UNIVERSIDADE DE SÃO PAULO
Instituto de Ciências Matemáticas e de Computação

Reconstruction of Network Phase Dynamics from Data

Zeray Hagos Gebrezabher

Tese de Doutorado do Programa de Pós-Graduação em Ciências de Computação e Matemática Computacional (PPG-CCMC)

ICMC USP
SÃO CARLOS

Zeray Hagos Gebrezabher

Reconstruction of Network Phase Dynamics from Data

Thesis submitted to the Instituto de Ciências Matemáticas e de Computação – ICMC-USP – in accordance with the requirements of the Computer and Mathematical Sciences Graduate Program, for the degree of Doctor in Science. *FINAL VERSION*

Concentration Area: Computer Science and Computational Mathematics

Advisor: Prof. Dr. Tiago Pereira da Silva

USP – São Carlos
July 2023

Ficha catalográfica elaborada pela Biblioteca Prof. Achille Bassi
e Seção Técnica de Informática, ICMC/USP,
com os dados inseridos pelo(a) autor(a)

G293r

Gebrezabher, Zeray Hagos
Reconstruction of Network Phase Dynamics from Data / Zeray Hagos Gebrezabher; orientador Tiago Pereira da Silva. -- São Carlos, 2023.
123 p.

Tese (Doutorado - Programa de Pós-Graduação em Ciências de Computação e Matemática Computacional) -- Instituto de Ciências Matemáticas e de Computação, Universidade de São Paulo, 2023.

1. Dynamical systems. 2. Coupled phase oscillators. 3. Network dynamics reconstruction. 4. Coupling functions. 5. Phase reduction. I. da Silva, Tiago Pereira, orient. II. Título.

Bibliotecários responsáveis pela estrutura de catalogação da publicação de acordo com a AACR2:
Gláucia Maria Saia Cristianini - CRB - 8/4938
Juliana de Souza Moraes - CRB - 8/6176

Zeray Hagos Gebrezabher

Reconstrução da Dinâmica de Fase de Rede a partir de Dados

Tese apresentada ao Instituto de Ciências Matemáticas e de Computação – ICMC-USP, como parte dos requisitos para obtenção do título de Doutor em Ciências – Ciências de Computação e Matemática Computacional. *VERSÃO REVISADA*

Área de Concentração: Ciências de Computação e Matemática Computacional

Orientador: Prof. Dr. Tiago Pereira da Silva

USP – São Carlos
Julho de 2023

ACKNOWLEDGEMENTS

I would like to express my deepest gratitude to Prof. Tiago Pereira for supervising this PhD and for offering me all the scientific opportunities that I had in this project, and in particular for giving me the freedom to explore my ideas, for his unreserved support throughout the course of my PhD.

I am also thankful to my colleagues and friends from the University of Sao Paulo for their support and the fruitful discussions I had during the course of my PhD. In particular, I am thankful to Edmilson Roque for the many discussions on phase oscillators and reconstruction from data and life in general. I am also thankful to Zheng Biang for his unreserved support during my difficult moments. Thanks should also go to many other people I had the chance to meet at the University of Sao Paulo and beyond. All of them had an impact on me. I am also grateful to my uncle, the late Samron Gebrehiwot, for his unreserved support during my studies until the last times of his life.

I wish to express my gratitude to my beloved wife, Tsega Girmay. Her unreserved and unconditional support, understanding, and encouragement helped me to get through my difficult times. I will never be grateful enough to her for raising our beautiful children, Melat and Abel, alone.

Last but not definitely least, I acknowledge CNPq-TWAS for the financial support under grant 120556/2017-0.

RESUMO

GEBREZABHER, Z. H. **Reconstrução da Dinâmica de Fase de Rede a partir de Dados**. 2023. 123 p. Tese (Doutorado em Ciências – Ciências de Computação e Matemática Computacional) – Instituto de Ciências Matemáticas e de Computação, Universidade de São Paulo, São Carlos – SP, 2023.

Muitos sistemas dinâmicos, tanto naturais quanto feitos pelo homem, são compostos de partes que interagem. Sistemas dinâmicos isolados, como neurônios, células cardíacas e circuitos elétricos, são de natureza periódica. Matematicamente, tais sistemas periódicos podem ser descritos por um oscilador de ciclo limite, que pode ser parametrizado em termos de fases. Hoje em dia é possível coletar e processar enormes quantidades de dados das unidades de muitos osciladores de ciclo limite de interação. No entanto, não temos modelos suficientes de tais sistemas para identificar e parametrizar as características cruciais que devem ser incorporadas ao modelo.

O objetivo principal desta tese é reconstruir modelos de sistemas dinâmicos a partir de dados de séries temporais disponíveis. Neste contexto, consideramos o caso em que os dados provêm de uma rede de unidades oscilatórias que interagem fracamente. Para tanto, pretendemos reconstruir a dinâmica de fases a partir de séries temporais em termos de fases. As fases podem ser estimadas a partir de cada série temporal de tais sistemas oscilatórios. Teoricamente, a estrutura de redução de fase é discutida para o caso de sistema dinâmico fracamente perturbado com um ciclo limite exponencialmente estável quando não perturbado, onde este também foi estendido para sistemas oscilatórios de interação fraca, usando o conceito de isócronas. A influência que um sistema dinâmico exerce sobre outro é descrita por uma função de acoplamento, e as funções de acoplamento extraídas das séries temporais de sistemas dinâmicos em interação são frequentemente variáveis no tempo.

Motivados pela variabilidade temporal das interações biológicas, incluindo as funções de interação cardiorrespiratória e neural delta-alfa que foram reconstruídas com base na inferência Bayesiana, estudamos a existência de transições de sincronização causadas por funções de acoplamento variantes no tempo, mesmo que o acoplamento líquido força é invariável. Também estudamos o surgimento de hiperredes ao reconstruir modelos de osciladores acoplados não linearmente a partir de dados. Em particular, quando os dados vêm de uma rede de osciladores Stuart-Landau fracamente acoplados, mostramos que métodos de recuperação esparsos revelam hiper-redes. Este resultado é verificado teoricamente usando a teoria de redução de fase de segunda ordem através do método de perturbação.

Palavras-chave: Sistemas dinâmicos, Osciladores de fase acoplados, Reconstrução dinâmica de rede, Funções de acoplamento, Redução de fase.

ABSTRACT

GEBREZABHER, Z. H. **Reconstruction of Network Phase Dynamics from Data**. 2023. 123 p. Tese (Doutorado em Ciências – Ciências de Computação e Matemática Computacional) – Instituto de Ciências Matemáticas e de Computação, Universidade de São Paulo, São Carlos – SP, 2023.

Many dynamical systems, both natural and man-made, are composed of interacting parts. Isolated dynamical systems such as the spiking of neurons, cardiac cells, and electrical circuits are periodic in nature. Mathematically, such periodic systems can be described by a limit cycle oscillator, which can be parameterized in terms of phases. Nowadays it is possible to collect and process enormous amounts of data from the units of many such interacting limit cycle oscillators. However, we do not have enough models of such systems to identify and parameterize the crucial features that must be incorporated into the model.

The main objective of this thesis is to reconstruct models of dynamical systems from available time-series data. In this context, we considered the case where the data comes from a network of oscillatory units that interact weakly. To this end, we aim to reconstruct phase dynamics from time series in terms of phases. The phases can be estimated from each time series of such oscillatory systems. Theoretically, the phase reduction framework is discussed for the case of a weakly perturbed dynamical system with an exponentially stable limit cycle when unperturbed, where this was also extended to weakly interacting oscillatory systems, using the concept of isochrons. The influence that one dynamical system exerts on another is described by a coupling function, and the coupling functions extracted from the time series of interacting dynamical systems are often found to be time-varying.

Motivated by the time-variability of biological interactions, including neural delta-alpha interaction functions which were reconstructed based on Bayesian inference, we studied the existence of synchronization transitions caused by time-varying coupling functions, even though the net coupling strength is invariant. We also studied the emergence of hypernetworks when reconstructing models of nonlinearly coupled oscillators from data. In particular, when the data comes from a network of weakly coupled Stuart-Landau oscillators, we showed that sparse recovery methods reveal hypernetworks. This result is verified theoretically using second-order phase reduction theory via the perturbation method.

Keywords: Dynamical systems, Coupled phase oscillators, Network dynamics reconstruction, Coupling functions, Phase reduction.

LIST OF FIGURES

LIST OF TABLES

LIST OF SYMBOLS

f — vector field

x — state vector in $\mathbb{R}^n$

φ — flow

γ — limit cycle

d — distance function

$\mathscr{B}(\gamma)$ — basin of attraction of γ

$\mathbb{S}^1$ — the circle of all phases $[0,1]$

$\theta, \vartheta, \psi, \phi$ — phase

Θ — asymptotic phase function

$\mathscr{I}(x_0)$ — Isochron passing through θ

Σ — cross section of a flow

$C^k(U,V)$ — space of k-times continuously differentiable functions

P — Poincaré map

g — time-one map of the flow φ

Z — phase sensitivity function

T — period

ω, Ω — angular frequencies

p — small perturbation function

N — Network size

h, q — Coupling function

$\boldsymbol{A}$ — Adjacency matrix

D, σ — Noise intensity

$\xi(t)$ — dynamical noise term

$\langle \cdot \rangle$ — Inner product

ε, α — Coupling parameters

$\mathscr{Y}, \Upsilon$ — time series data

$\mathscr{M}$ — set of unknown parameters

Δt — time sampling size

$\Delta \boldsymbol{W}$ — Wiener increments

$\boldsymbol{\zeta}_m$ — i.i.d. Gaussian random variable

$\ell(\mathscr{M}, \Upsilon)$ — likelihood function of the data Υ given parameters $\mathscr{M}$

S — minus-log-likelihood function

$p(\mathscr{M})$ — prior distribution of parameters $\mathscr{M}$

$\boldsymbol{\phi}_k$ — basis function

$\mathscr{L}$ — library of basis functions

$p(\mathscr{M} \mid \Upsilon)$ — poisterior distribution of parameters $\mathscr{M}$ given data Υ

$\boldsymbol{\Phi}$ — Library matrix of basis functions

$\boldsymbol{c}_i$ — coefficient vector of basis functions

M — number of data points

K — maximum number of basis functions

λ — sparsity thresholding parameter

wFP — weighted fraction of false positives

wFN — weighted fraction of false negatives

CONTENTS

CHAPTER

1

INTRODUCTION

Many complex systems, in nature and man-made, are composed of interacting units. Examples range from gene regulatory networks in the cell (DAVIDSON, 2010) and neural circuits in the brain (TAKEMURA *et al.*, 2013) to food webs in ecosystems (MCKANE *et al.*, 2003) and power grids (WITTHAUT; TIMME, 2012). Such systems can be described by dynamical units oscillating on complex networks. Knowledge of the network dynamics of such complex networked systems is essential to understanding and predicting sudden changes in behavior and controlling their functionality. However, in many real problems, network dynamics are often unknown but rather need to be reconstructed from available data.

Due to the advances in modern information technology, the availability of data that capture the structure and behavior of complex networked systems has greatly increased in recent years. Despite its increasing importance, reconstructing the governing equations of complex network dynamics remains a challenging problem due to the large-scale, noisy, and heterogeneous nature of the available data. Nonetheless, recent advances in computational and statistical methods, particularly in machine learning methods and graph theory, have greatly enhanced our capacity to reconstruct networks from various types of data, such as time series, "functional magnetic resonance imaging" (fMRI), and social media.

In this thesis, we focus on reconstructing network dynamics from data that come from networks of oscillatory dynamical systems. In particular, we consider data that come from networks of weakly interacting periodic systems. By weakly interacting we mean the effect of one dynamical system on another is small as compared to its own intrinsic dynamics. Dynamical systems such as periodic spiking of neurons (IZHIKEVICH, 2000), and cardiac cells (GLASS; MACKEY, 1988; WINFREE, 2001) when isolated are believed to exhibit stable rhythmic behavior. Mathematically, such periodic systems can be described by a limit cycle oscillator, which can be parameterized in terms of phases. A phase is a time-like variable bounded by the period of the limit cycle.

The notion of phases allows us to reduce the problem of studying the high-dimensional dynamical system into a one-dimensional phase dynamics equation using the phase reduction theory (PIETRAS; DAFFERTSHOFER, 2019), using the concept of "isochrons" (WINFREE, 1974). This can be extended to a system of weakly interacting dynamical systems (NAKAO, 2015). The impact that one dynamical system exerts on another can be described by its interaction function. Examples include Josephson junctions (WIESENFELD; COLET; STROGATZ, 1996), neuronal networks (CESSAC, 2010), the cardiorespiratory system (SCHÄFER *et al.*, 1998), cardiorespiratory-brain interactions (MORELLI *et al.*, 2018).

The dynamics of such systems often have external influences leading to time-variability in their mathematical description, e.g. time-varying frequency or a time-varying form of coupling function (Lucas; Newman; Stefanovska, 2018). These can lead to the existence of a qualitative change, such as synchronization transitions. By synchronization we mean the rhythmic adjustment of limit cycle oscillators caused due to their weak interactions. This phenomenon is greatly explored in (PIKOVSKY; ROSENBLUM; KURTHS, 2001), which is one of the hottest areas in recent studies. One of the main goals of this thesis is to study the effects of time-varying forms of coupling functions that induce a transition to synchronization. Coupling functions of interacting dynamical systems can be reconstructed from data (STANKOVSKI *et al.*, 2016).

Network of dynamical systems. Many of the networked dynamical systems examples mentioned above can be described in a network with pairwise interactions. In this setting, we consider a network of N pairwise coupled dynamical systems whose state equations can be described using stochastic differential equations as:

$$\frac{d}{dt}x_i(t) = f_i(x_i(t)) + \alpha \sum_{j=1}^{N} A_{ij} h_i(x_i(t), x_j(t)) + \xi_i(t), \quad i = 1, \ldots, N, \tag{1.1}$$

where $x_i(t)$ is the state variable of the ith node of the network at time t, possibly it could be higher-dimensional, say $x_i \in \mathbb{R}^m$ with $m > 1$; f_i is the vector field describing the isolated dynamics of node i; the coupling function h_i dictates a pairwise coupling function (STANKOVSKI *et al.*, 2017) of the ith node; and the adjacency matrix $A_{i,j}$ defines who is connected to whom: $A_{i,j} = 1$ if nodes i and j are connected and $A_{i,j} = 0$ otherwise. The constant α is the strength of the coupling. The term ξ_i is the dynamical noise added into the system to better mimic real situations. It can be seen that the system (1.1) is higher-dimensional and hence it might be challenging to make some important features about the network dynamics from it. For this reason, we might want to reduce the dynamics into phase equations. A straightforward question to ask would be:

Under what conditions can the network be effectively described using phase equations?

Before we give an adequate answer to this question, we consider the following assumptions on the network dynamics (1.1):

- When uncoupled (i.e. $\alpha = 0$), each system f_i exhibits an *exponentially stable limit cycle* γ_i with similar *natural frequencies* ω_i, and
- When coupled, we have a weak coupling, i.e., $\alpha \ll 1$.

Then the *normally hyperbolic invariant manifolds* (NHIMs) theory (HIRSCH; PUGH; SHUB, 1977; ELDERING, 2013a) guarantees that the network dynamics remain on an N-dimensional torus $\mathbb{T}^N$. For $N = 2$, it is demonstrated on figure 1. It remains to find the network phase equations on a manifold.

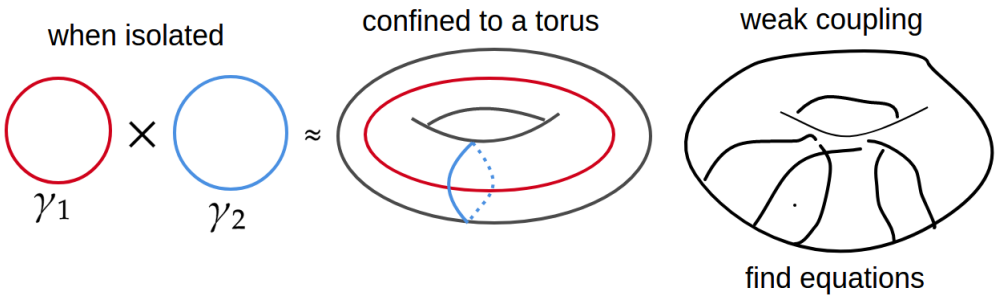

Figure 1 – The product of two isolated limit cycles γ_1 and γ_2 are confined in a torus $\mathbb{T}^2$ (middle), and if we impose a weak coupling, the normally hyperbolic invariant manifolds guarantee that the dynamics are on a torus (HIRSCH; PUGH; SHUB, 1977; ELDERING, 2013b), and we find the dynamics on a manifold (right).

Source: Elaborated by the author.

The phase reduction theory states that the network dynamics in equation (1.1) can be reduced to the phase equations:

$$\frac{d}{dt}\theta_i(t) = \omega_i + \alpha \sum_{j=1}^{N} A_{ij} q_i(\theta_i(t), \theta_j(t)) + \xi_i(t), \qquad i = 1, \ldots, N, \tag{1.2}$$

where θ_i is the phase of ith oscillator, and q_i is the *phase coupling function* between the ith oscillator and $j$the oscillator. Equation (1.2) is the reduced phase dynamics of the network of N nodes.

This project aims to

> *Reconstruct phase models of dynamical systems from available time-series data recorded from a network of weakly coupled limit cycle oscillators.*

In practice, we do not even have access to the time series in phases but we measure each state variable of the network. We first need to estimate the corresponding phases from the available data via e.g. *Hilbert transform* (ROSENBLUM; PIKOVSKY; KURTHS, 1996) or

angle variable. Then use these estimated phases to recover their phase dynamics. A schematic representation of the reconstruction problem is shown in figure 2.

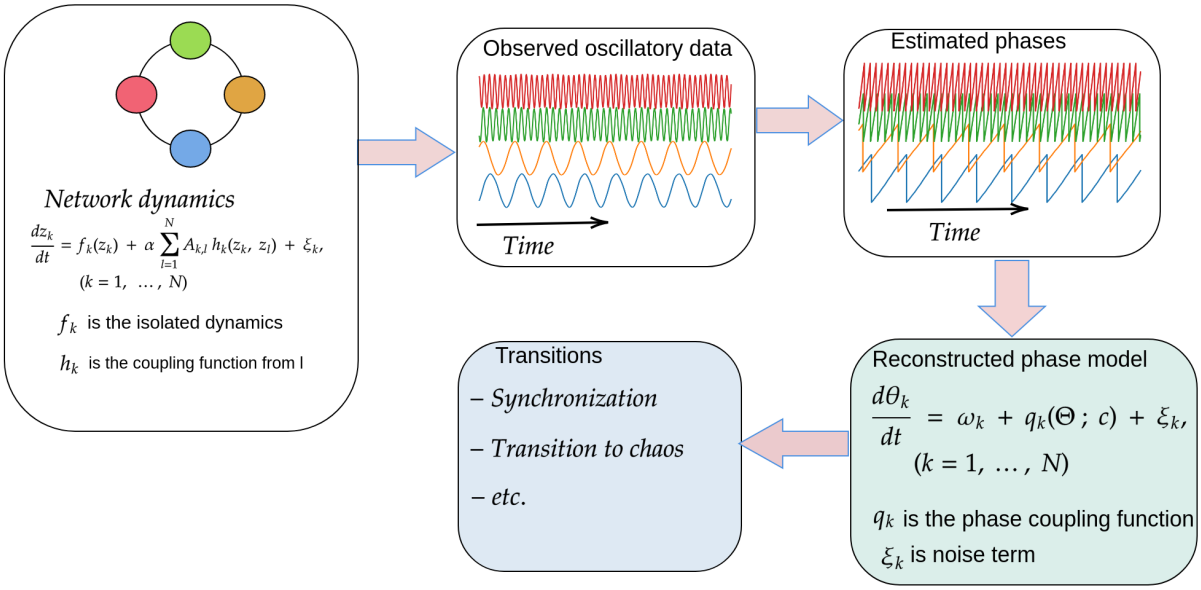

Figure 2 – Schematic diagram of the recovering phase coupling functions from observed rhythmic time series data. We assumed that we have access to multivariate time series of certain network dynamics. We then extract the phase time series followed by reconstructing the underlying phase dynamics. Finally, we deduce the underlying phenomenon, such as synchronization and/or transition to chaos.

Source: Elaborated by the author.

More precisely, we have two main results:

① Characterized the effects of time variability in the coupling functions. More precisely, we showed the existence of synchronization transitions caused by time-varying coupling functions example while the net coupling strength is kept constant.

② We reconstructed phase models of dynamical systems from oscillatory data. In particular, we showed the emergence of hypernetworks from ring networks of weakly coupled limit-cycle oscillators. This result was also verified theoretically by applying phase reduction followed by averaging theory. Also, we compared Bayesian inference and sparse recovery methods against the following parameters: computational cost vs sparsity; robust against noise vs not applicable. An insight is: by optimizing the phase of dynamical paths we may be able to get rid of some observational noise and better compare sparse recovery and Bayesian inference. These two reconstruction methods were applied to a network of three coupled phase oscillators subject to additive Gaussian noise.

In the next section, we present the organization of the rest of this thesis.

1.1 Organization

Chapter 2 presents the theoretical background of the project. Theoretically, the phase reduction framework is discussed for the case of a weakly perturbed dynamical system with an exponentially stable limit cycle when unperturbed. This was also extended to weakly interacting oscillatory systems. The phase coupling functions extracted from the time series of such interacting dynamical systems are often found to be time-varying.

In Chapter 3 we discuss the dynamics of phases. Motivated by the time-variability of biological interactions, including the cardio-respiratory and neural delta-alpha interaction functions which were reconstructed based on Bayesian inference, we studied the existence of synchronization transitions caused by time-varying coupling functions, even though the net coupling strength is invariant[1].

Chapter 4 is devoted to the reconstruction of phase models of coupled dynamical systems from data recorded from networks of weakly interacting oscillators based on Bayesian inference and sparse recovery methods. Moreover, we showed a case where although the dynamics in the network are purely pairwise, due to the nonlinearity of the coupling functions, we reveal hypernetworks – higher-order interaction terms. This result is verified theoretically using second-order phase reduction theory via the perturbation method[2].

Finally, Chapter 5 is devoted to the conclusions and future perspectives of our project.

[1] This result was published on the journal of the Royal Society (Hagos *et al.*, 2019)
[2] Part of these results is in process for submission in a journal

CHAPTER

2

THEORETICAL BACKGROUND

We review the dynamics of a weakly perturbed limit cycle.

2.1 Dynamics near a periodic orbit

Consider a system of ordinary differential equations

$$\frac{dx}{dt} = f(x), \tag{2.1}$$

where $f : U \to \mathbb{R}^n$ is continuously differentiable and $U \subset \mathbb{R}^n$ is open. By the *Picard theorem*, for every initial condition $x \in U$, there exist a time interval $I_x := (\alpha(x), \beta(x))$, for some $\alpha(x) < 0$ and $\beta(x) > 0$, and a unique continuously differentiable solution $\varphi : I_x \to U$ such that

$$\begin{aligned} &\varphi(0,x) = x, \\ &\frac{d\varphi(t,x)}{dt} = f(\varphi(t,x)) \quad \forall t \in (\alpha,\beta) =: I_x \subset \mathbb{R}. \end{aligned} \tag{2.2}$$

Thus, $\varphi(t,x)$ is the solution of the Cauchy initial value problem of the curves passing through the initial point x. We can construct a "local flow". Consider the set

$$M := \bigcup_{x \in U} I_x \times \{x\} \subset \mathbb{R} \times U. \tag{2.3}$$

Then we can define the "**local flow**" $\varphi : M \to U$ such that

1. $\varphi(0,x) = x$,
2. For all $x \in U$ and $s \in I_x$

$$\varphi(t+s,x) = \varphi(t, \varphi(s,x)) \quad \forall t \in I_x - s.$$

The condition 2 is called the *group property* of the flow $\varphi(t,x)$.

Recall that it is not always possible to extend the interval I_x to $\mathbb{R}$. If there is a *compact* set C such that $\varphi(t,x) \in C$ for each $t \in [0,\beta)$, then one can extend the solution to an interval $[0,\beta+\varepsilon)$ for some $\varepsilon > 0$. Thus if the solution never leaves a compact set we can extend the solution $\varphi(t,x)$ to $\mathbb{R}^+$. Similar construction can be done for $t < 0$.

We assume that the system (2.1) has an *exponentially stable limit cycle* with period 1, that is, $\gamma(t+1) = \gamma(t)$ for all $t \in \mathbb{R}$, that is, there exist constants $K > 0$ and $\lambda > 0$ such that, for each initial point x sufficiently close to γ,

$$d(\varphi(t,x),\gamma) \leq K\mathrm{e}^{-\lambda t}, \tag{2.4}$$

where $d(x,\gamma) = \inf_{x_0 \in \gamma} \|x - x_0\|$. Here $\|\cdot\|$ is the Euclidean norm. We can also consider the largest set that is attracted to the orbit

$$\mathscr{B}(\gamma) = \{x \in U \mid \lim_{t\to\infty} d(\varphi(t,x),\gamma) = 0\}, \tag{2.5}$$

known as the **basin of attraction** of γ (GUCKENHEIMER; HOLMES, 1983). It follows that $\mathscr{B}(\gamma)$ is open.

We can introduce a parametrization on the limit cycle γ in terms of its phase $\theta \in [0,1]$. Note that $[0,1]/\sim$ is *homeomorphic* to $\mathbb{S}^1$ via the homeomorphism which sends the equivalence class of $x \in [0,1]$ to $\exp(2\pi i x)$, so that $\mathbb{S}^1$ is identified with $\mathbb{R}/\mathbb{Z}$. Hence, θ has a unique extension $\bar{\theta}$ to $\mathbb{R}$ which is called the *lift* of θ. For the sake of simplicity, we will not distinguish the phase θ from its lift $\bar{\theta}$.

Small perturbations of the system (2.1) deviate the dynamics away from the limit cycle γ, hence the phase variable must be defined in some neighborhood of γ. This is accomplished with the concepts of "*asymptotic phase*" (WINFREE, 1967).

Asymptotic phase. Assume that $x \in \gamma$ and $y \in \mathscr{B}(\gamma)$, where φ, γ, and $\mathscr{B}(\gamma)$ are as defined above. We say that y is in asymptotic phase with a point $x \in \gamma$ if

$$\lim_{t\to\infty} \|\varphi(t,y) - \varphi(t,x)\| = 0. \tag{2.6}$$

The phase $\theta \in \mathbb{S}^1$ of the points $x \in \gamma$ correspond to the symmetry $t \mapsto t + \alpha$, where α is a shift. In other words, we choose the phase to increase uniformly in time. This can be seen by introducing the *normal coordinates*. Using the normal coordinates $(y,\theta) \in \mathbb{R}^{n-1} \times \mathbb{S}^1$ near the cycle γ, the system $\dot{x} = f(x)$ is equivalent to

$$\begin{aligned} \dot{y} &= Ay + F(\theta, y) \\ \dot{\theta} &= 1 \end{aligned}$$

with $F(\theta,0)=0, F_y(\theta,0)=0$.

Since γ is an exponentially stable limit cycle for each point $y \in \mathscr{B}(\gamma)$ and along the orbit there is no contraction, there is a unique asymptotic phase, denoted by $\Theta(y)$. Thus, we have a function defined by

$$\begin{aligned} \Theta \ : \ \mathscr{B}(\gamma) &\longrightarrow \mathbb{S}^1 \\ y &\longmapsto \Theta(y). \end{aligned} \tag{2.7}$$

such that

$$\lim_{t\to\infty} \|\varphi(t,y) - \gamma(t+\Theta(y))\| = 0. \tag{2.8}$$

This implies the solution starting from $y \in \mathscr{B}(\gamma)$ converges to γ and will have the same asymptotic phase with points on γ. Next, we introduce the concept of "isochrons".

2.2 Isochrons

Definition 2.2.1. The set of points x in $\mathscr{B}(\gamma)$ with constant asymptotic phase Θ with value θ are called **isochrons** denoted as $\mathscr{I}(x_0)$. Mathematically,

$$\mathscr{I}(x_0) = \{x \in \mathscr{B}(\gamma) \ : \ \Theta(x) = \theta\}.$$

This definition implies that an isochron is a level set of the asymptotic phase $\Theta(x) = \theta$. The set of points where isochrons cannot be defined is called a "*phaseless set*" (GUCKENHEIMER, 1975). We illustrate the isochrons and the asymptotic phase in Figure 3.

To characterize the isochrons we review some basic properties of the Poincaré map P associated with the flow φ on the limit cycle.

Recall that a set $\Sigma \subset \mathbb{R}^n$ is called a *submanifold of codimension one* (that is, its dimension is $n-1$), if it can be written as

$$\Sigma = \{x \in U \mid s(x) = 0\}, \tag{2.9}$$

where $U \subset \mathbb{R}^n$ is open, $s \in C^k(U,\mathbb{R}), k \geq 1$, and the gradient $\nabla s(x) \neq 0$ for each $x \in \Sigma$. The submanifold Σ is "*transversal*" to f if $\nabla s(x) \cdot f(x) \neq 0$ for each $x \in \Sigma$. In other words, we say that the vector $f(x)$ is transverse to Σ at x if $x \in \Sigma$ and $f(x) \notin T_x\Sigma$, where $T_x\Sigma$ denotes the the *tangent space* to Σ at x. If $f(x)$ is transverse to Σ at each $x \in \Sigma$, we say that Σ is a "*cross-section*" for the flow $\varphi(t,x)$ in U.

Assume that given $x_0 \in U$ there is τ_0 such that

$$\varphi(\tau_0, x_0) \in \Sigma.$$

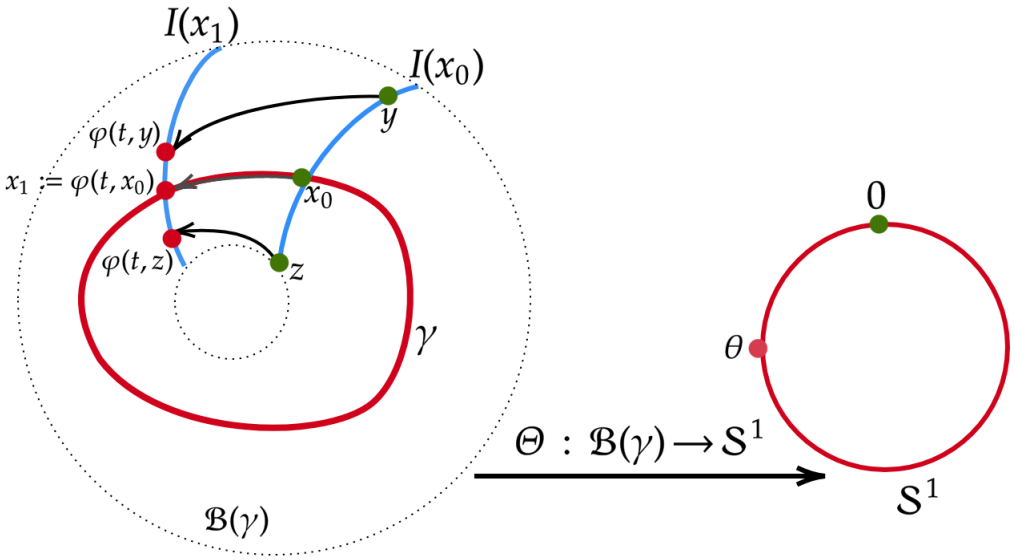

Figure 3 – An asymptotic phase $\Theta : \mathscr{B}(\gamma) \to \mathbb{S}^1$ associates to the base points x_0, x_1 in the basin of attraction $\mathscr{B}(\gamma)$, the asymptotic phases $0, \theta \in \mathbb{S}^1$, respectively. Shown are 2 isochrons $\mathscr{I}(x_0)$ and $\mathscr{I}(x_1)$ of the base points x_0 and x_1 associated to the phases θ_0, θ, respectively. An arbitrary chosen reference point $x_0 \in \gamma$ uses as the initial phase $\theta = 0$.

Source: Elaborated by the author.

Because the section Σ is transversal to f it follows from the implicit function theorem that there exist a neighborhood V of x_0 and a function $\tau : V \to \mathbb{R}$ such that for any $x \in V$ $\varphi(\tau(x), x) \in \Sigma$. Let us take a point $x_0 \in \gamma$ and a transversal section Σ such that x_0 belongs to Σ. We define the "*Poincaré map*" on Σ as $P : \Sigma \to \Sigma$ by

$$P(x) := \varphi(\tau(x), x), \tag{2.10}$$

where $\tau : \Sigma \to \mathbb{R}$ is the "*time of first return*" of the orbit $\varphi(t,x)$ to Σ and if $x_0 \in \gamma$, then $\tau(x) \to 1$ as $x \to x_0$. In that case x_0 is a fixed point of the map P .

Let us define the time-1 map defined on $\mathbb{R}^n$ as

$$\begin{aligned} g := \varphi(1, \cdot) \; : \; & \mathbb{R}^n \longrightarrow \mathbb{R}^n \\ & x \longmapsto g(x). \end{aligned} \tag{2.11}$$

By construction, $g(\gamma) = \gamma$.

The existence of isochrons is equivalent to the existence of cross-sections to the limit cycle γ for which the time of first return is identically the period of γ (GUCKENHEIMER, 1975). We seek a cross-section Σ of the limit cycle γ with $\{x\} = \Sigma \cap \gamma$ such that $\varphi(1, \Sigma) \subset \Sigma$.

If g is the time-1 map of the flow $\varphi(t,x)$ of equation (2.1), then for each $x_0 \in \gamma$, we have that $g(x_0) = \varphi(1, x_0) = x_0$. That is, x_0 is a fixed point of g. By the assumption on γ, there is a neighborhood V of γ such that $g(V) \subset V$ and $d(g(x), \gamma) < d(x, \gamma)$ for all $x \in V$.

We first present the definition of foliation. In the literature, there are several equivalent definitions of foliations. In this context, we offer the one that suits our discussion.

Definition 2.2.2. Let M be an n-dimensional manifold of class C^∞. An m-dimensional, class C^r $(r \geq 1)$ *foliation* of M is a maximum *atlas* $\mathscr{F}$ of class C^r in M with the following properties:

a) If $(U,\beta) \in \mathscr{F}$, then $\beta(U) = U_1 \times U_2 \subset \mathbb{R}^m \times \mathbb{R}^{n-m}$, where U_1 and U_2 are open disks of $\mathbb{R}^m$ and of $\mathbb{R}^{n-m}$ respectively.

b) If (U,β) and $(V,\chi) \in \mathscr{F}$ are such that $U \cap V \neq \emptyset$, then the change of coordinates $\chi \circ \beta^{-1}$: $\beta(U \cap V) \to \chi(U \cap V)$ is of the form

$$\chi \circ \beta^{-1}(u,v) = (h_1(u,v), h_2(v)), \quad (u,v) \in \mathbb{R}^m \times \mathbb{R}^{n-m}.$$

In this case, we say that M is *foliated* by $\mathscr{F}$.

Theorem 2.2.3. Consider the system (2.1), where f is $C^k(\mathbb{R}^n)$- smooth $(k \geq 1)$. Assume that γ, g, and φ are as defined above. For ε small enough through each $x_0 \in \gamma$, there is a unique isochron

$$\mathscr{I}_{loc}(x_0) := \{z \in B_\varepsilon \ : \ |g^m(z) - x_0| < Ce^{-\lambda m}, \lambda > 0\}. \tag{2.12}$$

which is a graph of a function. Moreover, the union of isochrons forms an invariant foliation of a small neighborhood V of γ. That is,

$$V = \bigcup_{x_0 \in \gamma} \mathscr{I}_{loc}(x_0) \quad \text{and} \quad \mathscr{I}_{loc}(x_0) \cap \mathscr{I}_{loc}(y_0) = \emptyset \text{ for } y_0 \neq x_0 \in \gamma.$$

The foliation is invariant in the following sense: The isochrons are mapped to isochrons under the action of the flow φ, that is, for any point $x_0 \in \gamma$ and $t > 0$ we have

$$\varphi(t, \mathscr{I}_{loc}(x_0)) \subset \mathscr{I}_{loc}(\varphi(t, x_0)).$$

For proof of this theorem, we refer the reader to Appendix A.

There are a few proofs in the literature about the isochrons. For example, in (GUCKENHEIMER, 1975) they showed for exponentially stable periodic orbits, isochrons are codimension-one stable submanifolds using the implicit function theorem. Moreover, the authors in (HIRSCH; PUGH; SHUB, 1977) showed isochrons as the persistence of normally hyperbolic invariant manifolds (NHIMs).

Remark 2.2.4. One can extend the local definition of the isochron to the basin of attraction. Theorem 2.2.3 shows that the basin of attraction $V := \mathscr{B}(\gamma)$ of the limit cycle γ is partitioned into stable manifolds of points $\mathscr{I}_{loc}(x_0), x_0 \in \gamma$ having the same asymptotic phase; which are the isochrons. In this case, x_0 is called the *base point* of the isochron through it. The foliation depends continuously smoothly on the base point $x_0 \in \gamma$.

From theorem 2.2.3, we note that the isochrons exist and they are mapped to isochrons under the flow φ, and they foliate V, each intersecting the limit cycle γ at x, which we call the base point. Since the foliation is continuous and invariant, we can extend the definition of the asymptotic phase $\Theta(x)$ to the small neighborhood V of γ.

Define

$$\theta(t,x) := \Theta(\varphi(t,x)).$$

By construction, all points x on an isochron $\mathscr{I}_{loc}(x_0)$ have a constant phase θ, and hence we establish the following proposition.

Proposition 2.2.5. Let $\varphi(t,x)$ be the solution of the system (2.1) passing through x in $\mathscr{B}(\gamma)$. Then the dynamics on the basin of attraction $\mathscr{B}(\gamma)$ of γ can be described by an asymptotic phase $\theta(t) := \Theta(\varphi(t,x))$ in such a way that

$$\frac{d\theta(t)}{dt} = 1. \tag{2.13}$$

Proof. From the result of theorem 2.2.3, we know that the asymptotic phase $\Theta(\varphi(t,x))$ increases uniformly in time t in such a way that

$$\frac{d\Theta(\varphi(t,x))}{dt} = 1, \tag{2.14}$$

By the chain rule, we obtain the phase equation

$$\frac{d\theta(t)}{dt} = \nabla\Theta(\varphi(t,x)) \cdot f(\varphi(t,x)) = 1 \tag{2.15}$$

for all points x in the basin of attraction $\mathscr{B}(\gamma)$ of γ. The gradient $\nabla\Theta(\varphi(t,x))$ can be computed at any $x \in \mathscr{B}(\gamma)$ for us of particular interest is the gradient along the limit cycle γ as $\nabla\Theta(\gamma(t))$. □

Remark 2.2.6. The existence of isochrons allows us to use the phase reduction framework.

Example 2.2.7. Consider the dynamical system

$$\begin{aligned} \dot{x} &= x - y - x(x^2+y^2), \\ \dot{y} &= x + y - y(x^2+y^2). \end{aligned} \tag{2.16}$$

In polar coordinates with $x = r\cos(\phi)$ and $y = r\sin(\phi)$, we obtain

$$\dot{r} = r(1-r^2); \quad \dot{\phi} = 1. \tag{2.17}$$

This system has an attracting limit cycle γ with radius $r = 1$, and basin of attraction $\mathscr{B}(\gamma) = \mathbb{R}^2 \setminus \{(0,0)\}$. An isochron is a curve that passes through $x_0 \in \gamma$ and moves at the same speed as x_0. Since the dynamics of ϕ does not depend on r, the isochrons are lines

$$\mathscr{I}_{loc}(x_0) := \{\phi = \theta\}$$

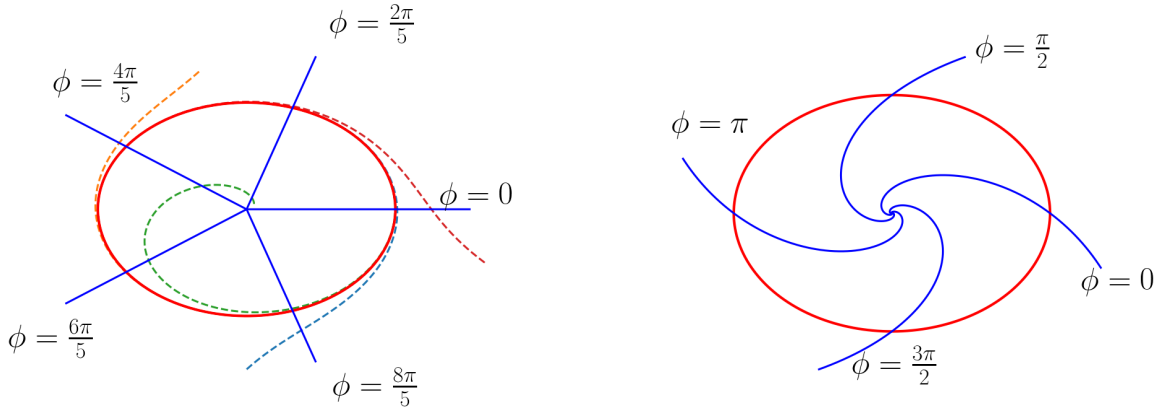

(a) (b)

Figure 4 – Isochrons and a stable periodic orbit. (a) A unique stable periodic orbit (red), five isochrons (blue) corresponding to phases $\phi = nT/5, n = 1,2,3,4,5$, where $T = 2\pi$ is the period of the orbit, of the system (2.16) in Theorem 2.2.7, and neighboring trajectories (dotted) with different initial conditions are attracted to the cycle. (b) Four isochrons (blue) of the periodic orbit (red) corresponding to phases $\phi = 0, \pi/2, \pi, 3\pi/2$, of the system (2.18) in Theorem 2.2.8.

Source: Elaborated by the author.

which are shown in figure 4a for 5 values of θ.

Gradient of the asymptotic phase. The asymptotic phase is

$$\Theta(r,\phi) = \phi = \theta.$$

The gradient of the asymptotic phase $\Theta(r,\phi)$ is given by

$$\nabla\Theta = \left(\frac{\partial\Theta}{\partial x}, \frac{\partial\Theta}{\partial y}\right).$$

Using the relations $r = \sqrt{x^2+y^2}$ and $\phi = \arctan(y/x)$, we have

$$\frac{\partial\Theta}{\partial x} = -\frac{1}{r}\sin(\theta), \quad \frac{\partial\theta}{\partial y} = \frac{1}{r}\cos(\theta).$$

Along the limit cycle γ, the gradient is

$$Z(\theta) := \nabla\Theta = (-\sin(\theta), \cos(\theta)).$$

Example 2.2.8. Consider the system which is adapted from (STANKOVSKI *et al.*, 2017)

$$\begin{aligned} \dot{x} &= x + (y-x)(x^2+y^2) \\ \dot{y} &= y + (x-y)(x^2+y^2). \end{aligned} \tag{2.18}$$

In polar coordinates with $x = r\cos(\phi)$ and $y = r\sin(\phi)$, the system (2.18) becomes

$$\dot{r} = r(1-r^2), \quad \dot{\phi} = r^2. \tag{2.19}$$

There is attracting periodic orbit γ with radius $r = 1$. Note that the phase ϕ along the orbit γ satisfies $\dot{\phi} = 1$. The asymptotic phase $\Theta(r,\phi)$ is a function of r and ϕ, and the isochrons of γ are the level sets of $\Theta(r,\phi)$.

Because r is independent of ϕ we use the ansatz

$$\theta(t) := \Theta(r,\phi) = \phi - \eta(r), \tag{2.20}$$

where $\eta(r)$ is unknown function of r to be determined.

Differentiating equation (2.20), we obtain

$$\dot{\Theta} = \dot{\phi} - \frac{d\eta}{dr}\frac{dr}{dt}. \tag{2.21}$$

Note that for points $x \in \mathscr{B}(\gamma)$, $\dot{\theta} = 1$. This implies from equation (2.19) above that

$$\frac{d\eta}{dr} = -\frac{1}{r}.$$

So that $\eta(r) = -\log(r) + C$, where C is constant. Hence, choosing $C = 0$, the isochrons are the set of points (r,ϕ) such that

$$\Theta(r,\phi) = \phi + \log(r) = \theta.$$

For different values of the constant θ, we construct the isochrons as shown in figure 4b.

Gradient of the asymptotic phase. The asymptotic phase is

$$\Theta(r,\phi) = \phi + \log(r).$$

Thus

$$\begin{aligned}\frac{\partial\Theta}{\partial x} &= \frac{\partial\Theta}{\partial r}\frac{\partial r}{\partial x} + \frac{\partial\Theta}{\partial\phi}\frac{\partial\phi}{\partial x} \\ &= \frac{1}{r}(\cos(\phi) - \sin(\phi))\end{aligned}$$

and

$$\begin{aligned}\frac{\partial\Theta}{\partial y} &= \frac{\partial\Theta}{\partial r}\frac{\partial r}{\partial y} + \frac{\partial\Theta}{\partial\phi}\frac{\partial\phi}{\partial y} \\ &= \frac{1}{r}(\cos(\phi) + \sin(\phi)).\end{aligned}$$

Along the limit cycle γ

$$Z(\theta) := \nabla\Theta = (\cos(\theta) - \sin(\theta), \cos(\theta) + \sin(\theta)).$$

Having already defined the concept of isochrons, in the next section, we present a reduction technique used to reduce higher-dimensional perturbed systems into phase models in terms of isochrons.

2.3 Phase reduction method

We consider the system (2.1) being perturbed as

$$\frac{dx}{dt} = f(x) + \varepsilon p(x,t), \quad x \in \mathbb{R}^n, \tag{2.22}$$

where $p(x,t+T) = p(x,t)$ for all t, and ε is a small parameter representing the intensity of the perturbation. Assume $T = \frac{2\pi}{\Omega}$, where Ω is the frequency of the perturbation.

When the function p is only a function of x, that is, $p = p(x)$, the periodic orbit γ of f persists by the implicit function theorem on the Poincaré map.

Under a weak perturbation $\varepsilon p(x,t)$, any solution of the perturbed system (2.22) that starts in the neighborhood of an exponentially stable limit cycle γ stays in its neighborhood. To see this, let us introduce a phase variable $\vartheta = \Omega t$. Then the system (2.22) can be transformed into an autonomous system on the extended phase space $\mathbb{R}^n \times \mathbb{S}^1$ as:

$$\begin{aligned} \frac{dx}{dt} &= f(x) + \varepsilon p(x,\vartheta) \\ \frac{d\vartheta}{dt} &= \Omega \end{aligned} \tag{2.23}$$

with $p(x,\vartheta + 2\pi) = p(x,\vartheta)$. Then the flow of the system (2.23) is represented as

$$(\varphi_\varepsilon(\vartheta,x,t,\varepsilon),\vartheta(t)).$$

A transversal cross-section can be defined as

$$\Sigma = \{(x,\vartheta) \in \mathbb{R}^n \times \mathbb{S}^1 \ : \ \vartheta = \vartheta_0\}. \tag{2.24}$$

Hence we define the Poincaré map on Σ. For the remainder of this section, we consider the system (2.23) under the following assumptions:

(A1) The functions f and p are continuously differentiable functions in their arguments.

(A2) The unperturbed system of (2.22) ($\varepsilon = 0$):

$$\frac{dx}{dt} = f(x), \quad x \in \mathbb{R}^n$$

has an exponentially stable limit cycle $\gamma \subset \mathbb{R}^n$ with period 1.

Then we have the following theorem.

Theorem 2.3.1. Consider the system (2.23) satisfying the assumptions (A1) and (A2). Then $\exists \varepsilon_0 > 0$ such that $\forall \varepsilon < \varepsilon_0$, there is a neighborhood $W := W(z, \frac{3\varepsilon}{1-k}) \subset \mathbb{R}^n$ of γ that is positively invariant

$$g_\varepsilon(W) \subset W,$$

where g_ε is the time-one map of the perturbed system (2.23).

The proof of theorem 2.3.1 can be found in appendix A. Theorem 2.3.1 implies that the perturbed orbit, denoted by $\tilde{\gamma}$ projected to $\mathbb{R}^n$ stays in a neighborhood of size $O(\varepsilon)$ of the unperturbed orbit, γ. This observation leads us to obtain an approximated equation of the orbit under perturbation, which is demonstrated in figure 5.

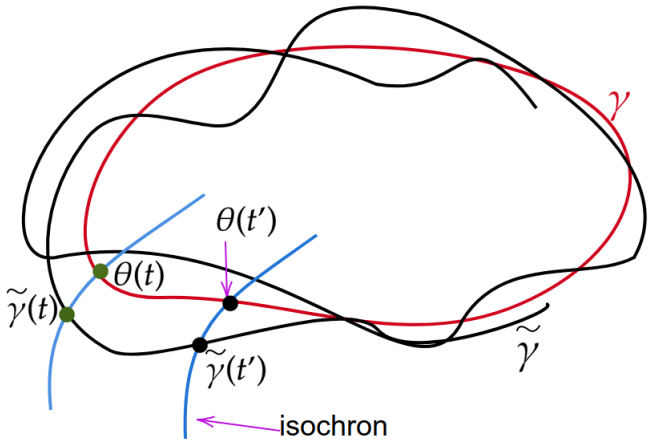

Figure 5 – Projection of the perturbed solution, $\tilde{\gamma}(t)$, to $\mathbb{R}^n$ stays in the neighborhood of the limit cycle, γ.

Source: Elaborated by the author.

Theorem 2.3.2. Consider the system (2.22) with $\tilde{\gamma}, \gamma$ as defined above, and let $\gamma(\theta)$ be a point on the limit cycle γ with the phase $\theta \in \mathbb{S}^1$. Assume that $\gamma(\theta)$, $\theta \in \mathbb{S}^1$, and $\varepsilon \ll 1$. Then the dynamics is reduced into a phase model

$$\frac{d\theta}{dt} = 1 + \varepsilon\Gamma(\theta,t) + \varepsilon^2 R(\theta,t,\varepsilon), \tag{2.25}$$

where the function Γ is defined using the inner product

$$\Gamma(\theta,t) := \nabla\Theta|_{\gamma(\theta)} \cdot p(\gamma(\theta),t) \tag{2.26}$$

and the function R is considered to be the remainder term.

Remark 2.3.3. In theorem 2.3.2, the equation of the phase dynamics (2.25) gives the result

$$\frac{d\Theta}{dt}(\varphi_\varepsilon(\vartheta,x,t,\varepsilon)) = 1 + \varepsilon\Gamma(\Theta(\varphi_\varepsilon(\vartheta,x,t,\varepsilon)),t) + \varepsilon^2 R(\Theta(\varphi_\varepsilon(\vartheta,x,t,\varepsilon)),t,\varepsilon). \tag{2.27}$$

Proof of Theorem 2.3.2. By construction, $\theta(t) = \Theta(\tilde{\gamma}(t))$ is already a phase in γ. Using equations (2.15) and (2.22), we obtain that the phase dynamics along the new orbit $\tilde{\gamma}$ is

$$\begin{aligned}\frac{d\theta(t)}{dt} &= \nabla\Theta(\tilde{\gamma}(t)) \cdot [f(\tilde{\gamma}(t)) + \varepsilon p(\tilde{\gamma}(t),t)] \\ &= 1 + \varepsilon\nabla\Theta(\tilde{\gamma}(t)) \cdot p(\tilde{\gamma}(t),t)\end{aligned} \tag{2.28}$$

where the gradient is evaluated along the new orbit $\tilde{\gamma}$. Here we have used the fact from proposition 2.2.5 that $\nabla\Theta(x) \cdot f(x) = 1$ in the basin of attraction of γ. Notice that there is no approximation in equation (2.28) as it depends explicitly on x, t, and θ. We want to reduce it to an equation of θ only.

Since the isochrons $\mathscr{I}_{loc}(x)$ smoothly depend on the base point x, then the gradient $\nabla\Theta(x)$ is differentiable for each x in a neighborhood of γ. We know that $\tilde{\gamma}(t)$ is assumed to be ε-close to the limit cycle γ, that is, $|\tilde{\gamma}(t) - \gamma(t)| = O(\varepsilon)$. By the Taylor expansion of $\nabla\Theta$ about $\tilde{\gamma}(t) - \gamma(t)$, we have

$$\nabla\Theta(\gamma(t) + \tilde{\gamma}(t) - \gamma(t)) = \nabla\Theta(\gamma(t)) + O(\varepsilon). \tag{2.29}$$

From assumption (A1) we know that p is differentiable, and hence by the Taylor expansion of p about $\tilde{\gamma}(t) - \gamma(t)$, we have

$$p(\gamma(t) + \tilde{\gamma}(t) - \gamma(t), t) = p(\gamma(t), t) + O(\varepsilon). \tag{2.30}$$

Hence, the first-order approximation phase dynamics of equation (2.28) along the orbit γ can be written as

$$\frac{d\theta(t)}{dt} = 1 + \varepsilon\nabla\Theta(\gamma(t)) \cdot p(\gamma(t),t) + O(\varepsilon^2) \tag{2.31}$$

which is the reduced phase equation of the perturbed system (2.22). □

Phase sensitivity function. The vector function

$$Z(\theta) := \nabla\Theta(x)|_{x=\gamma(\theta)} \tag{2.32}$$

is called the "*phase sensitivity function*" or "*infinitesimal phase response curve*" (NAKAO, 2015), and it measures how sensitively the oscillator responds to external perturbations (WINFREE, 1967; KURAMOTO, 1984b). $Z(\theta)$ is the isochron defined in $\mathscr{B}(\gamma)$. In the infinitesimal perturbations, we interpret the phase sensitivity function $Z(\theta)$ as a phase response curve that keeps track of linear response in the phase to infinitesimal perturbations.

Remark 2.3.4. If $Z(\theta)$ is known, the oscillator dynamics are fully determined for any weak perturbation.

Effective coupling on slow scales. In equation (2.25), considering $\vartheta := \Omega t$ as the phase of the external influence, $\Omega \approx 1$.

The problem will have slow scales

$$\psi = \theta - \Omega t. \tag{2.33}$$

Differentiating equation (2.33) with respect to t, we obtain that

$$\frac{d\psi(t)}{dt} = (1-\Omega) + \varepsilon Z(\psi + \Omega t) \cdot u(\psi + \Omega t, t), \tag{2.34}$$

where we have used $u(\psi + \Omega t, t) = p(\gamma(\psi + \Omega t), t)$. Equation (2.34) is still a non-autonomous differential equation, due to the explicit dependence on t, which is not easy to analyze in general. By assumption, $\Omega \approx 1$, and hence $1 - \Omega = \varepsilon\Delta$, where $\Delta = O(1)$. Hence we have that the dynamics of ψ is slow as compared to the dynamics of ϑ. That is, $\dot{\psi} = O(\varepsilon)$, $\dot{\vartheta} = O(1)$. We also assume that $\psi(t)$ is much slower that $p(t)$, allowing an approximation that replaces $\Gamma(\psi, t)$ by its *average*.

We now introduce the averaging theory to approximate and simplify the phase equation (2.34) into an autonomous equation. Here, we restate the simplest version of the averaging principle, called the *periodic averaging*.

Theorem 2.3.5 (Periodic Averaging, (SANDERS; VERHULST, 1985))**.** Consider a perturbed system of the form

$$\dot{x} = \varepsilon f(x, t, \varepsilon); \quad x \in U \subset \mathbb{R}^n, \quad 0 \leq \varepsilon \ll 1, \tag{2.35}$$

where $f : \mathbb{R}^n \times \mathbb{R} \times \mathbb{R}^+ \to \mathbb{R}^n$ is $C^k, k \geq 2$, bounded on bounded set U, and of period $T > 0$ in t. The associated "*autonomous averaged system*" is defined as

$$\dot{y} = \varepsilon \frac{1}{T} \int_0^T f(y, t, 0)\, dt =: \varepsilon \bar{f}(y). \tag{2.36}$$

Then there exists a C^k *change of coordinates* $x = y + \varepsilon w(y, t, \varepsilon)$ under which equation (2.35) becomes

$$\dot{y} = \varepsilon \bar{f}(y) + \varepsilon^2 f_1(y, t, \varepsilon), \tag{2.37}$$

where f_1 is of period T in t. Moreover

(i) If $x(t)$ and $y(t)$ are solutions of equations (2.35) and (2.36) starting at x_0 and y_0, respectively, at $t = 0$, and $|x_0 - y_0| = O(\varepsilon)$, then $|x(t) - y(t)| = O(\varepsilon)$ on a time scale $t \sim 1/\varepsilon$.

(ii) If p_0 is a hyperbolic fixed point of equation (2.36) then there exists $\varepsilon_0 > 0$ such that, for all $0 < \varepsilon \leq \varepsilon_0$, equation (2.35) possesses a unique hyperbolic periodic orbit $\gamma_\varepsilon(t) = p_0 + O(\varepsilon)$ of the same stability type as p_0.

By theorem 2.3.5, one can approximate the right hand side of equation (2.25) by integrating it over one period of the fast external forcing p, assuming that $\psi(t)$ does not vary within its period T, which is precisely the principle of averaging. It turns out that

$$\frac{d\psi(t)}{dt} = \varepsilon\Delta + \varepsilon\bar{\Gamma}(\psi), \tag{2.38}$$

where the coupling function is

$$\begin{aligned}\bar{\Gamma}(\psi) &= \frac{1}{T}\int_0^T \Gamma(\psi,t)\,dt \\ &= \frac{1}{T}\int_0^T Z(\psi+\Omega t)\cdot u(\psi+\Omega t,t)\,dt,\end{aligned} \tag{2.39}$$

where $T = 2\pi$ is the period of p as a function of $\vartheta = \Omega t$. This is summarized in the following theorem.

Theorem 2.3.6. Consider the reduced phase equation of the perturbed system (2.23)

$$\frac{d\psi}{dt} = \varepsilon\Delta + \varepsilon\Gamma(\psi,t) + O(\varepsilon^2),\ \varepsilon \ll 1, \tag{2.40}$$

where $\Gamma(\psi,t) = Z(\psi+\Omega t)\cdot u(\psi+\Omega t,t)$, and $\psi = \theta - \Omega t$ is a slowly varying phase as compared to the fast oscillation Ωt. Then, On a time scale of $t \sim 1/\varepsilon$ the equation (2.40) can be approximated by the phase equation

$$\frac{d\psi}{dt} = \varepsilon\Delta + \varepsilon\bar{\Gamma}(\psi), \tag{2.41}$$

where

$$\bar{\Gamma}(\psi) = \frac{1}{T}\int_0^T Z(\psi+\Omega t)\cdot u(\psi+\Omega t,t)\,dt. \tag{2.42}$$

Moreover, the solutions of the two equations are related by

$$|\theta(t) - \psi(t)| = O(\varepsilon). \tag{2.43}$$

The result of theorem 2.3.6 follows from the above assumptions on ψ, and using theorem 2.3.5(i). We note that equation (2.41) is the required reduced phase equation in ψ, and it can be analyzed graphically (see (NAKAO, 2015) for more discussion).

In summary, in the phase reduction approach, the dynamics of the oscillator is projected onto a single phase equation describing neutral dynamics along a one-dimensional stable limit cycle in the state space.

2.4 Examples of Phase Reduction

For a sufficiently small perturbation of a certain nonlinear oscillator or a network of weakly coupled oscillators, we can compute the corresponding phase sensitivity function or

infinitesimal PRC $Z(\theta)$. In this section, we consider three illustrative examples to compute $Z(\theta)$ analytically.

Phase oscillator. Consider the phase oscillator (IZHIKEVICH; ERMENTROUT, 2008) of the form

$$\dot{x} = f(x), \quad x \in \mathbb{S}^1 \tag{2.44}$$

where $f : \mathbb{R} \to \mathbb{R}$ such that $f(x) > 0$ is periodic. We note that the state variable x is a one-dimensional, defined on $\mathbb{S}^1$. Let $\gamma(t)$ be its periodic solution with some period $T > 0$. Let θ be the phase on the limit cycle γ at a point $\gamma(\theta)$ such that $\dot{\theta} = 1$. We follow *Kuramoto*'s approach to compute the phase sensitivity function $Z(\theta)$. Consider the asymptotic phase $\Theta(x)$. Using the rule for differentiating of inverse functions, the gradient of Θ along γ is given by

$$\nabla\Theta = \frac{1}{f(\gamma(\theta))}.$$

Saddle node infinite period (SNIPER). This bifurcation occurs when a saddle-node bifurcation of fixed points takes place on an invariant circle. Motivated by the results in (ERMENTROUT, 1996), we ignore the direction transverse to the periodic orbit and consider the one dimensional normal form

$$\dot{x} = \mu + x^2, \quad x \in \mathbb{R}. \tag{2.45}$$

Here x may represent a local arc length along the invariant circle. Note that the general solution to the equation is given by

$$x(t) = \sqrt{\mu}\tan[\sqrt{\mu}(t+c)]$$

where c is an arbitrary constant. We can see that for $\mu \leq 0$, there are two fixed points: $x = \pm\sqrt{-\mu}$, but for $\mu > 0$ there is no fixed point. This shows that the solution will "blow up" in finite time. Following (ERMENTROUT, 1996), the period T of the orbit can be approximated by computing the total time required for the solution $x(t)$ to send it from $x = -\infty$ to $x = +\infty$ and making the solution periodic, we obtain that $T = \frac{\pi}{\sqrt{\mu}}$, and hence the frequency $\omega = 2\sqrt{\mu}$.

Next, we introduce the asymptotic phase $\Theta(x) =: \theta(t)$ in such a way that it increases uniformly in time, i.e., $\frac{d\theta}{dt} = \omega$, and we need to compute its gradient.

$$\nabla\Theta = \frac{\partial\Theta}{\partial x} = \frac{\omega}{\frac{dx}{dt}|_{x(t)}} = \frac{\omega}{\mu + x(t)^2},$$

Using the periodic solution $x(t) = \sqrt{\mu}\tan(\sqrt{\mu}t)$, we have that

$$\nabla\Theta = \frac{\omega}{\mu(1+\tan^2(\sqrt{\mu}t))} = \frac{\omega}{\mu}\cos^2(\sqrt{\mu}t) = \frac{\omega}{2\mu}[1+\cos(2\sqrt{\mu}t)] = \frac{2}{\omega}[1+\cos(\theta)].$$

2.5 Networks of weakly coupled oscillators

In this section, we extend the phase reduction approach to a network of weakly coupled oscillators. In doing this, we first introduce the definition of networks that will be used throughout this thesis. For a comprehensive review of network theory we refer the reader to classical texts in the field (see, for instance, (NEWMAN; BARABÁSI; WATTS, 2006)).

Networks can be modeled as a labeled graph $G = (\mathscr{N}, \mathscr{E})$, where $\mathscr{N} = \{1, \ldots, N\}$ is a set of nodes and $\mathscr{E} \subset \mathscr{N} \times \mathscr{N}$ is a set of edges connecting the nodes. Vertex and link are terms that are often used as synonyms for nodes and edges, respectively. Here N is the total number of nodes, also known as the size of the network. The dynamics of such network G can be described by a set of oscillatory systems attached on top of each node.

The network dynamics of N weakly coupled oscillators can be described by the following system of differential equations

$$\frac{d}{dt}x_i(t) = f_i(x_i) + \varepsilon \sum_{j=1}^{N} A_{ij} h_i(x_i, x_j), \quad i = 1, \ldots, N \tag{2.46}$$

where $x_i(t) \in U_i \subset \mathbb{R}^n$ is the ith state variable of the underlying system at time t whose time evolution is given by $\frac{d}{dt}x_i(t)$, $f_i \colon U_i \to \mathbb{R}^n$ represents the isolated dynamics of the ith oscillator, and $h_i \colon U_i \times U_j \to \mathbb{R}^N$ is the pairwise coupling function of oscillator i. The network structure is encoded by the adjacency matrix $\boldsymbol{A} = (A_{ij})_{i,j=1}^{N}$, whose elements are defined as

$$A_{ij} = \begin{cases} 1 & \text{if there is a connection between nodes } i \text{ and } j, \\ 0 & \text{otherwise} \end{cases}$$

The parameter ε is the overall *coupling strength* which is assumed to be sufficiently small. Throughout this thesis, we assume that the functions f_i and h_i are smooth unless otherwise stated. Equation (2.46) is a higher dimensional dynamical system which would be difficult to give a detailed mathematical analysis. For this, we need to reduce it into a lower-dimensional model in terms of phases. To do this, we require the following additional assumptions.

We assume that each f_i is sufficiently close to some unknown function f, i.e., $\|f_i - f\| < \varepsilon$, where f exhibits an exponentially stable limit cycle γ of period T,. Applying the implicit function theorem, we can show that the isolated dynamics f_i has an exponentially stable limit cycle γ_i with period T_i and frequency $\Omega_i = \frac{2\pi}{T_i}$, and T_i is ε-close to T.

For each limit cycle γ_i, we can introduce a phase $\theta_i \in \mathbb{S}^1$. Let $\Theta_i(x) \in \mathbb{S}^1$ be the corresponding asymptotic phase for each f_i such that $\Theta_i(\varphi(t, x_i)) =: \theta_i(t)$, and $\|\Theta_i - \Theta\| < O(\varepsilon)$. Using the notion of isochrons, the isolated dynamics can be written as

$$\frac{d\theta_i}{dt} = \nabla\Theta_i(x_i) \cdot f_i(x_i) = \Omega_i. \tag{2.47}$$

By the chain rule, we have

$$\begin{aligned}\frac{d\theta_i}{dt} &= \nabla\Theta_i(x_i)\cdot\left[f_i(x_i)+\varepsilon\sum_{j=1}^{N}A_{ij}h_i(x_i,x_j)\right]\\ &= \Omega_i+\varepsilon\sum_{j=1}^{N}A_{ij}Z_i(\theta_i)\cdot h_i(\gamma_i(\theta_i),\gamma_j(\theta_j))+O(\varepsilon^2)\\ &= \Omega_i+\varepsilon Z_i(\theta_i)\cdot\sum_{j=1}^{N}A_{ij}p_{ij}(\theta_i,\theta_j)+O(\varepsilon^2).\end{aligned} \tag{2.48}$$

Let us assume that the natural frequencies of the oscillators are close to each other, i.e., $|\Omega_i-\Omega_j|=O(\varepsilon)$, for each $i\neq j$. Then, we can introduce a new phase variable

$$\psi_i(t)=\theta_i(t)-\Omega t,\quad i=1,\ldots,N, \tag{2.49}$$

where Ω is the mean frequency. Then we have $|\Omega_i-\Omega|=O(\varepsilon)=:\omega_i$. Then we transform the system (2.48) into the form

$$\frac{d\psi_i}{dt}=\omega_i+\varepsilon\sum_{j=1}^{N}A_{ij}Z_i(\psi_i+\Omega t)\cdot p_{ij}(\psi_i+\Omega t,\psi_j+\Omega t). \tag{2.50}$$

Applying the averaging theorem 2.3.5, we obtain

$$\frac{d\psi_i}{dt}=\omega_i+\varepsilon\sum_{j=1}^{N}A_{ij}q_i(\psi_j-\psi_i), \tag{2.51}$$

with the functions

$$\begin{aligned}q_i(\psi_j-\psi_i) &= \frac{1}{T}\int_0^T Z_i(\psi_i+\Omega t)\cdot p_{ij}(\psi_i+\Omega t,\psi_j+\Omega t)dt\\ &= \frac{1}{2\pi}\int_0^{2\pi} Z_i(s)\cdot p_{ij}(s,\psi_j-\psi_i)ds.\end{aligned} \tag{2.52}$$

describing the phase coupling function that measures the influence of the jth oscillator on the ith oscillator.

In terms of the phases θ_i, equation (2.51) can be rewritten as

$$\frac{d\theta_i}{dt}=\Omega_i+\varepsilon\sum_{j=1}^{N}A_{ij}q_i(\theta_i-\theta_j). \tag{2.53}$$

Note that if we measure the phases $\theta_i(t)$ for each oscillator i, we can numerically reconstruct the phase dynamics (2.53). In reality, however, we do not have access to the data $\theta_i(t)$ but rather we need to estimate them from an available time series data of the state variables $x_i(t)$, where we assumed that the data come from a system of weakly interacting oscillators. This problem is the central of chapter 4 of this project.

Theorem 2.5.1. Consider a periodic forcing $p(\vartheta,\psi)=:p(\vartheta)$ of an isolated oscillator near a Hopf bifurcation. Then the phase coupling function is given by

$$q(\psi_i-\psi_j)=\sin(\psi_i-\psi_j+\beta).$$

Proof. From hypothesis, the corresponding phase sensitivity function can be written as

$$Z(\theta) = (\sin\theta, \cos\theta). \tag{2.54}$$

We want to compute the coupling function. Then the coupling function, using the relation $p(\vartheta, \psi) =: p(\vartheta = \Omega t)$ and by equation (2.52), is given by

$$\begin{aligned} q(\psi_i - \psi_j) &= \frac{1}{2\pi}\int_0^{2\pi} \sin(\psi_i - \psi_j + s)p(s)\, ds \\ &= \frac{1}{2\pi}\int_0^{2\pi} \sin(\Delta\psi + s)p(s)\, ds \\ &= \frac{1}{2\pi}\int_0^{2\pi} \left(\sin(\Delta\psi)\cos(s) + \cos(\Delta\psi)sin(s)\right)p(s)\, ds \\ &= A\sin\left(\psi_i - \psi_j + \beta\right) \end{aligned} \tag{2.55}$$

where A is the amplitude and β is a phase shift. This completes the proof. □

2.6 Weakly coupled oscillators with noise

In this section we apply the phase reduction technique to a system of two weakly coupled oscillators driven by additive noise. This result was discussed in details by the authors in (KURAMOTO, 1984a; NAKAO, 2015). To this end, we consider a system of two weakly coupled oscillators described by the following differential equations with additive noise

$$\frac{dx_i}{dt} = f_i(x_i) + \varepsilon h_i(x_j, x_i) + \sqrt{D_i}\xi_i(t), \quad i, j = 1, 2; i \neq j, \tag{2.56}$$

where $x_i \in \mathbb{R}^n$ is the state variable of oscillator i, f_i is the isolated dynamics of the ith oscillator, h_i is the coupling function, and the coefficient $\varepsilon \ll 1$ is the coupling strength. The constant $\sqrt{D}$ scales the noise term $\xi_i(t)$ to ensure that it is $O(\varepsilon)$. The noise term $\xi_i(t)$ is assumed to be Gaussian white noise satisfying

$$\langle \xi_i(t) \rangle = 0, \tag{2.57}$$

$$\langle \xi_i(t)\xi_j(t') \rangle = \delta_{ij}\delta(t - t'), \tag{2.58}$$

where $\langle \cdot \rangle$ denotes an average. Assuming that each f_i has an exponentially stable limit cycle γ_i with period T_i and frequency Ω_i and that ε is sufficiently small. By phase reduction, the reduced phase equations can be written as

$$\frac{d\theta_i}{dt} = \Omega_i + \varepsilon Z_i(\gamma_i(\theta_i)) \cdot h_i(\gamma_j(\theta_j), \gamma_i(\theta_i)) + \sqrt{D_i}Z_i(\gamma_i(\theta_i))\xi_i(t) + O(\varepsilon^2) \tag{2.59}$$

$$=: \Omega_i + \varepsilon Z_i(\theta_i) \cdot h_i(\theta_j, \theta_i) + \sqrt{D_i}Z_i(\theta_i)\xi_i(t) + O(\varepsilon^2), \tag{2.60}$$

which can obtained applying the Ito formula (BJöRK, 2009, Theorem 4.16) to the asymptotic phase $\Phi_i(x_i)$ for each $i = 1, 2$. Assuming $|\Omega_i - \Omega_j| = O(\varepsilon)$ and introducing new phase variables

$\psi_i(t) = \theta_i(t) - \Omega t$, where Ω is the mean frequency, and applying the averaging theorem, we can arrive at the phase equations

$$\frac{d\psi_i}{dt} = \varepsilon\Omega_i + \varepsilon q_i(\psi_j - \psi_i) + \sqrt{D_i}\sigma_i\xi_i(t), \tag{2.61}$$

where σ comes from averaging the noisy phase equations (KURAMOTO, 1984a), and is defined as

$$\sigma_i = \left(\frac{1}{T}\int_0^T [Z_i(\tau)]^2\, d\tau\right)^{1/2}$$

and the phase coupling functions

$$q_i(\psi_j - \psi_i) = \frac{1}{T}\int_0^T Z_i(\tau)\cdot h_i(\psi_j - \psi_i, \tau)\, d\tau, \quad i \neq j = 1,2. \tag{2.62}$$

CHAPTER

3

TIME-VARYING COUPLING FUNCTIONS

This chapter presents the effects of time-varying phase equations in the transitions of collective dynamics. Such time-varying phase equations can be derived from weakly interacting limit cycle oscillators of higher-dimensional dynamical systems using the concept of phase reduction, which we have discussed in the previous chapter. More precisely, we study the effect of time-dependent interaction functions in phases.

3.1 Coupling functions: definition and examples

Complex systems are composed of many components or units which may interact with each other. Examples include Earth's global climate, organisms, the human brain, transportation or communication systems, an ecosystem, a living cell, and ultimately the entire universe. The interacting units of a complex system form a network, which can be modeled using networked dynamical systems. Examples include neuronal networks (CESSAC, 2010), the cardiorespiratory system (SCHÄFER *et al.*, 1998), cardiorespiratory-brain interactions (MORELLI *et al.*, 2018). Such dynamical systems often have external influences leading to time-variability in their mathematical description, e.g. time-varying form of coupling function (Stankovski, 2017).

Many of such networked dynamical systems described above are usually described using a system of deterministic differential equations or stochastic differential equations. The interacting components appearing in such equations are known as *coupling functions*. For instance, in the Kuramoto-Sakaguchi phase model (SAKAGUCHI; KURAMOTO, 1986; OMEL'CHENKO; WOLFRUM, 2012), a function of the form $q(\theta_i, \theta_j) = \sin(\theta_j - \theta_i - \beta)$ is a coupling function of oscillator i influenced by another oscillator j in the system of interest. Here, β denotes phase shift. Such coupling functions are vastly applicable in numerous scientific disciplines (ACEBRÓN *et al.*, 2005; STANKOVSKI *et al.*, 2017; SAKAGUCHI; KURAMOTO, 1986; OMEL'CHENKO; WOLFRUM, 2012). If such function q is explicitly time-dependent, we call it a time-dependent coupling function.

The coupling function can be described by its *net coupling strength*, and its *form* (STANKOVSKI *et al.*, 2017). The net coupling strength is just the norm or magnitude of the coupling function, and it quantifies only one aspect of the coupling function. On the other hand, the form of coupling function defines the functional law specifying the interactions, and it thereby introduces a new dimension and perspective (STANKOVSKI *et al.*, 2017; STANKOVSKI *et al.*, 2017; TICCINELLI *et al.*, 2017). Recent studies show that the effect of the net coupling strength on the dynamics of interacting dynamical systems is explored extensively.

In this chapter, we study the effect of time-varying functional forms of coupling functions on the collective dynamics of interacting systems. More precisely, we study the effects of time-varying functions that exhibit a transition to synchronization, while keeping the net coupling strength constant.

3.2 Motivation from biological interactions: the existence of time-varying coupling functions

Time-dependent interacting components can describe many dynamical systems in biology. For example, the coupling functions of cardiorespiratory interactions were found to vary in time in (STANKOVSKI *et al.*, 2012), where it was shown that the coupling strength and form of the coupling function vary over time.

In illustrating, we consider an example of time-varying delta-alpha neural coupling functions, calculated using simultaneous recordings from the same subject. More specifically, the delta and alpha brainwaves were extracted from an electroencephalogram (EEG) signal, measured in the resting state of the eyes opened. The data are drawn from an earlier study of neural cross-frequency coupling functions (STANKOVSKI *et al.*, 2017). The sampling frequency is 200 Hz. After that, the data are filtered to obtain the delta and alpha signals, $x_i(t)$. Then we aim to reconstruct the phase models of the delta-alpha neural brainwaves from it.

We first assumed that the phases $\phi_1(t)$ and $\phi_2(t)$ of the two interacting oscillators are governed by a differential equation of the general form equation (3.2) with the addition of Gaussian white noise, i.e.

$$\frac{d}{dt}\phi_i(t) = \omega_i + q_i(\phi_i(t), \phi_j(t)) + \xi_i(t), \quad i = 1,2,$$

where ω_i is the natural frequency of oscillator i, $\xi_i(t)$ is Gaussian white noise, and q_i is the coupling function describing the influence of oscillator j on the phase of oscillator i. Then, we extracted coupling functions from the phase dynamics using the dynamical Bayesian inference method (Luchinsky *et al.*, 2005; STANKOVSKI *et al.*, 2012; STANKOVSKI *et al.*, 2014). Reconstruction of phase models of non-time variable dynamical systems using the Bayesian inference method is discussed in detail in section 4.2.1 of the next chapter.

In our analysis, we aim in reconstructing the delta-alpha neural coupling function for the influence of δ brainwaves on α brainwaves, denoted by $q_\alpha(\phi_\delta, \phi_\alpha)$, from the recorded time series signals $x_i(t)$. In this case, we first estimate the corresponding phases of the delta brainwave ϕ_δ, and the alpha brainwave ϕ_α oscillations via the *Hilbert transform* followed by a transformation "protophase" to phase (More information on this procedure can be found in (KRALEMANN *et al.*, 2008)). The results are depicted in figure 6.

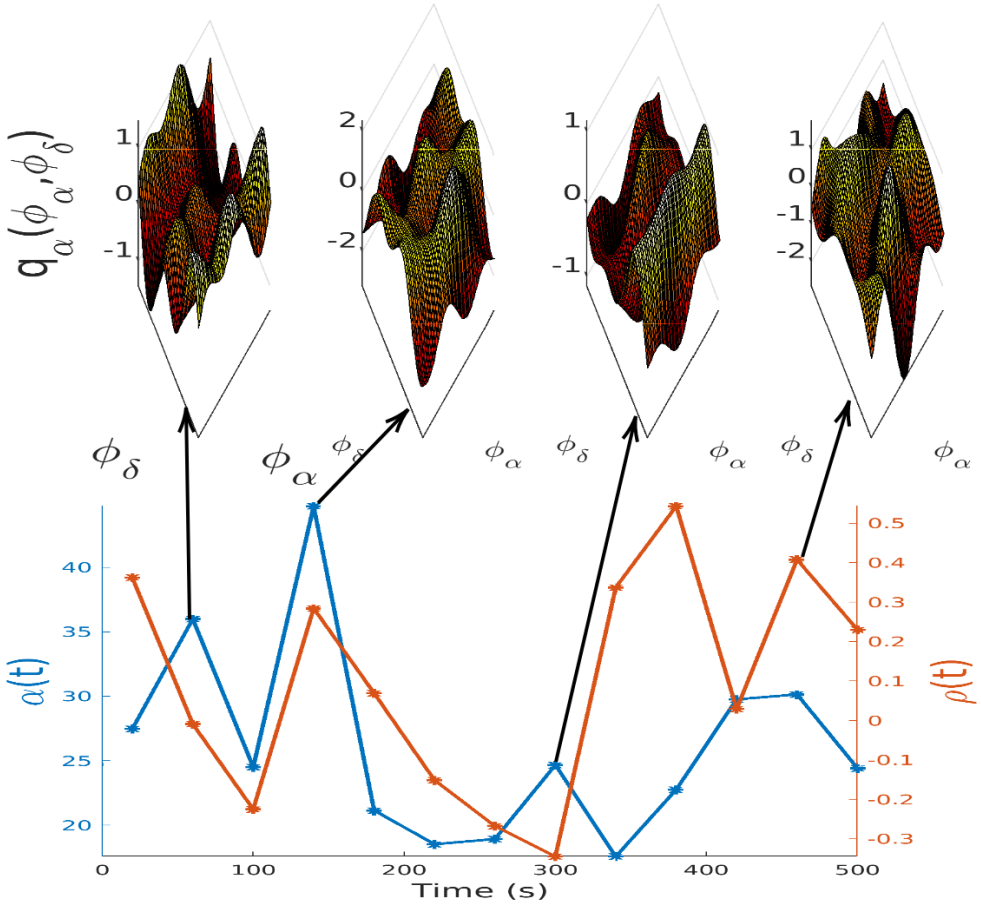

Figure 6 – Time-variability of delta-alpha neural interactions. Top panel: show results of phase coupling from delta brainwaves to alpha brainwaves. The four plots show the changes in the delta-alpha neural coupling function at different times; the time of each is indicated by a small arrow from the time axis in the bottom panel. Bottom panel: show plots of the time-variability of the similarity of form of coupling function $\rho(t)$ (orange line, right ordinate) and the net coupling strength $\alpha(t)$ (blue line, left ordinate) for the delta-alpha neural interactions. The similarity index $\rho(t)$ is calculated with respect to the time-averaged coupling function.

Source: Elaborated by the author.

Figure 6 shows the time-variability of delta-alpha coupling functions. Such time-variability are quantified using the "*similarity index*", $\rho(t)$, and the coupling strength, $\varepsilon(t)$. The definitions of these quantities are presented in section 3.4. This shows that the neural coupling changes more between different time windows and that the coupling strength and the form of the function often vary over time quite differently from each other. Hence, these characteristics can have

correspondingly different effects on the outcome and the possible transitions caused by the interactions – a phenomenon worth exploring further theoretically.

3.3 The model

In this section, we consider the dynamical system (2.46) for $N = 2$:

$$\frac{dx_i}{dt} = f_i(x_i) + \varepsilon h_i(x_i, x_j), \quad i \neq j = 1, 2,$$

Based on our discussion in section 2.5, the unperturbed system (i.e. $\varepsilon = 0$) can be reduced, on the limit cycle γ_i, to a one-dimensional phase equation

$$\frac{d\theta_i}{dt} = \omega_i, \quad i = 1, 2, \tag{3.1}$$

where $\omega_i = 2\pi/T_i$ is the natural frequency of the ith oscillator.

Little outside disturbances to each oscillator x_i, such as its interaction with the other oscillator x_j, may constrain x_i off the limit cycle γ_i of f_i. For this reason, we need to define the phases θ_i off the limit cycle γ_i. Based on the "isochrons" (WINFREE, 1967; WINFREE, 1980; KURAMOTO, 1984b), which is also discussed in more detail in chapter 2 of this thesis, one can amplify the definitions of the phases θ_i of the oscillators to the whole basin of attractions $\mathscr{B}(\gamma_i)$ of the limit cycles γ_i in such a way that they pivot consistently agreeing to equation (3.1), not as it were on the cycle but moreover in their comparing neighborhoods. Thus, the reduced phase equations of the two coupled limit-cycle oscillators can be written as

$$\frac{d\theta_i}{dt} = \omega_i + \varepsilon q_i(\theta_i, \theta_j), \quad i \neq j = 1, 2, \tag{3.2}$$

where the phase coupling functions $q_i(\theta_i, \theta_j)$ are 2π-periodic with respect to their arguments θ_1 and θ_2.

In our specific context where the isolated phase is uniform coupling function is just q defined as a mapping

$$q \; : \; M \times M \to M, \tag{3.3}$$

where M is the phase space. We assume that the coupling functions $q_{1,2}$ in equation (3.2) are smooth.

In (Hagos *et al.*, 2019), we examined a model of unidirectional coupling of the form

$$\begin{aligned} \frac{d\theta_1}{dt} &= \omega_1, \\ \frac{d\theta_2}{dt} &= \omega_2 + \varepsilon q_2(\theta_2, \theta_1), \end{aligned} \tag{3.4}$$

where q_2 is the coupling function of oscillator 2 influenced by oscillator 1 and is assumed to be time-dependent explicitly. To show an explicit time dependency, we write it as $q_2(\theta_1, \theta_2, t)$. We introduce the concepts of net coupling strength, similarity index, and synchronization transitions. After this, we carried out our numerical and theoretical analysis of the model.

3.4 Basic concepts

3.4.1 Net coupling strength

From the previous subsection, the coupling functions $q_1(\theta_1,\theta_2)$ and $q_2(\theta_1,\theta_2)$ defined in equation (3.2) are 2π-periodic in their arguments $\theta_i \in \mathbb{S}^1$, for each $i=1,2$. Hence, we can identify them on a 2-dimensional torus of the form $\mathbb{T}^2 = \mathbb{S}^1 \times \mathbb{S}^1$, where $\mathbb{S}^1 \cong \mathbb{R}/2\pi\mathbb{Z}$. Subsequently, the torus $\mathbb{T}^2$ can be distinguished by the square $[-\pi,\pi]^2$ or $[0,2\pi]^2$. We define the inner product in $L^2(\mathbb{T}^2,\mathbb{R})$ (RUDIN, 1987) by

$$\langle f,g\rangle = \frac{1}{4\pi^2}\int_{-\pi}^{\pi}\int_{-\pi}^{\pi} f(\theta_1,\theta_2)g(\theta_1,\theta_2)\,d\theta_1 d\theta_2 \quad \text{and the norm} \quad \|f\|_2^2 = \langle f,f\rangle.$$

If the coupling functions $q_1(\theta_1,\theta_2)$ and $q_2(\theta_1,\theta_2)$ defined in equation (3.2) are smooth, then we can decompose q_k into a Fourier series on the square $[-\pi,\pi]^2$ as

$$q_k(\theta_1,\theta_2) = \sum_{n,m=-\infty}^{\infty} c_{n,m}^{(k)}\, \mathrm{e}^{i2\pi(n\theta_1+m\theta_2)}, \quad k=1,2,$$

where $i^2=-1$, and $\{c_{n,m}^{(k)} \mid n,m\in\mathbb{Z}; k=1,2\}$ are the Fourier coefficients.

In applications, the coupling functions can be well-approximated by employing a finite number of Fourier terms. Each coupling function is regularly of the diffusive type (Hagos *et al.*, 2019)

$$\begin{aligned} q(\theta_1,\theta_2,t) &= c_1(t)\sin(\theta_1-\theta_2) + c_2(t)\cos(\theta_1-\theta_2) \\ &= (c_1(t)+c_2(t))\sin(\theta_1)\cos(\theta_2) + (c_2(t)-c_1(t))\cos(\theta_1)\sin(\theta_2), \end{aligned} \tag{3.5}$$

where $c_1(t)$ and $c_2(t)$ are assumed time-varying parameters. Using the second expression for q in equation (3.5) and by *Parseval's identity* (RUDIN, 1987), we obtain that

$$\|q\|_2 = \frac{1}{\sqrt{2}}\sqrt{c_1^2(t)+c_2^2(t)}. \tag{3.6}$$

The net coupling strength is analyzed quantitatively using the norm in equation (3.6). This quantity is denoted by $\varepsilon(t)$ in figure 6, which is shown to be a time-varying net coupling strength. However, the main goal of this chapter is the case where this net coupling strength remains constant in time, but of course with time-varying coupling functions.

3.4.2 Similarity index

Based on (Kralemann *et al.*, 2013; STANKOVSKI *et al.*, 2017), the similarity between the coupling functions $q_1(\theta_1,\theta_2)$ and $q_2(\theta_1,\theta_2)$ defined in equation (3.2) can be quantified by the correlation coefficient of their forms, irrespective of their amplitudes. The *similarity index* is then defined by the correlation coefficient ρ as

$$\rho(q_1,q_2) = \frac{\langle \tilde{q}_1,\tilde{q}_2\rangle}{\|\tilde{q}_1\|\|\tilde{q}_2\|}, \tag{3.7}$$

where $\langle\cdot\rangle$ denotes averaging over the two dimensional phase domain $0\le\theta_1,\theta_2\le 2\pi$, $\tilde{q}$ is a standard deviation defined by $\tilde{q}=q-\langle q\rangle$, and the norm $\|q\| = \langle q,q\rangle^{1/2}$.

3.4.3 Synchronization transitions

An adjustment of rhythmic behavior due to weak interaction is known as synchronization (PIKOVSKY; ROSENBLUM; KURTHS, 2001). The time variability of the coupling functions can cause transitions into or out of synchronization. The existence of such transitions results in the occurrence of epochs of synchrony – during which the phase difference remains nearly constant, as well as the occurrence of phase slips – when the phase difference changes rapidly. An example to illustrate these behaviors is shown in figures 7 and 8 plot the time series of the phase difference between two coupled oscillators, which occurs due to the time-variability of the form of the coupling function while keeping the net coupling strength constant.

3.5 Numerics

As introduced in section 3.3, we study a unidirectional coupling setting of the form provided in equation (3.4), but allowing the coupling function q_2 to be time-varying. More precisely, we study the effect of the time-variability of the coupling function while the net coupling strength is kept constant. We select this arrangement since it gives the clearest case where time-varying coupling functions can lead to synchrony and phase slips, whereas the net coupling strength remains steady.

We consider the *master-slave configuration* (Hagos *et al.*, 2019)

$$\begin{aligned} \frac{d\theta_1}{dt} &= \omega_1, \\ \frac{d\theta_2}{dt} &= \omega_2 + q(\theta_1, \theta_2, t), \end{aligned} \tag{3.8}$$

where ω_1, ω_2 are the natural frequencies of the oscillators, and the coupling function $q(\theta_1, \theta_2, t)$ is equal to the expression in equation (3.5). The presence of the coupling term $q(\theta_1, \theta_2, t)$ could cause the fundamental frequency of the driven oscillator (whose phase is represented by θ_2) to become different from its natural frequency ω_2, and to become time-dependent as $q := (\theta_1, \theta_2, t)$ varies over time.

From equation (3.6), the net coupling strength of the master-slave configuration q in equation (3.8) can be defined as

$$\|q\|_2 = \alpha(t) = \frac{1}{\sqrt{2}}\sqrt{c_1^2(t) + c_2^2(t)},$$

where $c_1(t)$ and $c_2(t)$ are the time-varying coupling parameters of the coupling functions (Stankovski, 2017). Throughout the thesis unless otherwise stated α denotes the net coupling strength.

Note that if the parameters $c_1(t)$ and $c_2(t)$ are constant in time, the two oscillators synchronize if the condition

$$\|q\|_2 = \alpha > \frac{1}{\sqrt{2}}|\omega_1 - \omega_2| \tag{3.9}$$

is satisfied (Stankovski, 2017). This conclusion is not necessarily true if the parameters $c_1(t)$ and $c_2(t)$ are time-dependent. This means that the oscillators in equation (3.8) might exhibit transitions between synchronization and phase slips even if the inequality in (3.9) is satisfied. This is one remark where a time-invariant net coupling strength does not give information about the dynamics of phase oscillators.

We analyze the phase synchronization of the two oscillators in the master-slave configuration (3.8) in terms of their phase difference

$$\psi(t) := \theta_1(t) - \theta_2(t).$$

Using equation (3.8) with q as in equation (3.5), the phase difference $\psi(t)$ obeys the equation

$$\frac{d\psi}{dt} = \Omega - c_1(t)\sin(\psi) - c_2(t)\cos(\psi), \tag{3.10}$$

where $\Omega = \omega_1 - \omega_2$ is the natural frequency difference (sometimes called the "frequency mismatch", or "detuning") between the oscillators, and the time-varying coupling parameters $c_1(t)$ and $c_2(t)$ are defined as (Hagos *et al.*, 2019)

$$c_1(t) = \sqrt{2}\alpha\cos(f(t)t) \quad \text{and} \quad c_2(t) = \sqrt{2}\alpha\sin(f(t)t), \tag{3.11}$$

where α is a constant parameter, and $f(t)$ is a T-periodic function defined by

$$f(t) = \begin{cases} \varepsilon & 0 \le t \le T_1 \\ \frac{\varepsilon(T/2-t)+k(t-T_1)}{T/2-T_1} & T_1 \le t \le T/2 \\ k & T/2 \le t \le T_2 \\ \frac{k(T-t)+\varepsilon(t-T_2)}{T-T_2} & T_2 \le t \le T \end{cases} \tag{3.12}$$

where ε, k, T_1, T_2 and T are constants with $k > \varepsilon \ge 0$, and with the values of ε, $\frac{T/2-T_1}{T}$ and $\frac{T-T_2}{T}$ being small. The expression for the function in equation (3.12) has been chosen to exhibit the existence of synchrony epochs and phase slips in the dynamics of the phase difference (Hagos *et al.*, 2019). From equation (3.11) and the formula for the net coupling strength, we obtain

$$\|q\|_2 = \alpha,$$

showing that the net coupling strength is constant for all time.

We carried out two experiments. In both experiments, the phase dynamics equation (3.10) via equation (3.13) is simulated with a sampling step of $\Delta t = 0.005$, where the length of the simulated time series is set to 6000 starting from an initial condition of $\psi(0) = 0$. In the first experiment, the parameter values are set to be: $\Omega = 1.05, \alpha = 1.8/\sqrt{2}, k = 100, \varepsilon = 0.01, T = 1500, T_1 = 740$, and $T_2 = 1490$. In the second experiment, we consider varying the parameter values of ε and k and set the tuple $(\varepsilon, k) \in \{(0.01, 100), (0.0005, 50), (0.0001, 10), (0, 5)\}$, and all the remaining parameters are fixed as in the first experiment. The time series of the phase

difference $\psi(t)$ (red) and the T-periodic function $f(t)$ (blue) of the first and second experiments are displayed in figures 7 and 8, respectively. The inset figure in the first experiment shows the transition to synchrony, even though the inequality (3.9) is satisfied as $\sqrt{2}\alpha > \Omega = \omega_1 - \omega_2$. For the sake of clarity, in both plots, the time axis was scaled by 100.

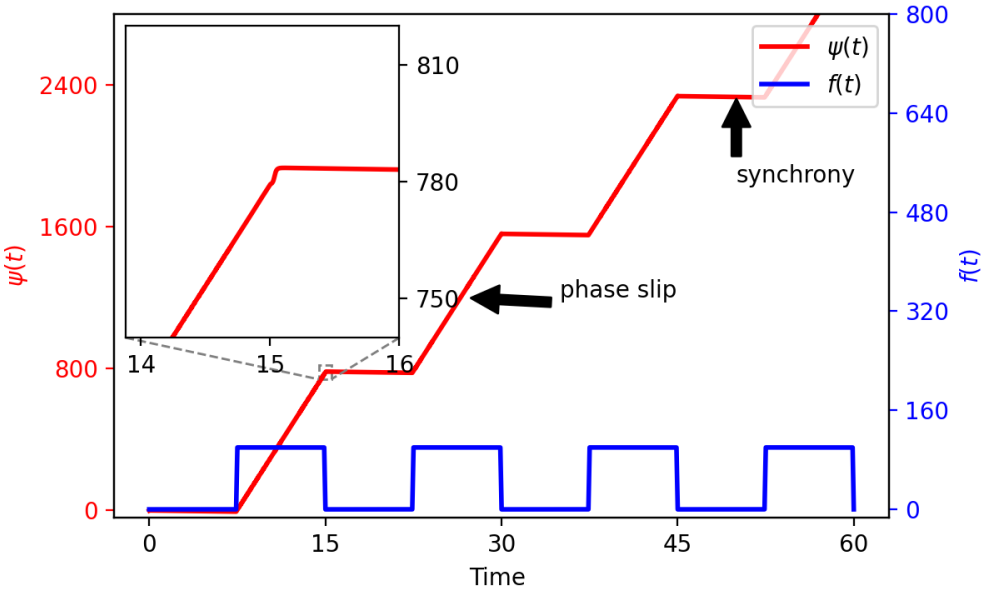

Figure 7 – Synchronization transitions in the model (equation (3.8)), due to a time-varying coupling function q in equation (3.5). Specifically, $c_1(t) = \sqrt{2}\alpha\cos(f(t)t)$ and $c_2(t) = \sqrt{2}\alpha\sin(f(t)t)$ as in equation (3.11), where $f(t)$ is the periodic function defined in equation (3.12). In red is shown the time series of the phase difference $\psi(t) = \theta_1(t) - \theta_2(t)$, and in blue is shown the periodic function $f(t)$. The parameters values were set to $\Omega = 1.05, \alpha = 1.8/\sqrt{2}, k = 100, \varepsilon = 0.01, T = 1500, T_1 = 740$, and $T_2 = 1490$. The inset shows the transition to synchronization. The plot of $\psi(t)$ is shown to alternate between synchrony states and phase slips, due to the time-variability of the coupling function q in equation (3.5) via the parameters $c_1(t)$ and $c_2(t)$ while the net coupling strength remains constant.

Source: Elaborated by the author.

In both experiments (figure 7 and figure 8(a)–(d)), we see transitions of synchronization, phenomena similar to that observed experimentally and numerically in (STEFANOVSKA; LUCHINSKY; MCCLINTOCK, 2001; Kenwright *et al.*, 2008; STANKOVSKI *et al.*, 2012; Lucas; Newman; Stefanovska, 2018): there is an alternation between synchronized epochs (plateaux) and phase slips (rapid increases) in the phase difference $\psi(t)$. Note that the T-periodic function $f(t)$ is small on the intervals $[nT, nT + T_1]$, whereas it is large on the intervals $[(n+\frac{1}{2})T, nT + T_2]$. In both cases, $n \in \mathbb{Z}^+ \cup \{0\}$. In both experiments, when the function $f(t)t$ is slowly varying we observe synchrony because the phase difference is bounded. On the other hand, if $f(t)t$ has rapid angular velocity, the dynamics of the phase oscillators in terms of the phase difference $\psi(t)$ has a sequence of rapid jumps (slips) separated by synchronous epochs and hence we observe phase slips.

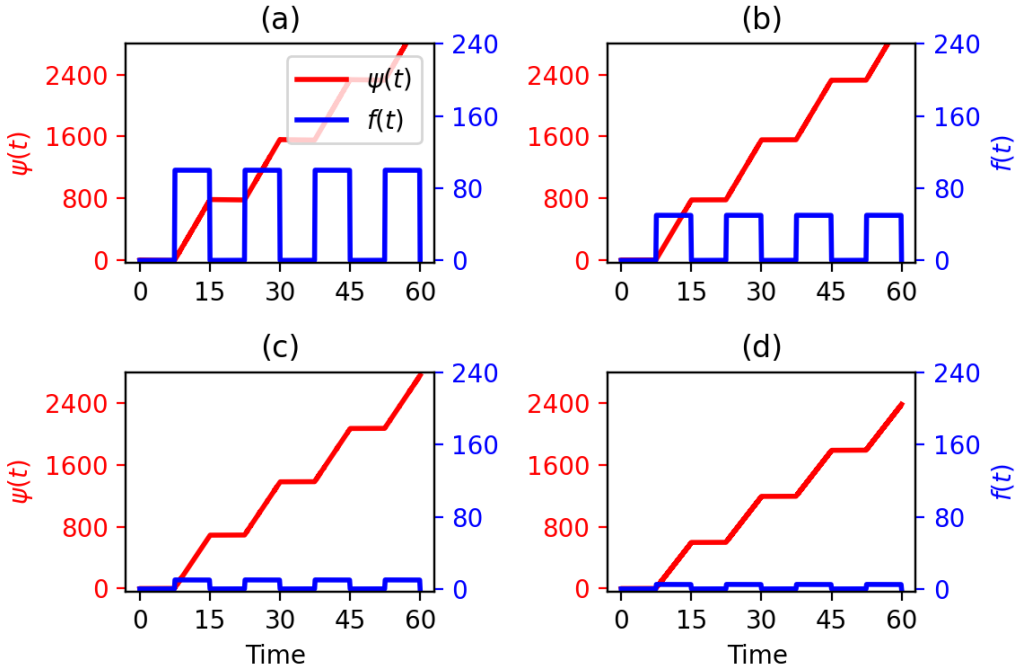

Figure 8 – Synchronisation transitions due to a time-varying coupling function, like in figure (7), with different values of the parameters ε and k for the function $f(t)$ in equation (3.12). In all four plots, in red is shown the time series of the phase difference $\psi(t)$, and in blue is shown the periodic function $f(t)$. The parameters ε and k were set to (a) $\varepsilon = 0.01, k = 100$, (b) $\varepsilon = 0.0005, k = 50$, (c) $\varepsilon = 0.0001, k = 10$, and (d) $\varepsilon = 0, k = 5$. In all four plots, the net coupling strength was set to $\alpha = 1.8/\sqrt{2}$. The plots of the phase difference $\psi(t)$ are shown to alternate between synchrony states and phase slips due to the time-variability of the coupling function while the net coupling strength remains constant.

Source: Elaborated by the author.

In summary, given that the net coupling strength between the oscillators was invariant, it is obvious that the proceeding variation between synchronization epochs and phase slips was just due to time variability within the coupling function. This shows that the net coupling strength does not in itself give us enough information to characterize the interactions of the oscillators. In section 3.6, we extend the results to a general choice of the coefficients $c_1(t)$ and $c_2(t)$.

3.6 Main theorems: generalization of numerical findings

We consider the coupling parameters $c_1(t)$ and $c_2(t)$ defined in equation (3.11) with an arbitrary function $\varphi(t)$ in place of $f(t)t$ to be of the form (Hagos *et al.*, 2019)

$$c_1(t) = \sqrt{2}\alpha\cos(\vartheta(t)) \quad \text{and} \quad c_2(t) = \sqrt{2}\alpha\sin(\vartheta(t)),$$

for some C^1 function $\vartheta\colon \mathbb{R} \to \mathbb{S}^1 \cong \mathbb{R}//2\pi\mathbb{Z}$, and α is the net coupling strength. Thus, the phase dynamics equation (3.10) can be written as

$$\frac{d\psi}{dt} = \Omega - \sqrt{2}\alpha\sin(\psi + \vartheta(t)). \tag{3.13}$$

This last equation is explicitly time-dependent and hence is a *nonautonomous* system. As shown in the numerics, we need to study the effect of both slow and fast variations of $\vartheta(t)$. Introducing a new variable $\phi(t) = \psi(t) + \vartheta(t)$, the dynamics of equation (3.13) is then equivalent to the dynamics of the equation

$$\frac{d\phi}{dt} = \Omega + \dot{\vartheta}(t) - \sqrt{2}\alpha \sin(\phi). \tag{3.14}$$

If $\sqrt{2}\alpha > |\Omega|$, let ϕ^* be the stable fixed point of the phase equation

$$\frac{d\phi}{dt} = \Omega - \sqrt{2}\alpha \sin(\phi). \tag{3.15}$$

We then state and prove the main theorems of this study on the effect of the time-varying coupling functions, while the net coupling strength is constant in time. In theorem 3.6.1 we consider the case where synchronization is exhibited for slowly varying $\vartheta(t)$. That means the function ϑ belongs to a set of the form:

$$M_\varepsilon := \{g : \mathbb{R} \to \mathbb{R} : \|g\|_{C^1} \leq \varepsilon\}.$$

Theorem 3.6.1. For all $\varepsilon > 0$ and $\psi(0) \in \mathbb{R}$, there exist $\varepsilon_0 = \varepsilon_0(\varepsilon, \psi(0)) > 0, T_0 = T_0(\varepsilon, \psi(0))$ such that for all $t > T_0$, if $\vartheta \in M_\varepsilon$, then the solution $\psi(t)$ of equation (3.13) with $\psi(0)$ satisfies $\psi(t) \in \mathscr{B}_{\varepsilon_0}(\phi^* - \vartheta(0))$ for all $t > T_0$.

Proof. The proof consists of two steps.

Step I. We want to show that the solution $\psi(t)$ enters a ball around the stable fixed point ϕ^* in finite time, that is, want to find an estimate

$$|\psi(t) - \phi^*| \leq \varepsilon T_0 \exp(\sqrt{2}\alpha T_0^2), \quad \forall t \in [0, T_0].$$

Consider the phase dynamics

$$\frac{d\eta}{dt} = \Omega - \sqrt{2}\alpha \sin(\eta), \tag{3.16}$$

which has a stable fixed point η^* if $\sqrt{2}|\alpha| > |\Omega|$ and $\Omega - \sqrt{2}\alpha \sin(\eta) = 0$. Consequently,

$$\eta^*(t) = \arcsin\left(\frac{\Omega}{\sqrt{2}\alpha}\right)$$

is a fixed point of the phase dynamics equation (3.16). Comparing equations (3.14) and (3.16), we obtain

$$\frac{d\phi}{dt} - \frac{d\eta}{dt} = \dot{\vartheta}(t) - \sqrt{2}\alpha(\sin(\phi) - \sin(\eta)). \tag{3.17}$$

Assume that there exists a $\varepsilon_1 > 0$ such that

$$|\phi(t) - \eta(t)| < \varepsilon_1, \tag{3.18}$$

at the beginning of the interval $t \in [0, T_0]$. Define a new function $u(t) = \phi(t) - \eta(t)$. Then it follows that $\frac{d\phi}{dt} - \frac{d\eta}{dt} = \frac{du}{dt}$.

By the Mean Value Theorem, there exists ζ between ϕ and η such that equation (3.17) is reduced to the equation

$$\frac{du}{dt} = \dot{\vartheta}(t) - \sqrt{2}\alpha\cos(\zeta)u. \tag{3.19}$$

Integrating both sides of equation (3.19) over the interval $[0,t]$, we get

$$u(t) = \int_0^t \dot{\vartheta}(s)\,ds - \sqrt{2}\alpha\int_0^t \cos(\zeta(s))u(s)\,ds \tag{3.20}$$

which implies that

$$|u(t)| \leq \int_0^t |\dot{\vartheta}(s)|\,ds + \sqrt{2}\alpha\int_0^t |\cos(\zeta(s))||u(s)|\,ds \leq \int_0^t |\dot{\vartheta}(s)|\,ds + \sqrt{2}\alpha\int_0^t |u(s)|\,ds. \tag{3.21}$$

Let $v(t) = |u(t)|$. Then Eq. (3.21) implies

$$v(t) \leq \varepsilon T_0 + \sqrt{2}\alpha\int_0^t v(s)\,ds. \tag{3.22}$$

By Gronwall's inequality on (3.22), we obtain that

$$\begin{aligned} v(t) &\leq \varepsilon T_1 \exp\left(\int_0^t \sqrt{2}\alpha\,ds\right), \quad \forall t \in [0, T_0] \\ &\leq \varepsilon T_1 \exp\left(\sqrt{2}\alpha T_0\right), \quad \forall t \in [0, T_0]. \end{aligned}$$

Hence

$$|\phi(t) - \eta(t)| \leq \varepsilon T_0 \exp\left(\sqrt{2}\alpha T_0\right), \quad \forall t \in [0, T_0].$$

Now we require

$$\varepsilon T_0 \exp\left(\sqrt{2}\alpha T_0\right) \leq \varepsilon_1.$$

Solving for $T_0 = T_0(\varepsilon, \alpha, \varepsilon_1)$ we obtain the required finite time for which $\phi(t) - \eta(t) = \mathscr{O}(\varepsilon)$, for all $t \in [0, T_0]$.

Step II. Motivated by the result of the generalization of (PEREIRA *et al.*, 2014, Lemma 8), we want to show that the solution $\psi(t)$ stays in the ball for all time t, that is, we want the estimate

$$|\psi(t) - \phi^*| \leq \varepsilon K, \quad \forall t \geq 0.$$

Consider a ball $\mathscr{B}_{\varepsilon_2}(\phi^*)$ of radius ε_2 around the equilibrium solution ϕ^*. Consider the phase dynamics equation (3.14)

$$\frac{d\phi}{dt} = \Omega - \sqrt{2}\alpha\sin(\phi) + \dot{\vartheta}(t) =: F(\phi, t) \tag{3.23}$$

Linearizing equation (3.23) about the fixed point ϕ^*, we obtain

$$\begin{aligned}\frac{d\phi}{dt} &= F(\phi+\phi^*,t)\\ &= F(\phi^*,t)+D_\phi F(\phi^*,t)(\phi-\phi^*)+R(\phi,t)\\ &\approx D_\phi F(\phi^*,t)(\phi-\phi^*)+h(t).\end{aligned}$$

Here $h(t) := F(\phi^*,t)$ and the remainder term $R(\phi,t)$ consists of higher order nonlinear terms. But $D_\phi F(\phi^*,t) = -\sqrt{2}\alpha\cos(\phi^*)$, and setting $\mu = \phi - \phi^*$, we get

$$\frac{d\mu}{dt} = -\lambda\mu + h(t), \tag{3.24}$$

where $\lambda = \sqrt{2}\alpha\cos(\phi^*)$.

By the Variation of Constants formula,

$$\mu(t) = \mathrm{e}^{-\lambda t}\mu_0 + \int_0^t \mathrm{e}^{-\lambda(t-s)}h(s)\,ds.$$

It turns out that

$$\begin{aligned}|\mu(t)| &\le |\mathrm{e}^{-\lambda t}||\mu_0| + \int_0^t |\mathrm{e}^{-\lambda(t-s)}||h(s)|\,ds\\ &= \mathrm{e}^{-\lambda t}|\mu_0| + \int_0^t \mathrm{e}^{-\lambda(t-s)}|h(s)|\,ds.\end{aligned}$$

Multiplying both sides of the last inequality by $\mathrm{e}^{-\lambda t}$, we obtain

$$\mathrm{e}^{\lambda t}|\mu(t)| \le |\mu_0| + \int_0^t \mathrm{e}^{\lambda s}|h(s)|\,ds \le |\mu_0| + \int_0^t \mathrm{e}^{\lambda s}|\mu(s)||h(s)|\,ds.$$

Since $h(t) = F(\phi^*,t) = \Omega - \sqrt{2}\alpha\sin(\phi^*) + \dot{\vartheta}(t)$, it follows that there exists a number $M > 0$ such that $|h(t)| \le M$ for all $t \in [0,T_0]$. Let us choose $M = \lambda/2$. Then the last inequality yields

$$\mathrm{e}^{\lambda t}|\mu(t)| \le |\mu_0| + \frac{\lambda}{2}\int_0^t \mathrm{e}^{\lambda s}|\mu(s)|\,ds.$$

Applying Gronwall's inequality to the last inequality, we obtain

$$\mathrm{e}^{\lambda t}|\mu(t)| \le |\mu_0|\mathrm{e}^{\frac{\lambda}{2}t},$$

it follows that

$$|\mu(t)| \le |\mu_0|\mathrm{e}^{-\frac{\lambda}{2}t}.$$

Hence $|\mu(t)| \to 0$ as $t \to \infty$ for all $t \ge 0$. It follows that

$$\phi(t) \in \mathscr{B}_{\varepsilon_0}(\eta^*),$$

for all time t. Since $\psi(t) = \phi(t) - \vartheta(t)$, it follows that $\psi^*(t) = \phi^*(t) - \vartheta(t)$. Hence there exists a finite time $T_0 > 0$ such that the solution $\psi(t)$ enters the ball of radius ε_0.

□

In a similar setup to theorem 3.6.1, a proof of the existence of synchronous states for the slowly varying function ϑ is also provided in (Hagos *et al.*, 2019, Theorem 6.1) followed by (Hagos *et al.*, 2019, Corollary 6.2).

Now in theorem 3.6.2 we consider the unbounded phase slips exhibited for fast-winding ϑ. The following theorem may be regarded as a kind of nonautonomous averaging principle. For a detailed exposition of averaging principles, it is presented in theorem 2.3.5, which was adapted from (SANDERS; VERHULST, 1985).

Theorem 3.6.2. (Hagos *et al.*, 2019) For all $\varepsilon_1, \varepsilon_2 > 0$ there exist $\beta_1, \beta_2 > 0$ such that if ϑ is twice differentiable on an interval $[0,t]$ with $\dot{\vartheta}(s) > \max(\beta_1, \beta_2\sqrt{|\ddot{\vartheta}(s)|})$ for all $s \in [0,t]$, then any solution ψ of equation (3.13) satisfies

$$|\psi(s) - \psi(0) - \Omega s| \leq \varepsilon_1 + \varepsilon_2 s$$

for all $s \in [0,t]$.

Proof. Let $F(\phi) := \Omega - \sqrt{2}\alpha\sin(\phi)$. First take arbitrary $\beta_1 > 0$ and $\beta_2 > \sqrt{2\pi}$, and suppose that $\dot{\vartheta}(s) > \max(\beta_1, \beta_2\sqrt{|\ddot{\vartheta}(s)|})$ for all $s \in [0,t]$. Define recursively a sequence $0 = t_0 < t_1 < \ldots < t_N < t$ by $t_{i+1} = t_i + \frac{2\pi}{\dot{\vartheta}(t_i)}$, with N being the largest possible such that $t_N < t$. It follows in particular that $t - t_N \leq \frac{2\pi}{\dot{\vartheta}(t_N)}$. For each $i < N$, we have that

$$\begin{aligned}\int_{t_i}^{t_{i+1}} F\left(\psi(t_i) + \vartheta(t_i) + \frac{2\pi(s-t_i)}{t_{i+1}-t_i}\right) ds &= \int_{t_i}^{t_{i+1}} \left(\Omega - \sqrt{2}\alpha\sin\left(\phi(t_i) + \frac{2\pi(s-t_i)}{t_{i+1}-t_i}\right)\right) ds \\ &= \Omega(t_{i+1}-t_i) - \frac{2\sqrt{2}\pi\alpha}{t_{i+1}-t_i}\int_{\phi(t_i)}^{\phi(t_i)+2\pi} \sin u\, du \\ &= \Omega(t_{i+1}-t_i),\end{aligned}$$

where we have used $\phi(t_i) := \psi(t_i) + \vartheta(t_i)$. Also, we have that

$$\begin{aligned}\int_{t_i}^{t_{i+1}} F(\psi(s) - \vartheta(s))\, ds = \int_{t_i}^{t_{i+1}} \left(\Omega - \sqrt{2}\alpha\sin(\psi(s) + \vartheta(s))\right) ds &= \int_{t_i}^{t_{i+1}} \dot{\psi}(s)\, ds \\ &= \psi(t_{i+1}) - \psi(t_i).\end{aligned}$$

It follows that

$$|\psi(t_{i+1}) - \psi(t_i) - \Omega(t_{i+1}-t_i)| \leq \int_{t_i}^{t_{i+1}} \left|F(\psi(s) + \vartheta(s)) - F\left(\psi(t_i) + \vartheta(t_i) + \frac{2\pi(s-t_i)}{t_{i+1}-t_i}\right)\right| ds. \tag{3.25}$$

Now we fix any $s \in (t_i, t_{i+1})$. Then we have that $s - t_i < \frac{2\pi}{\beta_1}$ and hence

$$|\psi(s) - \psi(t_i)| < \frac{2\pi(|\Omega| + \sqrt{2}\alpha)}{\beta_1}. \tag{3.26}$$

Also, by Taylor's theorem, we have that

$$\left|\vartheta(s)-\left(\vartheta(t_i)+\frac{2\pi(s-t_i)}{t_{i+1}-t_i}\right)\right| = \frac{1}{2}|\ddot{\vartheta}(\xi_1(s))|(s-t_i)^2 \leq \frac{2\pi^2|\ddot{\vartheta}(\xi_1(s))|}{\dot{\vartheta}(t_i)^2}$$

for some $\xi_1(s) \in (t_i, s)$. But by the mean value theorem, we have that for some $\xi_2(s) \in (t_i, \xi_1(s))$,

$$\frac{1}{\dot{\vartheta}(\xi_1(s))} = \frac{1}{\dot{\vartheta}(t_i)} - \frac{(\xi_1(s)-t_i)\ddot{\vartheta}(\xi_2(s))}{\dot{\vartheta}(\xi_2(s))^2} > \frac{1}{\dot{\vartheta}(t_i)}\left(1-\frac{2\pi}{\beta_2^2}\right),$$

and so

$$\left|\vartheta(s)-\left(\vartheta(t_i)+\frac{2\pi(s-t_i)}{t_{i+1}-t_i}\right)\right| \leq \frac{2\pi^2|\ddot{\vartheta}(\xi_1(s))|}{\dot{\vartheta}(\xi_1(s))^2}\left(1-\frac{2\pi}{\beta_2^2}\right)^{-2} \leq \frac{2\pi^2}{\beta_2^2}\left(1-\frac{2\pi}{\beta_2^2}\right)^{-2}. \quad (3.27)$$

Combining equations (3.25), (3.26) and (3.27), we have that

$$|\psi(t_{i+1})-\psi(t_i)-\Omega(t_{i+1}-t_i)| \leq \underbrace{\sqrt{2}\alpha\left(\frac{2\pi(|\Omega|+\sqrt{2}\alpha)}{\beta_1}+\frac{2\pi^2}{\beta_2^2}\left(1-\frac{2\pi}{\beta_2^2}\right)^{-2}\right)}_{=:\kappa(\beta_1,\beta_2)}(t_{i+1}-t_i).$$

Hence, for each $i \leq N$,

$$|\psi(t_i)-\psi(0)-\Omega t_i| \leq \kappa(\beta_1,\beta_2)t_i. \quad (3.28)$$

Now for any $s \in [0,t]$, taking the largest i with $t_i \leq s$, we have

$$|\dot{\psi}(\zeta)-\Omega| \leq \sqrt{2}\alpha \quad \forall \zeta \in [t_i, s]$$

and so

$$|\psi(s)-\psi(t_i)-\Omega(s-t_i)| \leq \sqrt{2}\alpha(s-t_i) < \underbrace{\frac{2\sqrt{2}\pi\alpha}{\beta_1}}_{=:\kappa_0(\beta_1)}. \quad (3.29)$$

Combining equations (3.28) and (3.29) gives that

$$|\psi(s)-\psi(0)-\Omega s| < \kappa_0(\beta_1)+\kappa(\beta_1,\beta_2)s$$

for all $s \in [0,t]$. So now, given any $\varepsilon_0, \varepsilon > 0$ choose β_1, β_2 sufficiently large that $\kappa_0(\beta_1) \leq \varepsilon_0$ and $\kappa(\beta_1,\beta_2) \leq \varepsilon$. □

Combining theorems 3.6.1 and 3.6.2, we see that the two oscillators exhibit transitions of synchronization. In this case, the function $\vartheta(t)$ has alternating epochs of slow variation and rapid oscillation, while the net coupling strength is kept constant but with time-varying coupling functions.

3.7 Concluding remarks

A model of two coupled oscillators with time-evolving coupling functions has been shown to exhibit transitions between synchronization states and phase slips while the net coupling strength is kept constant.

In general, time-variability can enter a system in different ways in such a way that the forms of the time-dependent driving oscillator lead to synchronization transitions. For example, it can enter a system through "modulation" of the natural frequency of the driving oscillator (Jensen, 2002; SUPRUNENKO; CLEMSON; STEFANOVSKA, 2013; Lucas; Newman; Stefanovska, 2018). As shown in (Jensen, 2002; Lucas; Newman; Stefanovska, 2018), for fixed-frequency driving, we have synchronization either all of the time or none of the time, but when the driving frequency is allowed to vary then the system can exhibit synchronization transitions.

In (Lucas; Newman; Stefanovska, 2018), they studied the theoretical and numerical considerations for a unidirectionally coupled pair of phase oscillators with time-variability of the driving frequency and shown to exhibit synchronization transitions. They extended these results to networks of phase oscillators (LUCAS; FANELLI; STEFANOVSKA, 2019). The considerations of our study can also be generalized to networks such as those considered in (PEREIRA *et al.*, 2013): network structure can also have an impact on the dynamics exhibited, such as synchronization (Pade; Poignard; Pereira, 2017; MAIA; MACAU; PEREIRA, 2016).

CHAPTER

4

RECONSTRUCTION OF NETWORK PHASE DYNAMICS FROM DATA

Complex systems such as ecological communities and neuron networks are essential to our everyday lives. Many such systems can be modeled using networked dynamical systems using systems of differential equations. Nowadays it is possible to collect and process enormous amounts of data from the units of such systems. Reconstructing models of dynamical systems from data is a crucial problem that has attracted a lot of attention.

This chapter deals with the reconstruction of network dynamics of oscillatory systems from time series data based on Bayesian statistics and sparse recovery methods. Moreover, we aim to show a case where although the dynamics in the network are purely pairwise, due to the nonlinearity of the coupling functions, we reconstruct higher-order interaction terms, given time-series data of networks of weakly interacting oscillators.

4.1 Reconstruction problem statement

We assume that we have access to an N- dimensional time series of observed oscillatory data

$$\mathscr{Y} := \{\boldsymbol{y}_m := \boldsymbol{y}(t_m) \mid t_m = m\Delta t, m = 1, \ldots, M\},$$

produced by M measurements performed at every sampling time interval Δt. We also assume that the data describes a system of N-dimensional stochastic process $\boldsymbol{\theta}(t) = (\theta_1(t), \ldots, \theta_N(t))^T$. Assume that the underlying dynamics of the system is described by a set of N-dimensional stochastic differential equations (SDEs) of the form:

$$\frac{d}{dt}\boldsymbol{\theta}(t) = \boldsymbol{F}(\boldsymbol{\theta}(t); \boldsymbol{c}) + \sqrt{\boldsymbol{D}}\boldsymbol{\xi}(t), \tag{4.1}$$

where $\boldsymbol{F} = (F_1, \ldots, F_N)^T$ denotes the deterministic vector field of the system, $\boldsymbol{c}$ is assumed to be a set of unknown model parameters that are embedded in $\boldsymbol{F}$. Without loss of generality, let $\boldsymbol{c} \in \mathbb{R}^L$.

The vector $\boldsymbol{\xi}(t) = (\xi_1(t), \ldots, \xi_N(t))^T$ denotes an N-dimensional dynamical noise induced into the system to better mimic real situations, and the constant matrix $\boldsymbol{D} \in \mathbb{R}^{N\times N}$ represents the noise intensity also known as the diffusion matrix. We assumed that the system is driven by white Gaussian noise satisfying

$$\begin{aligned}\langle \xi_i(t) \rangle &= 0,\\ \langle \xi_i(t)\xi_j(t') \rangle &= \delta_{ij}\delta(t-t') \quad (i,j = 1,\ldots,N),\end{aligned}$$

where $\langle\cdot\rangle$ the expected value of a quantity. The phase model (4.1) may describe a network of N coupled phase oscillators, with

$$\frac{d}{dt}\theta_i(t) = \Omega_i + \varepsilon \sum_{j=1}^{N} A_{ij} q_i(\theta_i, \theta_j) + \sqrt{D}\xi_i(t), \quad i = 1,\ldots,N, \tag{4.2}$$

where Ω_i is the natural frequency of node i, q_i is the pairwise coupling function of the ith oscillator with node j, and ε is the coupling strength. The adjacency matrix A defines who is connected to whom: $A_{i,j} = 1$ if nodes i and j are connected and $A_{i,j} = 0$ otherwise. The coupling function q may take the form $q(\theta_i, \theta_j) = \sin(\theta_j - \theta_i - \beta)$ where the parameter β denotes a phase shift. Phase equations with this form of coupling q are known as the Kuramoto-Sakaguchi (SAKAGUCHI; KURAMOTO, 1986; OMEL'CHENKO; WOLFRUM, 2012) and are widely applied across scientific disciplines (STANKOVSKI *et al.*, 2017). In real-world systems, the coupling may be heterogeneous (MORGAN; SOLTESZ, 2008). For simplicity, throughout this discussion, we considered a uniform noise strength D.

The data $\mathscr{Y}$ may be altered by measurement noise due to, for example, inaccuracies in measurements. In this thesis, however, we assume that there is no measurement noise imposed in the data. That is, we assume that we measure each component $\theta_i(t)$ of the N-dimensional process $\boldsymbol{\theta}(t) = (\theta_1(t), \ldots, \theta_N(t))^T$ and obtain a multivariate time series data

$$\Upsilon := \{\boldsymbol{\theta}_m := \boldsymbol{\theta}(t_m) \mid t_m = m\Delta t, m = 1,\ldots,M\} \tag{4.3}$$

such that the measurements are performed over M distinct time points t_m with the property $t_1 < t_2 < \cdots < t_M$, where Δt is the sampling time interval assumed to be uniform. If $\Delta t \ll 1$ we can compute the velocities of $\boldsymbol{\theta}$ in equation (4.1) numerically using e.g. the forward finite difference formula

$$\dot{\boldsymbol{\theta}}(t_m) \approx \frac{\boldsymbol{\theta}_{m+1} - \boldsymbol{\theta}_m}{\Delta t}$$

and if $M \gg 1$ we have sufficiently large samples to perform relevant data analysis e.g. in predicting future changes in the dynamics and critical transitions. Note that these conditions are not always available.

In equation (4.1) all the components of $\boldsymbol{F}$ are unknown, $\boldsymbol{c}$ is unknown and the noise matrix $\boldsymbol{D}$ is also unknown. Only the data (equation (4.3)) is available for analysis. The parameter

vector $\boldsymbol{c}$ is assumed to parameterize the vector field $\boldsymbol{F}$ using appropriate known functions. Hence, we can assume that the unknown parameters constitute the set

$$\mathscr{M} := \{\boldsymbol{c}, \boldsymbol{D}\}.$$

The reconstruction problem can be recast as follows:

> Given the available time series data Υ, which exhibit a periodic behavior and interact weakly, we aim to obtain the most probable parameters $\tilde{\mathscr{M}}$ that accurately describe the data.

Remark 4.1.1. In most practical problems, we do not even have access to the time series data in phases. In this case, we first need to extract the corresponding phases $\vartheta_i(t)$ from the given multivariate time-series data $\mathscr{Y}$ via e.g. *Hilbert transform* (ROSENBLUM; PIKOVSKY; KURTHS, 1996) or angle variable. Note that the phase $\vartheta_j(t)$ is not necessarily equal to $\theta_j(t)$, which increases uniformly in time (in the absence of coupling or noise), but all relevant information can be obtained from it. Hence we try to reconstruct the model of the data $\vartheta_j(t)$.

4.2 Review of reconstruction methods

In the literature there are a number of appropriate methods in reconstructing the underlying model, given a time series data of weakly interacting oscillators. In this thesis, we review some reconstruction techniques. In particular, we outline the Bayesian inference and sparse recovery methods in reconstructing networks from the available data.

4.2.1 Bayesian inference method

In Bayesian inference, all unknown parameters in $\mathscr{M}$ are treated as stochastic variables with certain probability distributions (BISHOP, 2006). In this section, we present the Bayesian inference method for stochastic differential equations that was originally proposed in (Luchinsky *et al.*, 2005; STANKOVSKI *et al.*, 2014) in reconstructing the phase dynamics (equation (4.1)) from the available data. This approach requires expert knowledge of the unknown parameters $\mathscr{M}$ before observing the data Υ. Based on Bayes' probability theory, the posterior distribution of the parameters $\mathscr{M}$ is updated via Bayes' theorem (BAYES, 1763):

$$p(\mathscr{M}|\Upsilon) = \frac{p(\Upsilon|\mathscr{M})p(\mathscr{M})}{\int p(\Upsilon|\mathscr{M})p(\mathscr{M})\, d\mathscr{M}}, \tag{4.4}$$

where $p(\Upsilon|\mathscr{M})$ is the likelihood function. The probabilities $p(\mathscr{M})$ and $p(\mathscr{M}|\Upsilon)$ are known as the *prior* and *posterior* distributions, respectively, of the parameters $\mathscr{M}$. Hence if we know the likelihood $p(\Upsilon|\mathscr{M})$ and the prior distribution $p(\mathscr{M})$, then using Bayes' theorem we obtain the updates of the parameters and hence reconstruct the model. The likelihood function describes

the process giving rise to the data Υ in terms of $\mathscr{M}$. In particular, the data Υ is kept fixed while reading the underlying information concerning the parameter values. We usually denote the likelihood function by

$$\ell(\mathscr{M},\Upsilon) := p(\Upsilon|\mathscr{M}).$$

Note that the integral $\int p(\Upsilon|\mathscr{M})p(\mathscr{M})\,d\mathscr{M}$ is not a function of $\mathscr{M}$. Thus, we can rewrite equation (4.4) in the simpler form

$$p(\mathscr{M}|\Upsilon) \propto \ell(\mathscr{M},\Upsilon)p(\mathscr{M}), \tag{4.5}$$

that is, "*the posterior is proportional to the prior times the likelihood*."

Based on the Bayesian probability theory (BROMILEY, 2013), we note that the following statement holds.

Theorem 4.2.1. If the prior $p(\mathscr{M})$ and the likelihood $\ell(\mathscr{M},\Upsilon)$ are Gaussian, then the posterior $p(\mathscr{M}|\Upsilon)$ is also Gaussian.

This shows that the problem of computing the posterior distribution $p(\mathscr{M}|\Upsilon)$ reduces to finding its two moments: the conditional mean and its covariance.

In formulating the Bayesian inference method, we assume that the prior distribution is known *a priori*. The task is therefore to determine the likelihood function and then the optimization of the posterior distribution with respect to $\mathscr{M}$. To this end, we formulate the likelihood function $\ell(\mathscr{M},\Upsilon)$ analytically. Under regularity conditions on the *drift* (the deterministic part) and *diffusion* (the stochastic part) coefficients of equation (4.1) (ØKSENDAL, 1992), assume that the SDE (equation (4.1)) has a unique solution $\boldsymbol{\theta}(t)$. However, an analytic solution $\boldsymbol{\theta}(t)$ is generally intractable. For this reason, the system is solved numerically, and hence the expression of the likelihood function $\ell(\mathscr{M},\Upsilon)$ will be constructed from it.

We first solve equation (4.1) numerically. To do this, we rewrite in the so-called Ito form as

$$d\boldsymbol{\theta}(t) = \boldsymbol{F}(\boldsymbol{\theta}(t);\boldsymbol{c})dt + \sqrt{\boldsymbol{D}}d\boldsymbol{W}(t) \tag{4.6}$$

in which $d\boldsymbol{W}(t) = \boldsymbol{\xi}(t)dt$ is the *Wiener Process* (ØKSENDAL, 1992). Let $\boldsymbol{\theta}_0 = \boldsymbol{\theta}(0)$ be an initial condition and $[0,T]$ the interval over which equation (4.1) must be integrated. The numerical solution for a trajectory of equation (4.1) by the Euler-midpoint approximation is then approximated by the Markov chain $\boldsymbol{\theta}_m$, in which the index m denotes the time dependence, defined recursively as

$$\boldsymbol{\theta}_{m+1} = \boldsymbol{\theta}_m + \Delta t\boldsymbol{F}(\boldsymbol{\theta}^*_m;\boldsymbol{c}) + \sqrt{\boldsymbol{D}}\Delta\boldsymbol{W}_m, \tag{4.7}$$

for $m = 0, 1, \ldots, M$, with $\Delta t = \frac{T}{M}$, $\boldsymbol{\theta}_m^* = \frac{\boldsymbol{\theta}_{m+1}+\boldsymbol{\theta}_m}{2}$ and the $\Delta \boldsymbol{W}_m$ are independent and identically distributed normal random variables with mean 0 and variance Δt . The explicit form of the term $\Delta \boldsymbol{W}_m$ is given by

$$\Delta \boldsymbol{W}_m = \sqrt{\Delta t}\boldsymbol{\zeta}_m \tag{4.8}$$

where $\boldsymbol{\zeta}_m$ is a random variable, distributed according to a Gaussian distribution, satisfying

$$\langle \zeta_i(t_m) \rangle = 0 \quad \text{and} \quad \langle \zeta_i(t_m)\zeta_j(t_n) \rangle = \delta_{ij}\delta_{mn}$$

for different times. Notice that in the above approximation $\Delta t \ll 1$.

Based on the approach proposed in (LUCHINSKY *et al.*, 2008) and the references therein, we then present the likelihood function $\ell(\mathscr{M}, \Upsilon)$ in the form of a "*path-integral*" over the random trajectories $\{\boldsymbol{\theta}_m\}$ of the system (Graham, 1977). Following the work of (Graham, 1977), we can write the likelihood function in the form of a path-integral over $\boldsymbol{\theta}(t)$ as

$$\ell(\mathscr{M}, \Upsilon) = p(\{\boldsymbol{\theta}_m\} \mid \mathscr{M}) = \pi(\boldsymbol{\theta}_0 \mid \mathscr{M}) \prod_{m=0}^{M} p(\boldsymbol{\theta}_m \mid \mathscr{M}), \tag{4.9}$$

where $\pi(\boldsymbol{\theta}_0 \mid \mathscr{M})$ represents the stationary probability distribution of equation (4.1), for simplicity, $\pi(\boldsymbol{\theta}_0 \mid \mathscr{M}) = 1$. The probability $p(\boldsymbol{\theta} \mid \mathscr{M})$ is the "probability density functional" to have given dynamical trajectory $\boldsymbol{\theta}(t)$ conditioned on fixed values of the model parameters $\mathscr{M}$ (FULLANA; ROSSI, 2002). Hence, it remains to compute $p(\boldsymbol{\theta}_m \mid \mathscr{M})$. The form of the conditional probability $p(\boldsymbol{\theta}_m \mid \mathscr{M})$ can be determined using known distributions for the independent source of white Gaussian noise $\{\zeta_i(t_m)\}$ (DYKMAN, 1990) in equation (4.7). From equation (4.7), one can see that the conditional probability $p(\boldsymbol{\theta}_{m+1}|\boldsymbol{\theta}_m; \mathscr{M})$ of fluctuational path $\{\boldsymbol{\theta}_m\}$ is related to the probability $p(\boldsymbol{\zeta}_m)$ corresponding to random realization $\{\boldsymbol{\zeta}_m\}$ because

$$\boldsymbol{\zeta}_m = \frac{1}{\sqrt{\Delta t}}[\sqrt{\boldsymbol{D}}]^{-1}\left(\boldsymbol{\theta}_{m+1} - \boldsymbol{\theta}_m - \Delta t \boldsymbol{F}(\boldsymbol{\theta}_m^*; \boldsymbol{c})\right).$$

Notice that the probability of a single realization $\boldsymbol{\zeta}_m$ is given by

$$\begin{aligned} p(\boldsymbol{\zeta}_m) &= \frac{d\boldsymbol{\zeta}_m}{\sqrt{(2\pi)^N}} \exp\left(-\frac{\boldsymbol{\zeta}_m^T \boldsymbol{\zeta}_m}{2}\right) \\ &= \frac{d\boldsymbol{\zeta}_m}{\sqrt{(2\pi)^N}} \exp\left(-\frac{1}{2\Delta t}\left(\boldsymbol{\theta}_{m+1} - \boldsymbol{\theta}_m - \Delta t \boldsymbol{F}(\boldsymbol{\theta}_m^*; \boldsymbol{c})\right)^T \boldsymbol{D}^{-1}\left(\boldsymbol{\theta}_{m+1} - \boldsymbol{\theta}_m - \Delta t \boldsymbol{F}(\boldsymbol{\theta}_m^*; \boldsymbol{c})\right)\right). \end{aligned} \tag{4.10}$$

By assumption, $\boldsymbol{\zeta}_m$ are independent, white Gaussian noise at each time step, and hence the joint probability of the realization $\{\boldsymbol{\zeta}_m\}$ as a product of the probabilities of each single realization $\boldsymbol{\zeta}_m$ is given by

$$p(\{\boldsymbol{\zeta}_m\}) = \prod_{m=0}^{M-1} p(\boldsymbol{\zeta}_m). \tag{4.11}$$

We note that the stochastic trajectory $\{\boldsymbol{\theta}_m\}$ exhibits the *Markov property*, i.e., the probability of having a particular value of the position at time $t = t_{m+1}$ depends only on the state location at time $t = t_m$ and not on the way it got to this location.

Thanks to the change of variables from $\boldsymbol{\zeta}_m$ to $\boldsymbol{\theta}_{m+1}(\boldsymbol{\zeta}_m)$ and the Markov property of $\boldsymbol{\theta}_m$ together with equations (4.7) and (4.11), we obtain the probability of realization of the whole process $\{\boldsymbol{\theta}_m\}$:

$$p(\{\boldsymbol{\theta}_{m+1}\}) = \prod_{m=0}^{M-1} \frac{d\boldsymbol{\theta}_{m+1}\det(\boldsymbol{J}(\boldsymbol{\theta}_m))}{\sqrt{(2\pi\Delta t)^N|\boldsymbol{D}|}} \times \exp\left(-\frac{1}{2\Delta t}[\boldsymbol{\theta}_{m+1} - \boldsymbol{\theta}_m - \Delta t\boldsymbol{F}(\boldsymbol{\theta}_m^*;\boldsymbol{c})]^T\boldsymbol{D}^{-1}[\boldsymbol{\theta}_{m+1} - \boldsymbol{\theta}_m - \Delta t\boldsymbol{F}(\boldsymbol{\theta}_m^*;\boldsymbol{c})]\right), \quad (4.12)$$

where $\boldsymbol{J}(\boldsymbol{\theta}_m)$ denotes the Jacobian of the transformation from noise variable $\boldsymbol{\zeta}_m$ to dynamical variable $\boldsymbol{\theta}_{m+1}$, defined as

$$\boldsymbol{J}(\boldsymbol{\theta}_m) = \frac{\partial(\zeta_{m,1},\ldots,\zeta_{m,N})}{\partial(\theta_{m+1,1},\ldots,\theta_{m+1,N})} \quad (4.13)$$

with entries of the Jacobian, J_{ij}, given by

$$J_{ij} := \delta_{ij} - \frac{\Delta t}{2}\frac{\partial(\boldsymbol{F}(\boldsymbol{\theta}_m^*;\boldsymbol{c}))_i}{\partial(\boldsymbol{\theta}_m^*)_j}.$$

Theorem 4.2.2. For a sufficiently small Δt, the determinant of the Jacobian of transformation $\boldsymbol{J}(\boldsymbol{\theta}_m)$ can be approximated as:

$$\det\boldsymbol{J}(\boldsymbol{\theta}_m) \approx \exp\left(-\frac{\Delta t}{2}(\boldsymbol{\nabla}\cdot\boldsymbol{F}(\boldsymbol{\theta}_m^*;\boldsymbol{c}))\right)$$

to leading order in Δt.

Proof. For a sketch of the proof see appendix A. □

Then, using equations (4.9) and (4.12) the required likelihood function can be written as

$$\ell(\mathscr{M},\Upsilon) = \prod_{m=0}^{M-1} \frac{1}{\sqrt{(2\pi\Delta t)^N|\boldsymbol{D}|}} \exp\left(-\frac{\Delta t}{2}[\dot{\boldsymbol{\theta}}_m - \boldsymbol{F}(\boldsymbol{\theta}_m^*;\boldsymbol{c})]^T\boldsymbol{D}^{-1}[\dot{\boldsymbol{\theta}}_m - \boldsymbol{F}(\boldsymbol{\theta}_m^*;\boldsymbol{c})]\right) \times \exp\left(-\frac{\Delta t}{2}\frac{\partial\boldsymbol{F}(\boldsymbol{\theta}_m^*;\boldsymbol{c})}{\partial\boldsymbol{\theta}_m^*}\right), \quad (4.14)$$

where we have used

$$\dot{\boldsymbol{\theta}}_m = \frac{\boldsymbol{\theta}_{m+1} - \boldsymbol{\theta}_m}{\Delta t}.$$

Taking the natural logarithm of equation (4.14) (for convenience), we obtain the *minus log-likelihood function*, $S := -\ln\ell(\mathscr{M},\Upsilon)$, given by

$$S = \frac{N}{2}\ln|\boldsymbol{D}| + \frac{\Delta t}{2}\sum_{m=0}^{M-1}\left(\frac{\partial\boldsymbol{F}(\boldsymbol{\theta}_m^*;\boldsymbol{c})}{\partial\boldsymbol{\theta}_m^*} + [\dot{\boldsymbol{\theta}}_m - \boldsymbol{F}(\boldsymbol{\theta}_m^*;\boldsymbol{c})]^T\boldsymbol{D}^{-1}[\dot{\boldsymbol{\theta}}_m - \boldsymbol{F}(\boldsymbol{\theta}_m^*;\boldsymbol{c})]\right) + N\ln(2\pi\Delta t). \quad (4.15)$$

This log-likelihood is asymptotically exact in the limit $\Delta t \to 0$ and $M \to \infty$ while $T = M\Delta t$ remains constant .

The next task is to maximize the posterior probability i.e. to fit the likelihood equation (4.15) to Bayes' theorem, in order to find the optimal probability of the parameter set $\mathscr{M}$ given the data Υ.

We assume a prior distribution $p(\mathscr{M})$ that is *Gaussian* in $\boldsymbol{c}$ and *uniform* in $\boldsymbol{D}$:

$$p(\mathscr{M}) = \frac{1}{\sqrt{(2\pi)^L |\boldsymbol{\Sigma}_{pr}|}} \exp\left(-\frac{1}{2}(\boldsymbol{c}-\boldsymbol{c}_{pr})^T \boldsymbol{\Sigma}_{pr}^{-1}(\boldsymbol{c}-\boldsymbol{c}_{pr})\right) \tag{4.16}$$

where $\boldsymbol{c}_{pr} \in \mathbb{R}^L$ is a vector of *a priori* model parameters and $\boldsymbol{\Sigma}_{pr}$ is its covariance matrix. It turns out from equations (4.15) and (4.16) that we can update the parameters $\mathscr{M}$ by the posterior distribution $p(\mathscr{M}|\Upsilon)$ via the Bayesian theorem.

Due to the highly non-linearity of the vector field $\boldsymbol{F}$, it is not always easy to apply Bayesian inference directly to equations (4.15) and (4.16). We assumed that we can rewrite the vector field $\boldsymbol{F}$ as a linear combination of certain known basis functions. Since we are dealing with phase equations, choosing K Fourier basis functions $\boldsymbol{\phi}_k(\boldsymbol{\theta})$:

$$\mathscr{L} = \{\boldsymbol{\phi}_1, \ldots, \boldsymbol{\phi}_K\} \tag{4.17}$$

we can parametrize $\boldsymbol{F}$ as a linear combination of the basis functions as:

$$\boldsymbol{F}(\boldsymbol{\theta};\boldsymbol{c}) = \boldsymbol{\Phi}(\boldsymbol{\theta})\boldsymbol{c} \tag{4.18}$$

where $\boldsymbol{\Phi} := \boldsymbol{\Phi}(\boldsymbol{\theta})$ is defined as

$$\boldsymbol{\Phi} := \begin{bmatrix} \begin{pmatrix} \boldsymbol{\phi}_1 & \ldots & 0 \\ \vdots & \ddots & \vdots \\ 0 & \ldots & \boldsymbol{\phi}_1 \end{pmatrix} & \ldots & \begin{pmatrix} \boldsymbol{\phi}_K & \ldots & 0 \\ \vdots & \ddots & \vdots \\ 0 & \ldots & \boldsymbol{\phi}_K \end{pmatrix} \end{bmatrix} \tag{4.19}$$

which is a matrix of $N \times N$ block matrices. Substituting this parametrization of $\boldsymbol{F}$ into equation (4.15) gives a quadratic log-likelihood function in respect of the parameters vector $\boldsymbol{c}$. By theorem 4.2.1, a multivariate normal distribution for the prior distribution $p(\mathscr{M})$ leads to a multivariate normal distribution for the posterior $p(\mathscr{M}|\Upsilon)$.

Finally, considering equations (4.15), (4.16) and (4.18), (4.16), the stationary point of the log-likelihood (and thus the posterior) can be calculated recursively with the following equations:

$$\boldsymbol{D} = \frac{\Delta t}{N} \sum_{m=0}^{M-1} [\dot{\boldsymbol{\theta}}_m - \boldsymbol{\Phi}_m \boldsymbol{c}]^T [\dot{\boldsymbol{\theta}}_m - \boldsymbol{\Phi}_m \boldsymbol{c}] \tag{4.20}$$

$$\boldsymbol{c} = \boldsymbol{\Xi}^{-1}(\boldsymbol{D})\boldsymbol{w}(\boldsymbol{D}), \tag{4.21}$$

where

$$\boldsymbol{w}(\boldsymbol{D}) := \boldsymbol{\Sigma}_{pr}^{-1}\boldsymbol{c}_{pr} + \Delta t \sum_{m=0}^{M-1}\left(\boldsymbol{\Phi}_m \boldsymbol{D}^{-1}\dot{\boldsymbol{\theta}}_m - \frac{1}{2}\frac{\partial \boldsymbol{\Phi}(\boldsymbol{\theta}_m^*)}{\partial \boldsymbol{\theta}_m^*}\right), \tag{4.22}$$

$$\boldsymbol{\Xi}(\boldsymbol{D}) := \boldsymbol{\Sigma}_{pr}^{-1} + \Delta t \sum_{m=0}^{M-1}\boldsymbol{\Phi}_m^T \boldsymbol{D}^{-1}\boldsymbol{\Phi}_m, . \tag{4.23}$$

Here, $\boldsymbol{\Phi}_m = \boldsymbol{\Phi}(\boldsymbol{\theta}_m)$, and $\boldsymbol{\Xi}$ is the inverse of the covariance matrix $\boldsymbol{\Xi} = \boldsymbol{\Sigma}^{-1}$ (often called concentration or precision matrix) of the parameters vector $\boldsymbol{c}$.

Following the work in (LUCHINSKY *et al.*, 2008; STANKOVSKI *et al.*, 2014), we can summarize the Bayesian inference algorithm as follows: starting from initial prior $\boldsymbol{\Sigma}_{pr}^{-1}$ and $\boldsymbol{c}_{pr}$, the noise matrix $\boldsymbol{D}$ can be calculated using equation (4.20), then given this $\boldsymbol{D}$, using equations (4.21)–(4.23) the parameter vector $\boldsymbol{c}$ can be calculated. The same procedure should be repeated recursively until $\boldsymbol{c}$ and $\boldsymbol{D}$ converge to stability. In the absence of any prior knowledge about the system, a *non-informative* initial prior can be used: $\boldsymbol{\Sigma}_{pr}^{-1} = 0$ and $\boldsymbol{c}_{pr} = 0$.

In summary: given a realization of $\Upsilon = \{\boldsymbol{\theta}_m\}$, basis functions $\boldsymbol{\phi}_k$, and quantities $\boldsymbol{c}_{pr}$ and $\boldsymbol{\Sigma}_{pr}$ of the prior distribution $p(\boldsymbol{c})$, the posterior distribution of the model parameters $\boldsymbol{c}$ is given by

$$p(\boldsymbol{c}|\Upsilon) = \frac{\sqrt{|\boldsymbol{\Xi}_{pt}|}}{\sqrt{(2\pi)^L}}\exp\left(-\frac{1}{2}(\boldsymbol{c}-\boldsymbol{c}_{pt})^T\boldsymbol{\Xi}_{pt}(\boldsymbol{c}-\boldsymbol{c}_{pt})\right), \tag{4.24}$$

where $\boldsymbol{c}_{pt}$ and $\boldsymbol{\Xi}_{pt}$ are the mean and covariance of the posterior $p(\boldsymbol{c}|\Upsilon)$, respectively. If a new sequential data block Υ' (obtained from the same dynamics) is given, we can use the posterior quantities $\boldsymbol{c}_{pt}$ and $\boldsymbol{\Xi}_{pt}$ from the first data-block Υ as the prior for the second one.

Remark 4.2.3. The Bayesian inference method presented here is to be implemented for reconstructing a non-time-varying noisy dynamical system from data. But it can be extended to a system with time variability. For the details of the procedure, the reader can refer to (STANKOVSKI *et al.*, 2014).

4.2.2 Sparse recovery methods

Given the data Υ in equation (4.3), we aim to reconstruct the phase dynamics (equation (4.1)). Rewriting equation (4.1) as

$$\frac{d}{dt}\boldsymbol{\theta}(t) = \boldsymbol{F}(\boldsymbol{\theta}(t);\boldsymbol{c}) \tag{4.25}$$

where we have assumed no dynamical noise, i.e., we considered the deterministic dynamical system. In the end, we will study the robustness of noise where the data comes from a stochastic phase equation.

Since, typically, nonlinear functional forms can be expanded as sums of terms belonging to a family of parameterized functions (see (LJUNG, 1999, Sec. 5.4) and (BILLINGS, 2013),

a usual approach to reconstructing models of complex systems is to search amongst a set of possible nonlinear terms (e.g., *basis functions*) for a parsimonious description coherent with the available data (HABER; UNBEHAUEN, 1990). A few choices of basis functions are provided by classical functional decomposition methods such as Taylor polynomial expansion or Fourier series (LJUNG, 1999; BILLINGS, 2013; BARAHONA; POON, 1996).

We assume that there exists a finite set of candidate library functions whose linear combination allows us to describe the dynamics of the system of interest. In particular, we assume that the components F_i of the vector field F can be written as a linear combination of a finite set $\mathscr{L}$ of candidate basis functions, defined as

$$F_i = \sum_{k=1}^{K} c_{i,k}\boldsymbol{\phi}_k(\boldsymbol{\theta}(t)), \tag{4.26}$$

where $\boldsymbol{\phi}_k(\boldsymbol{\theta}(t)) \in \mathscr{L}$ for each $k = 1,\dots,K$ are the candidate basis functions of the ith oscillator, and K is the maximum number of the candidate functions. The coefficients $\{c_{i,k} \mid i = 1,\dots,N; k = 1,\dots,K\}$ are the set of unknown parameters to be determined from available time-series data. By inserting equation (4.26) into equation (4.25) we obtain the system

$$\frac{d}{dt}\theta_i(t) = \sum_{k=1}^{K} c_{i,k}\boldsymbol{\phi}_k(\boldsymbol{\theta}(t)), \tag{4.27}$$

where we have assumed that the time derivatives $\frac{d}{dt}\theta_i(t)$, for each $i = 1,\dots,N$, are known. However, in real-life applications, these assumptions might not be applicable. If the sampling time interval Δt is sufficiently small, we can approximate the time derivatives $\dot{\theta}_i(t)$ numerically using, e.g., forward Euler difference as

$$\dot{\theta}_i(t_m) \approx \frac{\theta_i(t_{m+1}) - \theta_i(t_m)}{\Delta t}, \quad i = 1,\dots,N;\ m = 1,\dots,M-1.$$

The multivariate time-series data Υ of the process $\boldsymbol{\theta}(t)$ and their time derivatives $\dot{\boldsymbol{\theta}}(t)$ are arranged into $M \times N$ data matrices

$$\Theta := \begin{bmatrix} \theta_1(t_1) & \dots & \theta_N(t_1) \\ \vdots & \vdots & \vdots \\ \theta_1(t_M) & \dots & \theta_N(t_M) \end{bmatrix} \quad \text{and} \quad \dot{\Theta} := \begin{bmatrix} \dot{\theta}_1(t_1) & \dots & \dot{\theta}_N(t_1) \\ \vdots & \vdots & \vdots \\ \dot{\theta}_1(t_M) & \dots & \dot{\theta}_N(t_M) \end{bmatrix}. \tag{4.28}$$

Similarly, the chosen basis functions $\boldsymbol{\phi}_k$ are evaluated at each time step to obtain an $M \times K$ *library matrix* $\boldsymbol{\Phi} := \boldsymbol{\Phi}(\Theta)$ defined as

$$\boldsymbol{\Phi} = \begin{bmatrix} \boldsymbol{\phi}_1(\boldsymbol{\theta}(t_1)) & \dots & \boldsymbol{\phi}_K(\boldsymbol{\theta}(t_1)) \\ \vdots & \dots & \vdots \\ \boldsymbol{\phi}_1(\boldsymbol{\theta}(t_M)) & \dots & \boldsymbol{\phi}_K(\boldsymbol{\theta}(t_M)) \end{bmatrix}. \tag{4.29}$$

Using the matrices $\Theta, \dot{\Theta}$, and $\boldsymbol{\Phi}$, equation (4.27) becomes

$$\dot{\Theta} \approx \boldsymbol{\Phi}\boldsymbol{C}. \tag{4.30}$$

In sparse recovery methods, we aim to estimate a sparse set of parameters $\boldsymbol{C}$ that accurately fits the measured data in $\dot{\Theta}$. For each node $i = 1,\dots,N$, we solve a linear system of the form

$$\dot{\boldsymbol{\theta}}_i = \boldsymbol{\Phi}\boldsymbol{c}_i, \quad \text{for each} \quad i = 1,\dots,N, \tag{4.31}$$

where $\dot{\boldsymbol{\theta}}_i = (\dot{\theta}_i(t_1),\dots,\dot{\theta}_i(t_M))^T \in \mathbb{R}^M$ denotes the ith column of the time derivative data matrix $\dot{\Theta}$, and $\boldsymbol{c}_i$ is the ith column of the matrix of unknown coefficients

$$\boldsymbol{C} = \begin{bmatrix} c_{1,1} & c_{2,1} & \dots & c_{N,1} \\ \vdots & \vdots & \vdots & \vdots \\ c_{1,K} & c_{2,K} & \dots & c_{N,K} \end{bmatrix} = \begin{bmatrix} | & | & & | \\ \boldsymbol{c}_1 & \boldsymbol{c}_2 & \vdots & \boldsymbol{c}_N \\ | & | & & | \end{bmatrix}.$$

One can see that if $M < K$, the system (4.31) is known as *underdetermined*, i.e. there are fewer equations than unknowns, so that the system has infinitely many solutions, and we need a criterion to choose an optimal solution. On the other hand, if $M > K$, the system (4.31) is called *overdetermined*, i.e. there are more equations than unknowns, usually such a system has no exact solution since the data $\dot{\boldsymbol{\theta}}_i$ must be an element of the rank of the library matrix $\boldsymbol{\Phi}$, a proper subspace of $\mathbb{R}^M$. In both cases, it requires an optimization problem; in particular, it suggests the introduction of minimization problems. In our context, we assume that we have a long enough time series, i.e. $K \ll M$. In solving such problems, e.g. using the ℓ_p-norm the least-squares solution of system (4.31) is obtained by solving the following ℓ_2-norm minimization problem:

$$\hat{\boldsymbol{c}}_i = \underset{\boldsymbol{c}_i \in \mathbb{R}^K}{\arg\min} \|\dot{\boldsymbol{\theta}}_i - \boldsymbol{\Phi}\boldsymbol{c}_i\|_2. \tag{4.32}$$

By the *singular value decomposition* (SVD) (GOLUB; LOAN, 1996), the minimization problem (4.32) has an explicit solution

$$\boldsymbol{c}_i = \boldsymbol{\Phi}^{\dagger}\dot{\boldsymbol{\theta}}_i$$

where $\boldsymbol{\Phi}^{\dagger} = (\boldsymbol{\Phi}^T\boldsymbol{\Phi})^{-1}\boldsymbol{\Phi}^T$ is called the *Moore-penrose pseudo-inverse* of $\boldsymbol{\Phi}$. By assumption, the column vectors $\boldsymbol{c}_i$ of $\boldsymbol{C}$ are *sparse*, containing mostly zero entries, and the nonzero entries highlight the active terms in the dynamics of the F_i row of the dynamics. However, the least-squares solutions of Eq. (4.94) do not give satisfactory results. To this end, we need to impose a sparsity constraint on the least-squares solutions. In this case, we solve the following ℓ_0-norm:

$$\|\boldsymbol{c}_i\|_0$$

for each oscillator, which is defined as the number of non-zero elements in $\boldsymbol{c}_i$. Solving such a ℓ_0 problem is a combinatorial *NP-hard* problem. In this case, we try the ℓ_1-norm which also imposes sparsity. Another reconstruction technique that imposes sparsity is the least absolute shrinkage and selection operator (LASSO)(TIBSHIRANI, 1996). In LASSO, we solve the following problem:

$$\underset{\boldsymbol{c}_i \in \mathbb{R}^K}{\arg\min} \|\dot{\boldsymbol{\theta}}_i - \boldsymbol{\Phi}\boldsymbol{c}_i\|_2 \quad \text{subject to} \quad \|\boldsymbol{c}_i\|_1 \leq \beta \tag{4.33}$$

where β is a prespecified free parameter that determines the sparsity.

Definition 4.2.4. A vector is said to be s-sparse if it has at most s nonzero entries

$$\|x\|_0 \leq s. \tag{4.34}$$

In this context, we implement one of the recently developed sparse recovery methods known as Sparse identification of nonlinear dynamics (SINDy) (BRUNTON; PROCTOR; KUTZ, 2016), which is central to this section. In the SINDy algorithm, we attempt to obtain sparse solutions using regression techniques such as the sequentially thresholded least squares (STLSQ) with a thresholding parameter $\lambda > 0$. In this algorithm, we iteratively apply the least-squares method for the problem (4.31) with a hard thresholding parameter $\lambda > 0$. In particular, a sparse solution vector $\boldsymbol{c}_i$, for each $i = 1,\ldots,N$, which approximately solves equation (4.31) is generated by the following iterative scheme:

$$\boldsymbol{c}_i^{(0)} = \boldsymbol{\Phi}^{\dagger}\dot{\boldsymbol{\theta}}_i, \tag{4.35a}$$

$$S^{(n)} = \{1 \leq k \leq K \mid |c_{i,k}^{(n)}| \geq \lambda\},\ n \geq 0, \tag{4.35b}$$

$$\boldsymbol{c}_i^{(n+1)} = \underset{\boldsymbol{c}_i \in \mathbb{R}^K : \mathrm{supp}(\boldsymbol{c}_i) \subset S^{(n)}}{\arg\min} \|\dot{\boldsymbol{\theta}}_i - \boldsymbol{\Phi}\boldsymbol{c}_i\|_2,\ n \geq 0, \tag{4.35c}$$

where $\mathrm{supp}(\boldsymbol{c}_i)$ is the support set of $\boldsymbol{c}_i$, defined as the set of indices corresponding to its nonzero elements, $c_{i,k}^{(n)}$ is the kth component of the nth iteration $\boldsymbol{c}_i^{(n)}$. The procedure in equation (4.35) is iteratively repeated, for each oscillator $i \in \{1,\ldots,N\}$, until convergence or the maximum iteration is required. We denote the inferred sparse vector by $\hat{\boldsymbol{c}}_i$, for each i. In implementing the SINDy algorithm, we use *PySINDy*– an open-source software package that has been developed in Python (SILVA *et al.*, 2020).

Remark 4.2.5. It can be shown that the iterative scheme in equation (4.35) converges to a local minimum $\hat{\boldsymbol{c}}_i$ for each $i = 1,\ldots,N$ (BRUNTON; PROCTOR; KUTZ, 2016).

Model selection: the choice of the thresholding parameter. Note that the estimated sparse vector $\hat{\boldsymbol{c}}_i$ depends on the choice of the thresholding parameter λ. At each iteration, all the coefficients with $|c_{i,k}| < \lambda$ are set to zero. Hence, the parameter λ is important because if λ is too small, the SINDy recovery model contains many nonzero coefficients and hence the sparsity fails. Conversely, if λ is large then basis functions required to emulate the dynamics of the system may be removed, resulting in a model that does not resemble the data. Hence we need to select an appropriate value of λ.

We investigate the effects of the SINDy recovery for different values of λ. We use one of the statistical metrics, known as the *root-mean-squared error* (RMSE) in the predicted models. The approach is summarized below.

We first select *a priori* a set of r possible candidates $\boldsymbol{\lambda} = \{\lambda_1,\ldots,\lambda_r\}$ of the thresholding parameter λ. For each oscillator $i \in \{1,\ldots,N\}$, let $\hat{\boldsymbol{c}}_i(\lambda)$ denotes the inferred coefficient vector in search of the true coefficient vector $\boldsymbol{c}_i$ in equation (4.31) for a pre-chosen threshold value

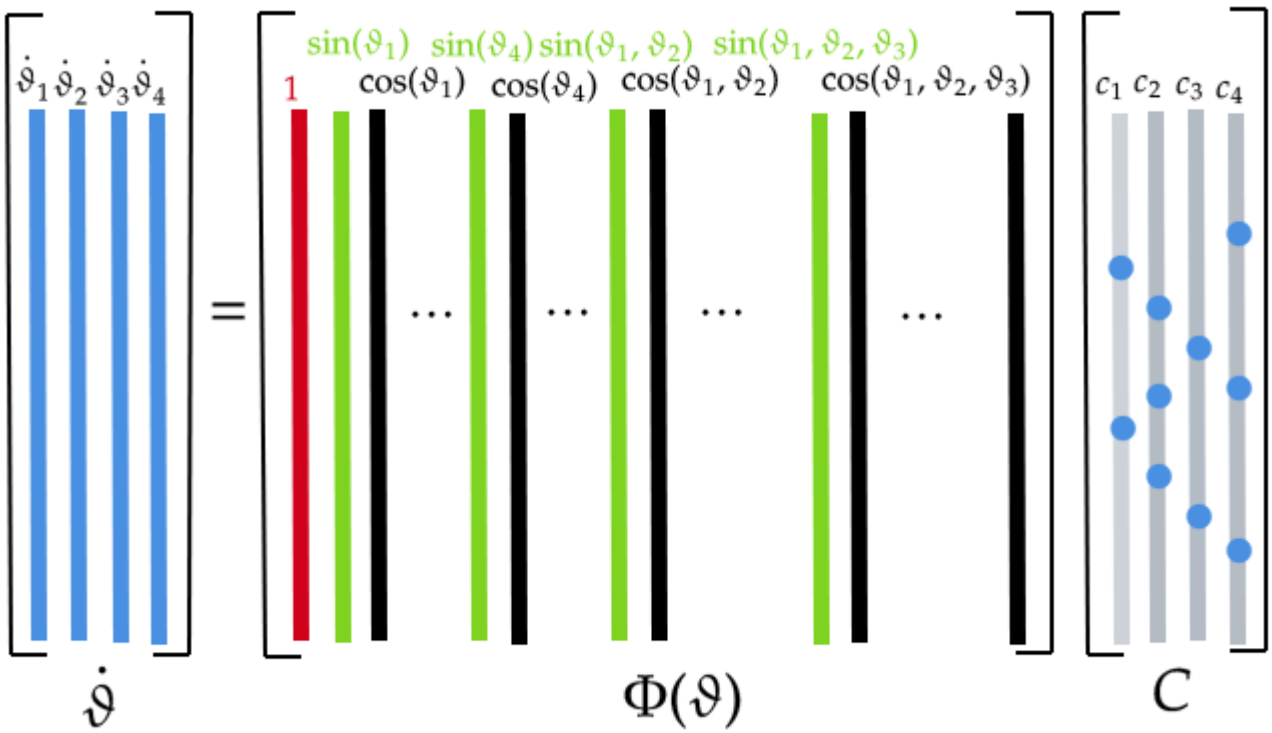

Figure 9 – Schematic of the SINDy algorithm. The active terms in the dynamics are identified by the nonzero elements in $\boldsymbol{C}$.

Source: Elaborated by the author.

$\lambda \in \boldsymbol{\lambda}$, and let $\hat{\dot{\boldsymbol{\theta}}}_i(\lambda)$ denotes the corresponding predicted value of the corresponding SINDy model $\boldsymbol{M}(\lambda)$. Hence, we have

$$\hat{\dot{\boldsymbol{\theta}}}_i(\lambda) \approx \boldsymbol{\Phi}\hat{\boldsymbol{c}}_i(\lambda) \quad \text{for each} \quad \lambda \in \boldsymbol{\lambda}.$$

Then the "best" thresholding parameter λ is the value such that the error between $\hat{\dot{\boldsymbol{\theta}}}_i(\lambda)$ and $\dot{\boldsymbol{\theta}}_i$ is minimum. To accomplish this, we split the time-series data into a training set for inferring the parameters and a test set for evaluating the predictions. Then, for each oscillator i, the RMSE of predicted values $\hat{\dot{\boldsymbol{\theta}}}_i(\lambda)$ can be defined as

$$RMSE(\hat{\boldsymbol{v}}_{i,m}(\lambda), \boldsymbol{v}_{i,m}) := \sqrt{\frac{1}{M_t}\sum_{m=1}^{M_t}(\hat{\boldsymbol{v}}_{i,m}(\lambda) - \boldsymbol{v}_{i,m})^2}, \tag{4.36}$$

where $\boldsymbol{v}_{i,m} := \dot{\theta}_i(t_m)$ is the time derivative of θ_i at time t_m for each $m \in \{1,\ldots,M_t\}$ and each $i = 1,\ldots,N$, where M_t is the number of data points in the validation set.

The "best" thresholding parameter $\lambda \in \boldsymbol{\lambda}$ is then the solution to the following minimization problem:

$$\lambda_{opt} := \arg\min_{\lambda \in \boldsymbol{\lambda}} \frac{1}{N}\sum_{i=1}^{N} RMSE(\hat{\boldsymbol{v}}_{i,m}(\lambda), \boldsymbol{v}_{i,m}). \tag{4.37}$$

4.3 Comparisons of Bayesian inference and sparse recovery methods

In this section, we will present a few examples to illustrate the reconstruction methods under consideration, from measurements or simulated data. We first consider the phase model driven by additive Gaussian noise and then we consider coupled Van der Pol oscillators driven by additive Gaussian noise.

4.3.1 Reconstruction from a network of three oscillators

We consider a model of three interacting phase oscillators of the form:

$$\begin{aligned}\dot{\theta}_1 &= F_1(\theta_1,\theta_2,\theta_3)+\sqrt{D_1}\xi_1(t),\ F_1=\omega_1+\alpha\sin(\theta_3-\theta_1)\\ \dot{\theta}_2 &= F_2(\theta_1,\theta_2,\theta_3)+\sqrt{D_2}\xi_2(t),\ F_2=\omega_2+\alpha\sin(\theta_3-\theta_2)\\ \dot{\theta}_3 &= F_3(\theta_1,\theta_2,\theta_3)+\sqrt{D_3}\xi_3(t), F_3=\omega_3+\beta\sin(\theta_3),\end{aligned} \tag{4.38}$$

where θ_i is the phase of the ith oscillator with natural frequency ω_i, and α is the coupling strength. The noise term $\xi_i(t)$ is assumed to be white Gaussian noise with zero-mean and $\langle\xi_j(t)\xi_i(t')\rangle=\delta_{ij}\delta(t-t')$ and D_i is the noise intensity. Equation (4.38) can describe a network of three nodes, where each node i is represented by $\dot{\theta}_i$. The system shows that oscillator 3 influences the other two oscillators 1 and 2 without being influenced by any of the two oscillators, and such a system is also known as a *master-slave configuration*, as shown in figure 10. Such configurations are widely found in biology (JOSHI; SEN; KAR, 2020), physics (AHMAD *et al.*, 2015) and engineering applications (RIGATOS, 2014). In the absence of coupling and noise, the oscillators move with their own frequencies ω_i. We aim to reconstruct the phase dynamics of

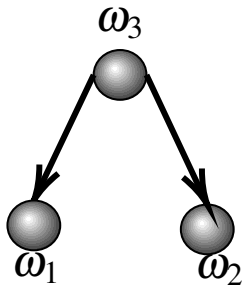

Figure 10 – Schematic diagram showing a master-slave configuration of three oscillators where oscillator 3 directly influences oscillators 1 and 2 with a coupling function of the form $q_i(\theta_3,\theta_i) := \alpha\sin(\theta_3-\theta_i)$ for $i=1,2$ and $q_3=\beta\sin\theta_3$.

Source: Elaborated by the author.

these three oscillators from the data. In this problem, the model is known *a priori*, and we have access to the time series of all the three oscillators θ_i, which can be obtained from simulating the system.

Generating input data from a stochastic phase model. We first obtain synthetic test data by simulating the system (4.38) using the Euler-Maruyama method from $t=0$ to $t=2000$

with a uniform time step $\Delta t = 0.001$ starting from initial conditions $\theta_i(0)$, which are uniformly distributed random numbers in the interval $[0, 2\pi]$, forming $M = 2 \times 10^6$ data points. In our simulations, we choose the parameter values $\omega_1 = 1 - \delta, \omega_2 = 1 + \delta, \omega_3 = 1.0, \alpha = 0.03$, and $\beta = 0.91$, with $\delta = 0.1$, and a noise intensity $D_i = D = 0.0005$. To simulate the influence of Gaussian white noises ξ_i, we use the generator of *pseudo random* numbers. We need a sample of independent random variables $\xi_i(t_m)$ at each of the values of the time $t_m = mh\,(m = 1, \ldots, M)$ in the discretization, distributed as $\sqrt{\Delta t}\mathcal{N}(0,1)$. Hence, we obtain a numerical multivariate time series $\Upsilon = \{\theta_i(t_m)\}_{t_m=1}^{2000}$ that represents the network dynamics (4.38), which are depicted in figure 11.

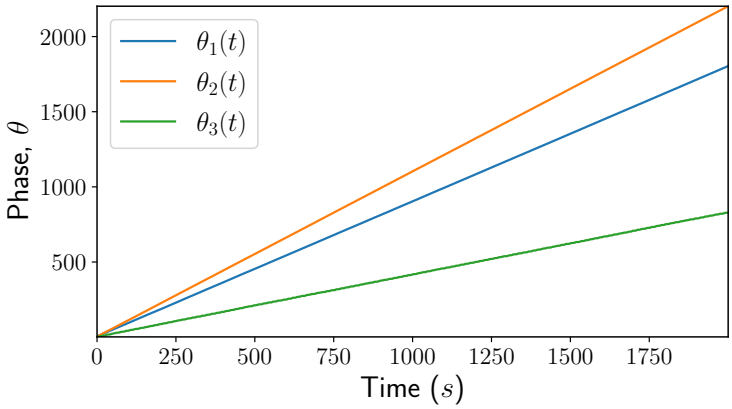

Figure 11 – The time series of the three oscillators described by the master-slave configuration (equation (4.38)). Parameter values are $\omega_1 = 1 - \delta, \omega_2 = 1 + \delta, \omega_3 = 1.0, \beta = 0.91$, and $\alpha = 0.03$, where $\delta = 0.1$. The system was simulated from time $t = 0$ to $t = 2000$ with a uniform time-step $\Delta t = 0.001$ using the Euler-Maruyama scheme, starting from initial conditions $\theta_i(0)$, which were uniformly distributed random numbers in the interval $[0, 2\pi]$.

Source: Elaborated by the author.

Reconstruction of the phase dynamics. Using the data obtained in the previous section, we aim to reconstruct the phase dynamics from it. In doing this, we first choose appropriate base functions. Because of their oscillatory nature and periodic solutions, we use Fourier basis functions. We choose the following 13 basis functions $\boldsymbol{\phi}_k(\boldsymbol{\theta})$:

$$\mathscr{L} = \{1, \sin(\theta_i), \cos(\theta_i), \sin(\theta_i - \theta_j), \cos(\theta_i - \theta_j)\}, \tag{4.39}$$

for each $i, j \in \{1, 2, 3\}$ and $i \neq j$. This counts for $K = 1 + 2(3) + 3(3-1) = 13$ basis functions.

In reconstructing the phase equations from data, we assume that the time derivatives $\dot{\theta}_i(t)$, which can be obtained numerically, can be written as a linear combination of the pre-chosen basis functions as

$$\frac{d}{dt}\theta_i(t) = \sum_{k=1}^{13} c_{i,k}\boldsymbol{\phi}_k(\boldsymbol{\theta}(t)) + \sqrt{D_i}\xi_i(t) \tag{4.40}$$

where $\boldsymbol{c}_i := \{c_{i,1}, \ldots, c_{i,13}\}$ are the unknown coefficients to be estimated from a 3-dimensional time series data $\{\theta_i(t_m)\}_{m=1}^{M}$ of M discrete time points $t_m = m\Delta t$, where Δt is the sampling interval.

In reconstructing the phase dynamics, we implement Bayesian inference. The phase time series $\{\theta_i(t)\}$ and the pre-chosen basis set $\mathscr{L}$ will be used as input for Bayesian inference to infer the set of parameters $\mathscr{M} = \{c_{i,k}, D_i\}$, for each $i = 1,2,3$ and $k = 1,\ldots,13$, over a single block of data of size $M = 2\times 10^6$.

Moreover, we will compare the inferred mean values of the parameters $\{c_{i,k}\}$ obtained using Bayesian inference with that of sparse recovery methods. To this end, we solve a sparse linear regression problem

$$\dot{\boldsymbol{\theta}}_i = \boldsymbol{\Phi}\boldsymbol{c}_i + \boldsymbol{\nu}_i, \tag{4.41}$$

for each oscillator i, using SINDy algorithm with a thresholding parameter $\lambda > 0$. Here, $\dot{\boldsymbol{\theta}}_i \in \mathbb{R}^M$ denotes the numerical derivatives of the time series of the ith oscillator, $\boldsymbol{\Phi} \in \mathbb{R}^{M\times K}$ denotes the matrix of basis functions evaluated at each time series, known as the *library matrix*, and is defined as

$$\boldsymbol{\Phi} = \begin{bmatrix} 1 & \sin(\theta_1(t_1)) & \ldots & \cos(\theta_1(t_1)) & \ldots & \sin(\theta_1(t_1)-\theta_2(t_1)) & \ldots & \cos(\theta_2(t_1)-\theta_3(t_1)) \\ 1 & \sin(\theta_1(t_2)) & \ldots & \cos(\theta_1(t_2)) & \ldots & \sin(\theta_1(t_2)-\theta_2(t_2)) & \ldots & \cos(\theta_2(t_2)-\theta_3(t_2)) \\ \vdots & \vdots & \ldots & \vdots & \ldots & \vdots & \ldots & \vdots \\ 1 & \sin(\theta_1(t_M)) & \ldots & \cos(\theta_1(t_M)) & \ldots & \sin(\theta_1(t_M)-\theta_2(t_M)) & \ldots & \cos(\theta_2(t_M)-\theta_3(t_M)) \end{bmatrix}$$

and $\boldsymbol{c}_i \in \mathbb{R}^K$ is the vector of constant coefficients to be estimated. The vector $\boldsymbol{\nu} \in \mathbb{R}^M$ is a noise term, assumed to be white and Gaussian. In SINDy, we heuristically consider a thresholding parameter $\lambda = \frac{\alpha}{10}$, where α is the coupling parameter of oscillators 1 and 2.

The recovered coefficients from a single block of data are presented in table 1. Table 1 shows that Bayesian inference is accurate with an error of 0.0163%. Both methods predict well.

Effect of the length of the time series on model reconstruction. Here we discuss the accuracy of the model reconstruction on the number of data points $M = T/\Delta t$. What is the minimum time required to obtain an accurate model reconstruction?

In such network reconstruction problems, typically, there are two types of errors: true connections might be absent in the reconstruction or non-existing connections may present in the reconstruction. We quantify such binary classification into two types of errors:

- *False positives* – non-existing connections that are nevertheless present in the reconstruction
- *False negatives* – existing connections that are not present in the reconstruction

Let $\mathscr{P}$ denote the set of indices of the interactions in the library $\mathscr{L}$. By reconstruction, we have

$$\mathscr{P} := \{1 \le k \le 12 : \boldsymbol{\phi}_k \in \mathscr{L}\}.$$

Table 1 – Model reconstruction from a 3-dimensional time series data of length $M = 2 \times 10^6$ obtained by simulating system (4.38) with model parameter values $\omega_1 = 0.9, \omega_2 = 1.1, \omega_3 = 1.0, \alpha = 0.03$, and $\beta = 0.91$ and noise intensity $D = 5 \times 10^{-4}$. Bayesian inference is implemented for a single block of data of time $t = 2000\ s$ to obtain the inferred mean values of the coefficients $\{c_{i,k}\}$. SINDy is implemented with a thresholding parameter of $\lambda = \frac{\alpha}{10}$. In both case, we considered $K = 13$ basis functions $\boldsymbol{\phi_k} \in \mathscr{L}$.

index	$\boldsymbol{\phi}_k \in \mathscr{L}$	Bayesian Inference			Sparse recovery		
		$\dot{\theta}_1$	$\dot{\theta}_2$	$\dot{\theta}_3$	$\dot{\theta}_1$	$\dot{\theta}_2$	$\dot{\theta}_3$
0	1	0.900	1.10	1.00	0.900	1.101	1.000
1	$\sin\theta_1$	0	0	0	0	0	0
2	$\sin\theta_2$	0	0.001	0	0.	0.	0.
3	$\sin\theta_3$	0	0.001	0.911	0.	0.	0.911
4	$\cos\theta_1$	0	0	0	0.	0.	0.
5	$\cos\theta_2$	0.002	0	0	0.	0.	0.
6	$\cos\theta_3$	0	0	0.001	0.	0.	0.
7	$\sin(\theta_1 - \theta_2)$	0	0	0	0.	0.	0.
8	$\sin(\theta_1 - \theta_3)$	-0.03	0	0	-0.03	0.	0.
9	$\sin(\theta_2 - \theta_3)$	-0.001	-0.03	0	0.	-0.03	0.
10	$\cos(\theta_1 - \theta_2)$	0	0	0	0.	0.	0.
11	$\cos(\theta_1 - \theta_3)$	0	0	0	0.	0.	0.
12	$\cos(\theta_2 - \theta_3)$	0	0	0	0.	0.	0.

Source: Elaborated by the author.

For each oscillator i, let $\mathscr{P}_i$ denote the set of indices of active interaction functions of node i of the original network. Then we have

$$\mathscr{P}_i := \{k \in \mathscr{P} : \boldsymbol{\phi}_k \text{ is an active basis element in the dynamics of node } i\}.$$

From the given phase equations, we see that $\sin(\theta_3 - \theta_1), \sin(\theta_3 - \theta_2)$, and $\sin\theta_3$, respectively, are the corresponding active basis elements of oscillators $1, 2$, and 3.

Let $\hat{\mathscr{P}}_i$ denote the set of indices of the reconstructed basis elements of node $i \in \{1,2,3\}$, respectively, using the SINDy and Bayesian inference methods. Let the estimated links of the reconstruction for node i be denoted by $w_{i,k} \in \{|\hat{c}_{i,k}| \ | k \in \hat{\mathscr{P}}_i\}$. Then we define the weighted fractions of false positives, wFP , and the weighted fractions of false negatives, wFN, in the reconstruction for each node i as:

$$wFP_i := \frac{\sum_{k\in\mathscr{P}} w_{i,k} \mathbb{1}_{\hat{\mathscr{P}}_i \cap \mathscr{P}_i^c}(k)}{\sum_{k\in\mathscr{P}} \left(w_{i,k} \mathbb{1}_{\hat{\mathscr{P}}_i \cap (\mathscr{P}_i)^c}(k) + \mathbb{1}_{(\hat{\mathscr{P}}_i)^c \cap (\mathscr{P}_i)^c}(k) \right)}, \tag{4.42}$$

$$wFN_i := \frac{\sum_{k\in\mathscr{P}} \mathbb{1}_{(\hat{\mathscr{P}}_i)^c \cap \mathscr{P}_i}(k)}{\sum_{k\in\mathscr{P}} \mathbb{1}_{\mathscr{P}_i}(k)}, \tag{4.43}$$

where $\mathbb{1}_A$ is the indicator function of the set A, defined as

$$\mathbb{1}_A(k) = \begin{cases} 1 & \text{if } k \in A \\ 0 & \text{if } k \notin A. \end{cases}$$

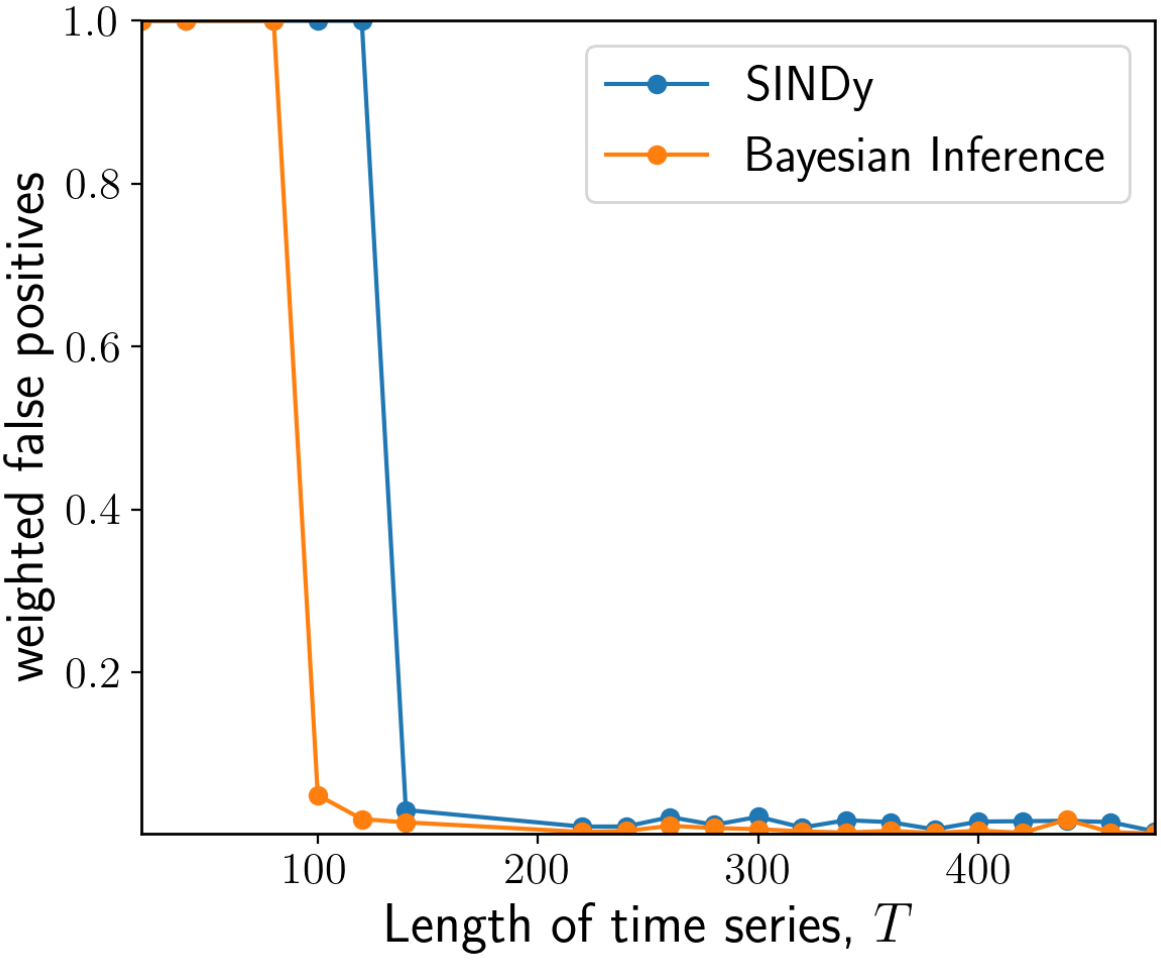

Figure 12 – Bayesian inference and SINDy are compared against the effects of varying the length of the time series. We plotted weighted fractions of false positive links vs. length of time series. The length of the time series varied from $T = 50$ to $T = 1000$. At all times, the noise level was set to be $D_i = 5 \times 10^{-4}$.

Figure 12 shows that Bayesian inference predicts better when the time series is relatively short. We also observe that both methods are accurate as the length of the time series increases.

Robustness to noise. We study the robustness of the techniques by plotting the false positive links of the reconstruction against the noise intensity D. The results are illustrated in figure 13. It shows that both methods give accurate results when the noise intensity is small enough. Bayesian inference predicts better when the noise intensity is relatively large.

4.3.2 Reconstruction from coupled Van der Pol oscillators

In practice, we do not observe phases directly but rather some variables from which we need to calculate phases. To this end, we consider two weakly coupled Van der Pol oscillators

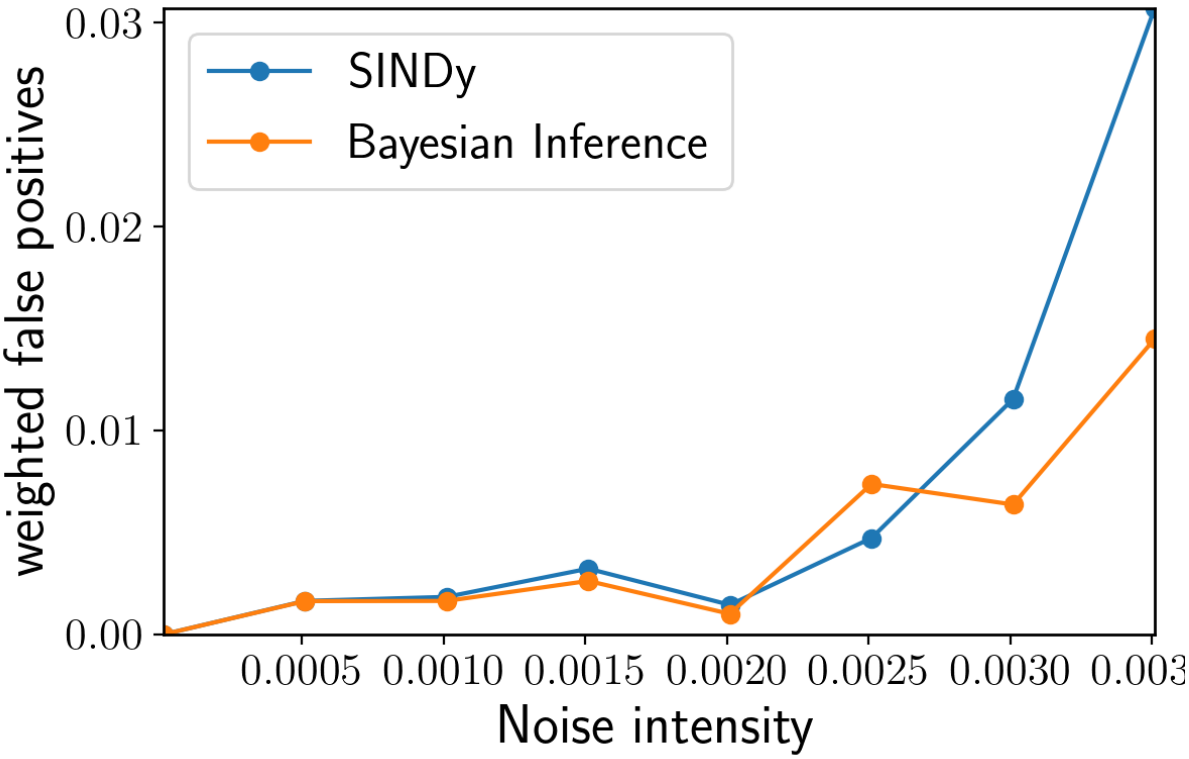

Figure 13 – Bayesian inference and SINDy are compared against the effects of noise. We plotted weighted fractions of false positive links vs. the noise level D. The noise levels were varying on the interval $[10^{-5}, 0.006]$ in steps of 5×10^{-4}. In all cases, the length of the time series was fixed to be $T = 1000$ with time step 0.001.

with additive noise, defined as:

$$\begin{aligned} \frac{d^2x_1}{dt^2} &= \mu(1-x_1^2)\frac{dx_1}{dt} - \omega_1^2 x_1 + \alpha(x_2 - x_1) + \sqrt{D_1}\xi_1(t), \\ \frac{d^2x_2}{dt^2} &= \mu(1-x_2^2)\frac{dx_2}{dt} - \omega_2^2 x_2 + \alpha(x_1 - x_2) + \sqrt{D_2}\xi_2(t), \end{aligned} \tag{4.44}$$

where $x_i(t)$ is the state variable of the ith oscillator at time t, μ is a constant parameter, α is the coupling strength, and ω_i is the natural frequency of the ith oscillator. The noise term ξ_i is assumed Gaussian white noise with $\langle \xi_i(t) \rangle = 0$ and $\langle \xi_i(t)\xi_j(t') \rangle = \delta_{ij}\delta(t-t')$, and $D_i \in \mathbb{R}$ represents the strength of the noise term assumed to be $O(\alpha)$.

When the oscillators are uncoupled and in the absence of noise, the system (4.44) is reduced to

$$\frac{du_i}{dt} = f_i(u_i), \quad i = 1, 2, \tag{4.45}$$

where $u_i = [x_i, \dot{x}_i]^T$ represents the state of the ith Van der Pol oscillator, and the vector field $f_i = [\dot{x}_i, \mu(1-x_i^2)\dot{x}_i - \omega_1^2 x_i]^T$ denotes the isolated dynamics of the ith oscillator. It can be shown that f_i has an exponentially stable limit cycle γ_i with period $T_i = \frac{2\pi}{\omega_i}$.

In this context, we assume that the coupling strength α is sufficiently small. Then, we can introduce a phase $\theta_i \in \mathbb{S}^1$ and define the corresponding asymptotic phase $\Theta_i(u) \in \mathbb{S}^1$ for each f_i

such that $\Theta_i(u) = \theta_i(t)$. Therefore, by virtue of the phase reduction method and equation (2.59), the system (4.44) can be reduced into the following first-order phase equations of the form

$$\frac{d\theta_i}{dt} = \omega_i + \alpha q_i(\theta_i, \theta_j) + \eta_i(t) + O(\alpha^2), \tag{4.46}$$

where θ_i is the phase of the ith oscillator which increases uniformly in the absence of coupling and noise, and q_i the phase coupling function of the ith oscillator, and takes the form

$$q_i(\theta_i, \theta_j) = Z_i(\theta_i) \cdot h_i(\theta_j, \theta_i) \tag{4.47}$$

and the noise induced in the dynamics $\eta_i(t)$ takes the form

$$\eta_i(t) = \sqrt{D_i} Z_i(\theta_i) \xi_i(t), \tag{4.48}$$

where $Z_i(\theta_i) = \nabla \Theta_i(u_i)|_{u_i = \gamma_i(\theta_i)}$ is the phase sensitivity function.

We aim to reconstruct the phase dynamics of the two coupled Van der Pol oscillators when only the variables x_i are observable.

Phase dynamics reconstruction. The first ingredient is to obtain time-series data. To do this, we first simulate the system (4.44) using the Euler-Maruyama method with time step $\Delta t = 0.01$ and use $M = 10^5$ data points each starting from initial conditions $[x_i(0), \dot{x}_i(0)]^T$. In our simulations, we set the parameter values $\omega_1 = 1.02, \omega_2 = 0.98$, and $\alpha = 0.01$. We consider noise levels $D_1 = D_2 = D = 0.0005$. To simulate the influence of Gaussian white noises ξ_i, we use the generator of *pseudo random* numbers. We need a sample of independent random variables $\xi_i(t_m)$ at each of the values of the time $t_m = m\Delta t$ $(m = 1, \ldots, M)$ in the discretization, distributed as $\sqrt{\Delta t}\mathcal{N}(0,1)$. Hence, we obtain the data set

$$\mathscr{Y} := \{[x_i(t_m), \dot{x}_i(t_m)]^T : t_m = m\Delta t, m = 1, \ldots, M; i = 1, 2\}.$$

The next step is to estimate the phases from each time series. There are a number of techniques. In this section, we obtain the time series of the oscillations' unwrapped phases $\{\vartheta_i(t_1), \ldots, \vartheta_i(t_M)\}$ from the time series of $x_i(t)$ and $\dot{x}_i(t)$ using the formula

$$\vartheta_i(t) = -\arctan\left(\frac{\dot{x}_i(t)}{x_i(t)}\right), \quad i = 1, 2, \tag{4.49}$$

where the arctan is defined as a four-quadrant operation. This phase $\vartheta_i(t)$ is a surrogate and not necessarily equal to the true phase $\theta_i(t)$, but all relevant information can be obtained from it. In figure 14, we show the trajectories of the state variables $x_i(t)$ and the time series of the phases $\vartheta_i(t)$. The resulting phase time series $\{\vartheta_i(t_m) : t_m = m\Delta t, m = 1, \ldots, M; i = 1, 2\}$ of $M = 10^5$ data points are used as the input for reconstructing the phase dynamics equations of each oscillator. This number of data points corresponds to approximately 160 periods of each oscillator as $\omega_i \approx 1, i = 1, 2$.

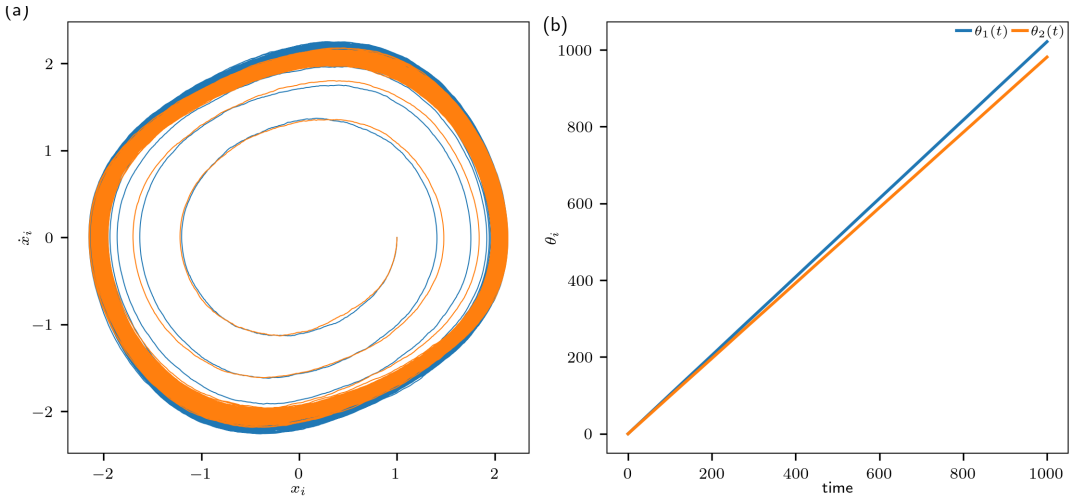

Figure 14 – **Simulations of the coupled Van der Pol oscillators** (Eq. (4.44). (a) Trajectories of the state variables $x_i(t)$. (b) Time series of the unwrapped phases $\vartheta_i(t)$. The parameter values are $\omega_1 = 1.02, \omega_2 = 0.98$, and $\alpha = 0.01$. The system was integrated using the Euler-Maruyama method with a time step $\Delta t = 0.01$ and $M = 10^5$ data points each starting from initial conditions $[x_i(0), \dot{x}_i(0)]^T = [1, 0]$.

Source: Elaborated by the author.

In reconstructing the phase equations, the next step is to compute numerically the derivatives of all phases $\vartheta_i(t)$, and we aim to fit the unknown coefficients of the phase model of each oscillator which can be described by the following stochastic differential equations

$$\frac{d\vartheta_i}{dt} = F_i(\vartheta_i, \vartheta_j) + \eta_i(t), \quad i = 1, 2, \tag{4.50}$$

from the data $\dot{\vartheta}_i(t)$. In practice, we assume that the function F_i can be written as a linear combination of a finite set $\mathscr{L}$ of candidate functions as

$$F_i(\vartheta_i, \vartheta_j) = \sum_{k=1}^{K} c_{i,k} \boldsymbol{\phi}_k(\boldsymbol{\vartheta}(t)) \tag{4.51}$$

where $\boldsymbol{\phi}_k(\boldsymbol{\vartheta}(t)) \in \mathscr{L}$ are K pre-chosen basis functions, and the coefficients $\{c_{i,k}\}$ are unknown parameters to be determined from the data. In this case, we choose the following trigonometric basis functions:

$$\mathscr{L} = \{1, \sin(\vartheta_i), \cos(\vartheta_i), \sin(\vartheta_i - \vartheta_j), \cos(\vartheta_i - \vartheta_j)\}, \tag{4.52}$$

for each $i, j = 1, 2$ and $i \neq j$. This counts for $K = 7$ basis functions.

The results obtained using Bayesian inference and SINDy are displayed in table 2. The results in table 2 show that the only terms that survive in the dynamics of ϑ_i are the natural frequencies ω_i and the diffusive coupling $\cos(\vartheta_1 - \vartheta_2)$ with coupling parameter ~ 0.005, correct to three decimal places. This conclusion agrees with both methods. In Bayesian inference, the noise terms $\eta_i(t)$ are also estimated.

Table 2 – Model reconstruction from a 2-dimensional time series data of length $M = 10^5$ obtained by simulating system (4.44) with model parameter values $\omega_1 = 0.1.02, \omega_2 = 0.98$, and $\alpha = 0.01$ and noise intensity $D = 5 \times 10^{-4}$. Bayesian inference is implemented for a single block of data of time $t = 1000\ s$ to obtain the inferred mean values of the coefficients $\{c_{i,k}\}$. SINDy is implemented with a thresholding parameter of $\lambda = \frac{\alpha}{10}$. In both case, we considered $K = 7$ basis functions $\boldsymbol{\phi_k} \in \mathscr{L}$.

index	$\boldsymbol{\phi}_k \in \mathscr{L}$	Bayesian Inference		SINDy	
		$\dot{\theta}_1$	$\dot{\theta}_2$	$\dot{\theta}_1$	$\dot{\theta}_2$
0	1	1.022	0.982	1.0216	0.9816
1	$\sin\theta_1$	0.	0.	0.	0.
2	$\sin\theta_2$	0.	0.	0.	0.
3	$\cos\theta_1$	0.	0.	0.	0.
4	$\cos\theta_2$	0.	0.	0.	0.
5	$\sin(\theta_1 - \theta_2)$	0.	0.	0.	0.
6	$\cos(\theta_1 - \theta_2)$	-0.0055	-0.004487	-0.0055	-0.0045

Source: Elaborated by the author.

4.4 Emergence of hypernetworks from networks of weakly coupled oscillators

4.4.1 Introduction

Many natural systems ranging from biology (ASHRAF *et al.*, 2016), physics (NIXON *et al.*, 2013; MATHENY *et al.*, 2014), and chemistry (SEBEK; TÖNJES; KISS, 2016) to neuroscience (ERMENTROUT; TERMAN, 2012) are rhythmical in nature and can be well modeled using networks of coupled limit-cycle oscillators. The collective dynamics of such systems can be studied and derived from the interactions of such networks (OMEL'CHENKO; WOLFRUM, 2012). Moreover, other emergent phenomena of such systems can be derived from the pairwise interactions of such networks. The phase reduction theory (NAKAO, 2015) can be used to analyze such networks of coupled oscillators by explicitly introducing the phases to reduce the dynamics. Phase reduction of first-order approximation is usually valid for small coupling. Derivation of higher-order corrections would extend the validity of the phase reduction beyond small coupling strength. This would help us understand complex networks' dynamics and other emergent phenomena.

In this section, we aim to show a case where although the dynamics in the network are purely pairwise, due to the nonlinearity of the coupling functions, we reveal higher-order interaction terms (hypernetworks). We first employ the perturbative theory to explicitly obtain phase equations with higher-order interaction terms. We demonstrate this by deriving the second-order phase equations followed by the averaging approach for a ring network of four weakly coupled limit cycle oscillators. Finally, we verify the result using sparse model recovery from simulated data.

4.4.2 Network dynamics of coupled limit-cycle oscillators

We consider a network of N coupled oscillators, where the governing equations of each oscillator $j \in \{1,\dots,N\}$ is given by

$$\dot{z}_j = f_j(z_j) + \alpha \sum_{k=1}^{N} A_{jk} h_j(z_j, z_k), \tag{4.53}$$

where $z_j \in \mathbb{C}$ is the state of the jth oscillator, $f_j : \mathbb{C} \to \mathbb{C}$ is its isolated vector field, $h_j : \mathbb{C} \times \mathbb{C} \to \mathbb{C}$ is the pairwise coupling function, $\boldsymbol{A} = (A_{jk})_{j,k=1}^{N}$ is the adjacent matrix describing the network structure, and $\alpha > 0$ is the coupling strength. We assume that the isolated dynamics of the oscillators are described by

$$f_j(z_j) = (\gamma + i\omega_j) z_j + \beta_j |z_j|^2 z_j \tag{4.54}$$

where $i^2 = -1$, the parameter $\lambda \in \mathbb{R}$, and $\omega_j \in \mathbb{R}$ are the natural frequency of the ith oscillator. Throughout we fix $\beta_j = -1$, but this value is immaterial.

Assumptions on ω_j and α. The frequencies ω_j satisfy the resonance condition:

$$\omega_1 + \omega_3 - \omega_2 \approx 0 \text{ and } \omega_1 + \omega_3 - \omega_4 \approx 0$$

and the coupling is assumed small, i.e., $\alpha \ll 1$.

The network structure is a 4-node ring. We consider a 4-node ring network (figure 15a) with a coupling function of the form

$$h(z, w) = (z + z^2)\bar{w}. \tag{4.55}$$

In rectangular coordinates $z_k = x_k + iy_k$, we may re-express the dynamics (4.53) in a $2N$-dimensional Euclidean space, via

$$\begin{aligned} \dot{x}_k &= \gamma x_k - \omega_k y_k + \beta(x_k^2 + y_k^2)x_k + \alpha \sum_{l=1}^{N} A_{kl} \left[((x_k + (x_k^2 - y_k^2))x_l + (y_k + 2x_k y_k)y_l \right] \\ \dot{y}_k &= \gamma y_k + \omega_k x_k + \beta(x_k^2 + y_k^2)y_k + \alpha \sum_{l=1}^{N} A_{kl} \left[(y_k + 2x_k y_k)x_l - (x_k + (x_k^2 - y_k^2))y_l \right]. \end{aligned} \tag{4.56}$$

In the absence of coupling (i.e. $\alpha = 0$), using polar coordinates $z_k = r_k e^{i\theta_k}$, the equations for the amplitude r_k and the angle variable θ_k can be decoupled into:

$$\begin{aligned} \dot{r}_k &= r_k(\gamma - r_k^2), \\ \dot{\theta}_k &= \omega_k \end{aligned}$$

for each $k = 1,2,3,4$. Hence for $\gamma > 0$ and $\alpha = 0$ there is an exponentially limit cycle $\{u(t)\}$ with a radius $r_k = r_*(\gamma) = \sqrt{\gamma}$, and with angular frequency ω_k. So, when the oscillators are uncoupled, there is an attracting 4-torus $\mathbb{T}^4$.

(a) The original network (b) Emergent hypernetwork

Figure 15 – (a) The emergent hypernwtwork from the original ring network with a coupling function of the form $h(z,w) = (z+z^2)\bar{w}$. The frequencies ω_k satisfy resonance conditions $\omega_2 \approx \omega_1 + \omega_3 \approx \omega_4$. We also observe the emergence of diffusive coupling of oscillators 2 and 4.

Source: Elaborated by the author.

For small coupling, the 4-torus is persistent, due to the exponentially stable limit cycle (HIRSCH; PUGH; SHUB, 1977; ELDERING, 2013b). In this case, the phase reduction method guarantees us that the network dynamics can be reduced to phase equations (KURAMOTO, 1984b; NAKAO, 2015), and the most relevant information about the system can be obtained from it.

4.4.3 Phase dynamics via phase reduction

Introducing the amplitudes and the phase variables according to $z_k = r_k \exp(i\theta_k)$, we obtain a system of equations in the form:

$$\dot{r}_1 = \gamma r_1 - r_1^3 + \alpha\left[r_1 r_4 \cos(\theta_4) + r_1 r_2 \cos(\theta_2) + r_1^2 r_4 \cos(\theta_1 - \theta_4) + r_1^2 r_2 \cos(\theta_1 - \theta_2)\right] \tag{4.57}$$

$$\dot{r}_2 = \gamma r_2 - r_2^3 + \alpha\left[r_2 r_1 \cos(\theta_1) + r_2 r_3 \cos(\theta_3) + r_2^2 r_1 \cos(\theta_2 - \theta_1) + r_2^2 r_3 \cos(\theta_2 - \theta_3)\right] \tag{4.58}$$

$$\dot{r}_3 = \gamma r_3 - r_3^3 + \alpha\left[r_3 r_2 \cos(\theta_2) + r_3 r_4 \cos(\theta_4) + r_3^2 r_2 \cos(\theta_3 - \theta_2) + r_3^2 r_4 \cos(\theta_3 - \theta_4)\right] \tag{4.59}$$

$$\dot{r}_4 = \gamma r_4 - r_4^3 + \alpha\left[r_4 r_3 \cos(\theta_3) + r_4 r_1 \cos(\theta_1) + r_4^2 r_3 \cos(\theta_4 - \theta_3) + r_4^2 r_1 \cos(\theta_4 - \theta_1)\right] \tag{4.60}$$

$$\dot{\theta}_1 = \omega_1 + \alpha\left[-r_4 \sin(\theta_4) - r_2 \sin(\theta_2) + r_1 r_4 \sin(\theta_1 - \theta_4) + r_1 r_2 \sin(\theta_1 - \theta_2)\right] \tag{4.61}$$

$$\dot{\theta}_2 = \omega_2 + \alpha\left[-r_1 \sin(\theta_1) - r_3 \sin(\theta_3) + r_2 r_1 \sin(\theta_2 - \theta_1) + r_2 r_3 \sin(\theta_2 - \theta_3)\right] \tag{4.62}$$

$$\dot{\theta}_3 = \omega_3 + \alpha\left[-r_2 \sin(\theta_2) - r_4 \sin(\theta_4) + r_3 r_2 \sin(\theta_3 - \theta_2) + r_3 r_4 \sin(\theta_3 - \theta_4)\right] \tag{4.63}$$

$$\dot{\theta}_4 = \omega_4 + \alpha\left[-r_3 \sin(\theta_3) - r_1 \sin(\theta_1) + r_4 r_3 \sin(\theta_4 - \theta_3) + r_4 r_1 \sin(\theta_4 - \theta_1)\right] \tag{4.64}$$

In the zero-order of α, the amplitude dynamics, equations (4.57)–(4.60), become

$$r_k = \sqrt{\gamma} + O(\alpha), \tag{4.65}$$

Substituting these expressions of r_k in the expressions of $\dot{\theta}_k$, equations (4.61)–(4.64), we obtain the phase equations in the leading order of α as:

$$\begin{aligned}
\dot{\theta}_1 &= \omega_1 - \alpha\sqrt{\gamma}[\sin\theta_2 + \sin\theta_4] + \alpha\gamma[\sin(\theta_1-\theta_2) + \sin(\theta_1-\theta_4)] + O(\alpha^2),\\
\dot{\theta}_2 &= \omega_2 - \alpha\sqrt{\gamma}[\sin\theta_1 + \sin\theta_3] + \alpha\gamma[\sin(\theta_2-\theta_1) + \sin(\theta_2-\theta_3)] + O(\alpha^2),\\
\dot{\theta}_3 &= \omega_3 - \alpha\sqrt{\gamma}[\sin\theta_2 + \sin\theta_4] + \alpha\gamma[\sin(\theta_3-\theta_2) + \sin(\theta_3-\theta_4)] + O(\alpha^2),\\
\dot{\theta}_4 &= \omega_4 - \alpha\sqrt{\gamma}[\sin\theta_1 + \sin\theta_3] + \alpha\gamma[\sin(\theta_4-\theta_1) + \sin(\theta_4-\theta_3)] + O(\alpha^2).
\end{aligned} \tag{4.66}$$

In the first order in α, we see that the coupling structure of the original network is preserved. However, we aim to recover hypernetworks from data. To this end, we introduce new phase variables as

$$\vartheta_k(t) := \theta_k(t) - \Omega_k t, \quad k \in \{1,\dots,N\}, \tag{4.67}$$

where each frequency Ω_k satisfies the resonance condition

$$\Omega_1 - \Omega_2 + \Omega_3 = 0 \text{ and } \Omega_1 - \Omega_4 + \Omega_3 = 0. \tag{4.68}$$

In terms of the new phases $\vartheta_k(t)$, the phase equations (4.66) are reduced into:

$$\begin{aligned}
\dot{\vartheta}_1 &= \delta_1 - \alpha\left(\sqrt{\gamma}[\sin(\vartheta_2+\Omega_2 t) + \sin(\vartheta_4+\Omega_4 t)] - \gamma[\sin(\vartheta_1-\vartheta_2-\Omega_3 t) + \sin(\vartheta_1-\vartheta_4-\Omega_3 t)]\right)\\
&\quad + O(\alpha^2),\\
\dot{\vartheta}_2 &= \delta_2 - \alpha\left(\sqrt{\gamma}[\sin(\vartheta_1+\Omega_1 t) + \sin(\vartheta_3+\Omega_3 t)] - \gamma[\sin(\vartheta_2-\vartheta_1+\Omega_3 t) + \sin(\vartheta_2-\vartheta_3+\Omega_1 t)]\right)\\
&\quad + O(\alpha^2),\\
\dot{\vartheta}_3 &= \delta_3 - \alpha\left(\sqrt{\gamma}[\sin(\vartheta_2+\Omega_2 t) + \sin(\vartheta_4+\Omega_4 t)] - \gamma[\sin(\vartheta_3-\vartheta_2-\Omega_1 t) + \sin(\vartheta_3-\vartheta_4-\Omega_1 t)]\right)\\
&\quad + O(\alpha^2),\\
\dot{\vartheta}_4 &= \delta_4 - \alpha\left(\sqrt{\gamma}[\sin(\vartheta_1+\Omega_1 t) + \sin(\vartheta_3+\Omega_3 t)] - \gamma[\sin(\vartheta_4-\vartheta_1+\Omega_3 t) + \sin(\vartheta_4-\vartheta_3+\Omega_1 t)]\right)\\
&\quad + O(\alpha^2),
\end{aligned} \tag{4.69}$$

where $\delta_k := \omega_k - \Omega_k \approx O(\alpha)$, for each k. It can be easily seen that each $\dot{\vartheta}_k$ is $O(\alpha)$. Then, $\vartheta_k(t)$ is a slowly varying variable, while $\Omega_k t$ varies rapidly. Thus, we may approximate the right-hand side of the last equation by integrating it over one period T of the fast oscillation, assuming that $\vartheta_k(t)$ does not vary within T.

The last equations can be rewritten as

$$\dot{\vartheta}_k = \delta_k + \alpha\Gamma_k(\boldsymbol{\vartheta}, t) + O(\alpha^2), \quad k \in \{1,2,3,4\}, \tag{4.70}$$

where Γ_k is the phase coupling function of oscillator k. The idea is to apply the averaging theorem (SANDERS; VERHULST; MURDOCK, 2007, Theorem 4.3.6) on equation (4.70). We notice that Γ_k is a sum of periodic functions in t, and hence is almost periodic in t. In particular, we can apply (SANDERS; VERHULST; MURDOCK, 2007, Lemma 4.6.5) which corresponds to our

case, in which the vector field is decomposed as a finite sum of periodic vector fields. Without loss of generality, we can decompose Γ_1 as a finite sum of m periodic vector fields

$$\Gamma_1(\boldsymbol{\vartheta},t) = \sum_{k=1}^{m} \Gamma_1^k(\boldsymbol{\vartheta},t).$$

It follows that the averaged vector field is given by

$$\begin{aligned}\bar{\Gamma}_1(\boldsymbol{\vartheta}) &:= \lim_{T\to 0} \frac{1}{T}\int_0^T \Gamma_1(\boldsymbol{\vartheta},t)\,dt = \lim_{T\to 0} \frac{1}{T}\int_0^T \sum_{k=1}^{m} \Gamma_1^k(\boldsymbol{\vartheta},t)\,dt \\ &= \lim_{T\to 0} \sum_{k=1}^{m} \frac{1}{T_k}\int_0^{T_k} \Gamma_1^k(\boldsymbol{\vartheta},t)\,dt.\end{aligned}$$

In particular, we see that the first two terms in the sum are of period $T = \frac{2\pi}{\Omega_2}$, whereas the last two terms in the sum are of period $\frac{2\pi}{\Omega_3}$. Let us introduce new phase variables

$$\varphi_1 = \vartheta_2 + \Omega_2 t, \varphi_2 = \vartheta_4 + \Omega_4 t, \varphi_3 = \vartheta_1 - \vartheta_2 - \Omega_3 t, \varphi_4 = \vartheta_1 - \vartheta_4 - \Omega_3 t.$$

So, we apply the averaging theorem as follows:

$$\begin{aligned}\bar{\Gamma}_1(\boldsymbol{\vartheta}) &:= \frac{\sqrt{\gamma}}{2\pi}\left\{\int_0^{2\pi} \sin(\varphi_1)d\varphi_1 + \int_0^{2\pi} \sin(\varphi_2)d\varphi_2\right\} + \frac{\gamma}{2\pi}\left\{\int_0^{2\pi} \sin(\varphi_3)d\varphi_3 + \int_0^{2\pi} \sin(\varphi_4)d\varphi_4\right\} \\ &= 0.\end{aligned}$$

We see that the whole interaction terms which are linear in α vanish. This shows that the phase reduction in the leading order of α is not enough to analyze the network dynamics. And hence we require higher-order phase reduction. In this context, we only focus on the second-order phase reduction. In doing this, instead of the amplitude dynamics given in equation (4.65) where the amplitudes r_k are assumed constant and equal to the amplitude of the stable limit cycle, we assume that the amplitudes r_k is a function of the phases (GENGEL *et al.*, 2020), where they studied theoretical analysis of higher-order phase reduction in networks of coupled oscillators.

Second-order phase reduction. Applying the perturbation method (KURAMOTO, 1984a; GENGEL *et al.*, 2020), we assume that the amplitude r_k is a function of the phases:

$$r_k = \sqrt{\gamma} + \alpha R_k^{(1)}(\theta_1,\theta_2,\dots) + \alpha^2 R_k^{(2)}(\theta_1,\theta_2,\dots) + \dots, \quad k = 1,2,3,4, \tag{4.71}$$

where $R_k^{(1)}, R_k^{(2)}, \dots$ are unknown functions of the phases to be determined. Since we are limiting our discussion to second-order phase approximations, obtaining $R_k^{(1)}$ for each $k = 1,2,3,4$ would be enough in this context. We see that

$$\begin{aligned} r_m r_k &= \gamma + \alpha\sqrt{\gamma}\left(R_m^{(1)} + R_k^{(1)}\right) + \dots; \\ r_m^2 r_k &= \gamma^{3/2} + \alpha\gamma\left(R_k^{(1)} + 2R_m^{(1)}\right) + \dots, \quad m,k = 1,2,3,4.\end{aligned}$$

Substituting the last expressions of r_k in equations (4.61)–(4.64), we obtain the following expressions for the dynamics of the phases, up to the order α^2:

$$\begin{aligned}
\dot{\theta}_1 &= \omega_1 - \alpha\sqrt{\gamma}(\sin(\theta_4)+\sin(\theta_2)) + \alpha\gamma(\sin(\theta_1-\theta_4)+\sin(\theta_1-\theta_2)) - \alpha^2(R_4^{(1)}\sin\theta_4 + R_2^{(1)}\sin\theta_2) \\
&\quad + \alpha^2\sqrt{\gamma}(R_1^{(1)}+R_4^{(1)})\sin(\theta_1-\theta_4) + \alpha^2\sqrt{\gamma}(R_1^{(1)}+R_2^{(1)})\sin(\theta_1-\theta_2) + \dots, \\
\dot{\theta}_2 &= \omega_2 - \alpha\sqrt{\gamma}(\sin(\theta_1)+\sin(\theta_3)) + \alpha\gamma(\sin(\theta_2-\theta_1)+\sin(\theta_2-\theta_3)) - \alpha^2(R_1^{(1)}\sin\theta_1 + R_3^{(1)}\sin\theta_3) \\
&\quad + \alpha^2\sqrt{\gamma}(R_1^{(1)}+R_2^{(1)})\sin(\theta_2-\theta_1) + \alpha^2\sqrt{\gamma}(R_3^{(1)}+R_2^{(1)})\sin(\theta_2-\theta_3) + \dots, \\
\dot{\theta}_3 &= \omega_3 - \alpha\sqrt{\gamma}(\sin(\theta_2)+\sin(\theta_4)) + \alpha\gamma(\sin(\theta_3-\theta_2)+\sin(\theta_3-\theta_4)) - \alpha^2(R_2^{(1)}\sin\theta_2 + R_4^{(1)}\sin\theta_4) \\
&\quad + \alpha^2\sqrt{\gamma}(R_2^{(1)}+R_3^{(1)})\sin(\theta_3-\theta_2) + \alpha^2\sqrt{\gamma}(R_4^{(1)}+R_3^{(1)})\sin(\theta_3-\theta_4) + \dots, \\
\dot{\theta}_4 &= \omega_4 - \alpha\sqrt{\gamma}(\sin(\theta_3)+\sin(\theta_1)) + \alpha\gamma(\sin(\theta_4-\theta_3)+\sin(\theta_4-\theta_1)) - \alpha^2(R_3^{(1)}\sin\theta_3 + R_1^{(1)}\sin\theta_1) \\
&\quad + \alpha^2\sqrt{\gamma}(R_3^{(1)}+R_4^{(1)})\sin(\theta_4-\theta_3) + \alpha^2\sqrt{\gamma}(R_1^{(1)}+R_4^{(1)})\sin(\theta_4-\theta_1) + \dots.
\end{aligned} \tag{4.72}$$

Next, we have to evaluate the function $R_k^{(1)}$. This is accomplished by substituting expressions (4.71) in the equations for the amplitudes in equations (4.57)–(4.59) and (4.60). To this end, we get

$$\alpha\frac{dR_1^{(1)}}{dt} + \dots = \alpha\left\{(-2\gamma)R_1^{(1)} + \gamma(\cos(\theta_4)+\cos(\theta_2)) + \gamma^{3/2}(\cos(\theta_1-\theta_4)+\cos(\theta_1-\theta_2))\right\} + \dots.$$

Equating the terms of powers of α, we obtain that

$$\frac{dR_1^{(1)}}{dt} = -2\gamma R_1^{(1)} + \gamma(\cos(\theta_4)+\cos(\theta_2)) + \gamma^{3/2}(\cos(\theta_1-\theta_4)+\cos(\theta_1-\theta_2)), \tag{4.73}$$

and so on. Here the time derivatives are calculated according to the chain rule, as the function $R_k^{(1)}$ is assumed to be a function of phases θ_k.

$$\frac{dR_1^{(1)}}{dt} = \frac{\partial R_1^{(1)}}{\partial\theta_1}\dot{\theta}_1 + \frac{\partial R_1^{(1)}}{\partial\theta_2}\dot{\theta}_2 + \frac{\partial R_1^{(1)}}{\partial\theta_3}\dot{\theta}_3 + \frac{\partial R_1^{(1)}}{\partial\theta_4}\dot{\theta}_4 \approx \frac{\partial R_1^{(1)}}{\partial\theta_1}\omega_1 + \frac{\partial R_1^{(1)}}{\partial\theta_2}\omega_2 + \frac{\partial R_1^{(1)}}{\partial\theta_3}\omega_3 + \frac{\partial R_1^{(1)}}{\partial\theta_4}\omega_4, \tag{4.74}$$

we have used the zero-order expressions for the derivatives $\dot{\theta}_k$, i.e. we assumed $\dot{\theta}_k \approx \omega_k$.

We can rewrite equation (4.73) as:

$$\frac{\partial R_1^{(1)}}{\partial\theta_1}\omega_1 + \frac{\partial R_1^{(1)}}{\partial\theta_2}\omega_2 + \frac{\partial R_1^{(1)}}{\partial\theta_3}\omega_3 + \frac{\partial R_1^{(1)}}{\partial\theta_4}\omega_4 + 2\gamma R_1^{(1)} = \mathscr{G}_1(\theta_1,\dots,\theta_4), \tag{4.75}$$

where

$$\mathscr{G}_1(\theta_1,\dots,\theta_4) := \gamma(\cos(\theta_4)+\cos(\theta_2)) + \gamma^{3/2}(\cos(\theta_1-\theta_4)+\cos(\theta_1-\theta_2)) \tag{4.76}$$

We notice that the problem of determining the function $R_1^{(1)}$ is reduced to solving a partial differential equation (PDE).

Notice that $\mathscr{G}_1(\theta_1,\ldots,\theta_4)$ is 2π-periodic in its arguments $\theta_1\ldots,\theta_4$, and hence can be expressed using Fourier series as

$$\mathscr{G}_1(\theta_1,\ldots,\theta_4)=\sum_{m_1,\ldots,m_4} g_{m_1,\ldots,m_4}\mathrm{e}^{i(m_1\theta_1+\cdots+m_4\theta_4)}.$$

This implies the right-hand side of the amplitude dynamics r_k can be expressed using the Fourier series.

We consider the following ansatz for the function $R_1^{(1)}$ as:

$$R_1^{(1)}=\sum_{m_1,\ldots,m_4}\rho_{m_1,\ldots,m_4}\mathrm{e}^{i(m_1\theta_1+\cdots+m_4\theta_4)}.$$

where the Fourier coefficients $\rho_{m_1,\ldots,m_4}$ are unknown to be determined. Then, the partial derivatives of $R_1^{(1)}$ with respect to the phases θ_k are

$$\begin{aligned}
\frac{\partial R_1^{(1)}}{\partial\theta_1}&=im_1\sum_{m_1,\ldots,m_4}\rho_{m_1,\ldots,m_4}\mathrm{e}^{i(m_1\theta_1+\cdots+m_4\theta_4)}=im_1R_1^{(1)},\\
\frac{\partial R_1^{(1)}}{\partial\theta_2}&=im_2\sum_{m_1,\ldots,m_4}\rho_{m_1,\ldots,m_4}\mathrm{e}^{i(m_1\theta_1+\cdots+m_4\theta_4)}=im_2R_1^{(1)},\\
\frac{\partial R_1^{(1)}}{\partial\theta_3}&=im_3\sum_{m_1,\ldots,m_4}\rho_{m_1,\ldots,m_4}\mathrm{e}^{i(m_1\theta_1+\cdots+m_4\theta_4)}=im_3R_1^{(1)},\\
\frac{\partial R_1^{(1)}}{\partial\theta_4}&=im_4\sum_{m_1,\ldots,m_4}\rho_{m_1,\ldots,m_4}\mathrm{e}^{i(m_1\theta_1+\cdots+m_4\theta_4)}=im_4R_1^{(1)}.
\end{aligned}$$

Substituting these last expressions into equation (4.75) and equating the coefficients of the Fourier terms, we obtain the Fourier coefficients of $R_1^{(1)}$. It follows that the Fourier coefficients of $R_1^{(1)}$ are given by

$$\rho_{m_1,\ldots,m_4}=\frac{g_{m_1,\ldots,m_4}}{2\gamma+i(\omega_1m_1+\omega_2m_2+\omega_3m_3+\omega_4m_4)}. \tag{4.77}$$

Using this last expression and equation (4.75), we obtain that

$$\begin{aligned}
R_1^{(1)}&=a_4'\cos(\theta_4)+b_4'\sin(\theta_4)+a_2'\cos(\theta_2)+b_2'\sin(\theta_2)+c_{1,4}'\cos(\theta_1-\theta_4)+d_{1,4}'\sin(\theta_1-\theta_4)\\
&\quad+c_{1,2}'\cos(\theta_1-\theta_2)+d_{1,2}'\sin(\theta_1-\theta_2), &(4.78)\\
R_2^{(1)}&=a_1'\cos(\theta_1)+b_1'\sin(\theta_1)+a_3'\cos(\theta_3)+b_3'\sin(\theta_3)+c_{2,1}'\cos(\theta_2-\theta_1)+d_{2,1}'\sin(\theta_2-\theta_1)\\
&\quad+c_{2,3}'\cos(\theta_2-\theta_3)+d_{2,3}'\sin(\theta_2-\theta_3), &(4.79)\\
R_3^{(1)}&=a_2'\cos(\theta_2)+b_2'\sin(\theta_2)+a_4'\cos(\theta_4)+b_4'\sin(\theta_4)+c_{3,2}'\cos(\theta_3-\theta_2)+d_{3,2}'\sin(\theta_3-\theta_2)\\
&\quad+c_{3,4}'\cos(\theta_3-\theta_4)+d_{3,4}'\sin(\theta_3-\theta_4), &(4.80)\\
R_4^{(1)}&=a_3'\cos(\theta_3)+b_3'\sin(\theta_3)+a_1'\cos(\theta_1)+b_1'\sin(\theta_1)+c_{4,3}'\cos(\theta_4-\theta_3)+d_{4,3}'\sin(\theta_4-\theta_3)\\
&\quad+c_{4,1}'\cos(\theta_4-\theta_1)+d_{4,1}'\sin(\theta_4-\theta_1), &(4.81)
\end{aligned}$$

where we have used the definitions

$$a'_m = \frac{2\gamma^2}{4\gamma^2+\omega_m^2}, \quad b'_m = \frac{\omega_m\gamma}{4\gamma^2+\omega_m^2},$$
$$c'_{m,k} = \frac{2\gamma^2}{4\gamma^2+(\omega_m-\omega_k)^2}, \quad d'_{m,k} = \frac{(\omega_m-\omega_k)\gamma^{3/2}}{4\gamma^2+(\omega_m-\omega_k)^2}. \tag{4.82}$$

Substitution of the expressions $R_1^{(1)}, R_2^{(1)}, R_3^{(1)}$, and $R_4^{(1)}$ in equation (4.72) completes the second-order phase reduction and yields closed equations for $\dot{\theta}_k$ for each $k = 1,2,3,4$. In this case, we obtain the phase equations

$$\dot{\theta}_1 = \omega_1 - \alpha\sqrt{\gamma}(\sin(\theta_4)+\sin(\theta_2)) + \alpha\gamma(\sin(\theta_1-\theta_4)+\sin(\theta_1-\theta_2)) + \alpha^2\Gamma_1^2(\theta_1,\theta_2,\theta_3,\theta_4), \tag{4.83}$$

$$\dot{\theta}_2 = \omega_2 - \alpha\sqrt{\gamma}(\sin(\theta_1)+\sin(\theta_3)) + \alpha\gamma(\sin(\theta_2-\theta_1)+\sin(\theta_2-\theta_3)) + \alpha^2\Gamma_2^2(\theta_1,\theta_2,\theta_3,\theta_4), \tag{4.84}$$

$$\dot{\theta}_3 = \omega_3 - \alpha\sqrt{\gamma}(\sin(\theta_2)+\sin(\theta_4)) + \alpha\gamma(\sin(\theta_3-\theta_2)+\sin(\theta_3-\theta_4)) + \alpha^2\Gamma_3^2(\theta_1,\theta_2,\theta_3,\theta_4), \tag{4.85}$$

$$\dot{\theta}_4 = \omega_4 - \alpha\sqrt{\gamma}(\sin(\theta_3)+\sin(\theta_1)) + \alpha\gamma(\sin(\theta_4-\theta_3)+\sin(\theta_4-\theta_1)) + \alpha^2\Gamma_4^2(\theta_1,\theta_2,\theta_3,\theta_4) \tag{4.86}$$

in order of α^2.

The expressions of the functions $\Gamma_k^2(\cdot)$ are given in the appendix B in equations (B.1)–(B.3) and (B.4). From these expressions, we now explain the terms that appear in the second order of α.

Considering the dynamics of $\dot{\theta}_1$, for example, we observe that in the second order approximation; there are constant terms and terms containing the second harmonics of the phase difference, e.g. $\sim \cos(2\theta_1 - 2\theta_2)$. These terms do not arise from the interaction within the network. Moreover, there are higher-order interactions such as $\sim \sin(\theta_1+\theta_3-\theta_4)$ and $\sim \cos(2\theta_2-\theta_3-\theta_1)$ appear in the dynamics. This shows the emergence of hypernetworks from only pairwise couplings. The goal is to recover hypernetworks from data.

Introducing new phase variables

$$\vartheta_k(t) = \theta_k(t) - \Omega_k t, \quad k \in \{1,\ldots,N\}, \tag{4.87}$$

where each frequency Ω_k satisfies the resonance conditions in equation (4.68). In terms of the new phases, we have

$$\dot{\vartheta}_k = \delta_k + \alpha\Gamma_k^1(\vartheta_1,\vartheta_2,\vartheta_3,\vartheta_4;t) + \alpha^2\Gamma_k^2(\vartheta_1,\vartheta_2,\vartheta_3,\vartheta_4;t) + O(\alpha^3), \quad k \in \{1,2,3,4\}, \tag{4.88}$$

where $\delta_k = \omega_k - \Omega_k \approx O(\alpha)$, and the phase coupling functions $\Gamma_k^1(\cdot)$ and $\Gamma_k^2(\cdot)$, respectively, are of order $\sim \alpha$ and $\sim \alpha^2$ terms in equations (4.83)–(4.86), which are periodic functions in t. In particular, the functions $\Gamma_k^1(\cdot)$ and $\Gamma_k^2(\cdot)$ can be decomposed as a finite sum of periodic

functions in t. Hence, we can apply the results of (SANDERS; VERHULST; MURDOCK, 2007, Lemma 4.6.5) as in the previous discussion. In doing so, in the averaging sense, Γ_k^1 vanishes for each $k = 1,2,3,4$. Notice that $\theta_2 - \theta_4 = \vartheta_2 - \vartheta_4, \theta_1 + \theta_3 - \theta_2 = \vartheta_1 + \vartheta_3 + \vartheta_2$, and $\theta_1 + \theta_3 - \theta_4 = \vartheta_1 + \vartheta_3 - \vartheta_4$. Hence, the only terms which survive in the function Γ_k^2 are the constant terms, diffusive terms with pairwise resonant $\sim \vartheta_2 - \vartheta_4$, and the triplet interactions with triplet resonants $\sim \vartheta_1 + \vartheta_3 - \vartheta_2$ and $\sim \vartheta_1 + \vartheta_3 - \vartheta_4$. That means all non-resonant terms in α^2 are discarded. Setting

$$\begin{aligned}\phi_1 &:= \vartheta_1 + \vartheta_3 - \vartheta_2,\\ \phi_2 &:= \vartheta_1 + \vartheta_3 - \vartheta_4.\end{aligned}$$

we obtain the reduced second-order phase equation in order of α^2 as:

$$\begin{aligned}
\dot{\vartheta}_1 &= \varepsilon_1 - \alpha^2\gamma^{3/2}\left\{B_3\left[\cos(\phi_1)+\cos(\phi_2)\right] - A_3\left[\sin(\phi_1)+\sin(\phi_2)\right]\right\} + \alpha^2\gamma^2(D_{1,2}+D_{1,4})\cos(\vartheta_2-\vartheta_4)\\
\dot{\vartheta}_2 &= \varepsilon_2 - \alpha^2\gamma^{3/2}\left\{(A_1+A_3)\sin(\phi_1) - (B_1+B_3)\cos(\phi_1)\right\} + \alpha^2\gamma^2(C_{1,4}+C_{3,4})\sin(\vartheta_2-\vartheta_4)\\
&\quad + \alpha^2\gamma^2(D_{1,4}+D_{3,4})\cos(\vartheta_2-\vartheta_4)\\
\dot{\vartheta}_3 &= \varepsilon_3 - \alpha^2\gamma^{3/2}\left\{B_1\left[\cos(\phi_1)+\cos(\phi_2)\right] - A_1\left[\sin(\phi_1)+\sin(\phi_2)\right]\right\} + \alpha^2\gamma^2(D_{3,2}+D_{3,4})\cos(\vartheta_2-\vartheta_4)\\
\dot{\vartheta}_4 &= \varepsilon_4 - \alpha^2\gamma^{3/2}\left\{(A_1+A_3)\sin(\phi_2) - (B_1+B_3)\cos(\phi_2)\right\} + \alpha^2\gamma^2(C_{3,2}+C_{1,2})\sin(\vartheta_2-\vartheta_4)\\
&\quad + \alpha^2\gamma^2(D_{3,2}+D_{1,2})\cos(\vartheta_2-\vartheta_4)
\end{aligned} \tag{4.89}$$

where the constant coefficients $A_m, B_m, C_{m,k}$, and $D_{m,k}$ are defined by

$$\begin{aligned}
A_m &= \frac{1}{2}\frac{2\gamma}{4\gamma^2+\omega_m^2};\ B_m = \frac{1}{2}\frac{\omega_m}{4\gamma^2+\omega_m^2}, \quad \text{for } m = 1,3;\\
C_{m,k} &= \frac{1}{2}\frac{2\gamma}{4\gamma^2+(\omega_m-\omega_k)^2};\ D_{m,k} = \frac{1}{2}\frac{\omega_m-\omega_k}{4\gamma^2+(\omega_m-\omega_k)^2}, \quad \text{for } m,k \in \{1,2,3,4\}.
\end{aligned}$$

The constants ε_m in equation (4.89) are given by

$$\varepsilon_m = \left(\delta_m + \alpha^2\gamma^2 B_0^{(m)}\right), \quad m \in \{1,2,3,4\},$$

where

$$B_0^{(m)} = \begin{cases} 2(D_{m,2}+D_{m,4}), & \text{for } m = 1,3\\ -2(D_{1,m}+D_{3,m}), & \text{for } m = 2,4. \end{cases}$$

The phase dynamics equations (4.89) show the emergence of hypernetworks while the interaction of oscillators in the original 4-ring network is pairwise. The dynamics of oscillators 1 and 3 are impacted by both triplet interactions: ϕ_1 and ϕ_2, however, the dynamics of oscillators 2 and 4 are impacted by triplet interactions ϕ_1 and ϕ_2, respectively. All the oscillators are impacted by the pairwise interaction $\vartheta_2 - \vartheta_4$. Therefore, we can conclude that the phase dynamics of the oscillators coupled in a ring can be described by a hypernetwork shown in figure 15b.

Note that if $\gamma \ll 1$, then we see that $\gamma^2 \ll \gamma^{3/2}$. Hence, we can approximate the phase equations (4.89) and get rid of the diffusive coupling term containing $\vartheta_2 - \vartheta_4$ to obtain

$$\begin{aligned}
\dot{\vartheta}_1 &= \varepsilon_1 - \alpha^2\gamma^{3/2}\{B_3[\cos(\phi_1)+\cos(\phi_2)] - A_3[\sin(\phi_1)+\sin(\phi_2)]\} \\
\dot{\vartheta}_2 &= \varepsilon_2 - \alpha^2\gamma^{3/2}\{(A_1+A_3)\sin(\phi_1) - (B_1+B_3)\cos(\phi_1)\} \\
\dot{\vartheta}_3 &= \varepsilon_3 - \alpha^2\gamma^{3/2}\{B_1[\cos(\phi_1)+\cos(\phi_2)] - A_1[\sin(\phi_1)+\sin(\phi_2)]\} \\
\dot{\vartheta}_4 &= \varepsilon_4 - \alpha^2\gamma^{3/2}\{(A_1+A_3)\sin(\phi_2) - (B_1+B_3)\cos(\phi_2)\}.
\end{aligned} \tag{4.90}$$

These last expressions of the phase equations agree with the results in (NIJHOLT *et al.*, 2022), where they obtained only hypernetworks when the isolated dynamics are close to a Hopf bifurcation using normal forms.

In the next section, we aim at reconstructing the phase equations, given multivariate time series data $\vartheta_k(t)$, and compare the results with the theoretical findings.

4.4.4 Reconstruction of phase dynamics from data

The first ingredient is to obtain multivariate time-series data from the units of the ring. To do this, we first simulate the system (4.56) using the Runge-Kutta method of order 4 or 5 (RK45) with a uniform time step $\Delta t = 0.01$ and use $M = 1 \times 10^5$ data points each starting from the initial conditions $z_k(0) = x_k(0) + iy_k(0) = r_k(0)e^{i\theta_k(0)}$ with $r_k(0) = 1$ and the initial phases $\theta_k(0)$ are uniformly distributed and randomly chosen in the interval $[0, 2\pi]$. In our simulations, we fix the parameter values $\omega_1 = 1.01, \omega_2 = 2.5, \omega_3 = 1.5, \omega_4 = 2.49, \beta = -1, \alpha = 0.18$, and $\gamma = 1$. Hence, we obtain a multivariate time series data

$$\mathscr{Y} := \{z_k^m := z_k(t_m) : t_m = m\Delta t, m = 1,\ldots,M'; k = 1,\ldots,N\}.$$

We only store M' data points by discarding the first 5000 points as a transient time. The trajectories of the state variables $z_k(t)$ are displayed in the left panel of figure 16(a).

The next step is to estimate the phases from each time series. There are several techniques in the literature. In this subsection, we extract the unwrapped phases $\theta_k(t)$ of each oscillator from the time series of the state variables z_k using the polar decomposition $z_k(t) = r_k(t)e^{i\theta_k(t)}$, where $\theta_k(t) = \arctan(y_k(t)/x_k(t))$. The time series of the phases $\theta_k(t)$ are depicted on the right panel of figure 16(b). Figure 16(b) shows that each phase θ_k has a frequency close to ω_k, which shows that the phases increase almost linearly in time with a small coupling α.

Since the coupling is assumed small, we won't be able to recover the coupling terms from the data θ_k, or either we require a sufficiently long time series. For this reason, we need to subtract the linear trends from $\theta_k(t)$ to obtain a new data set. To this end, we introduce new phases

$$\vartheta_k(t) := \theta_k(t) - \Omega_k t, \quad k \in \{1,\ldots,N\},$$

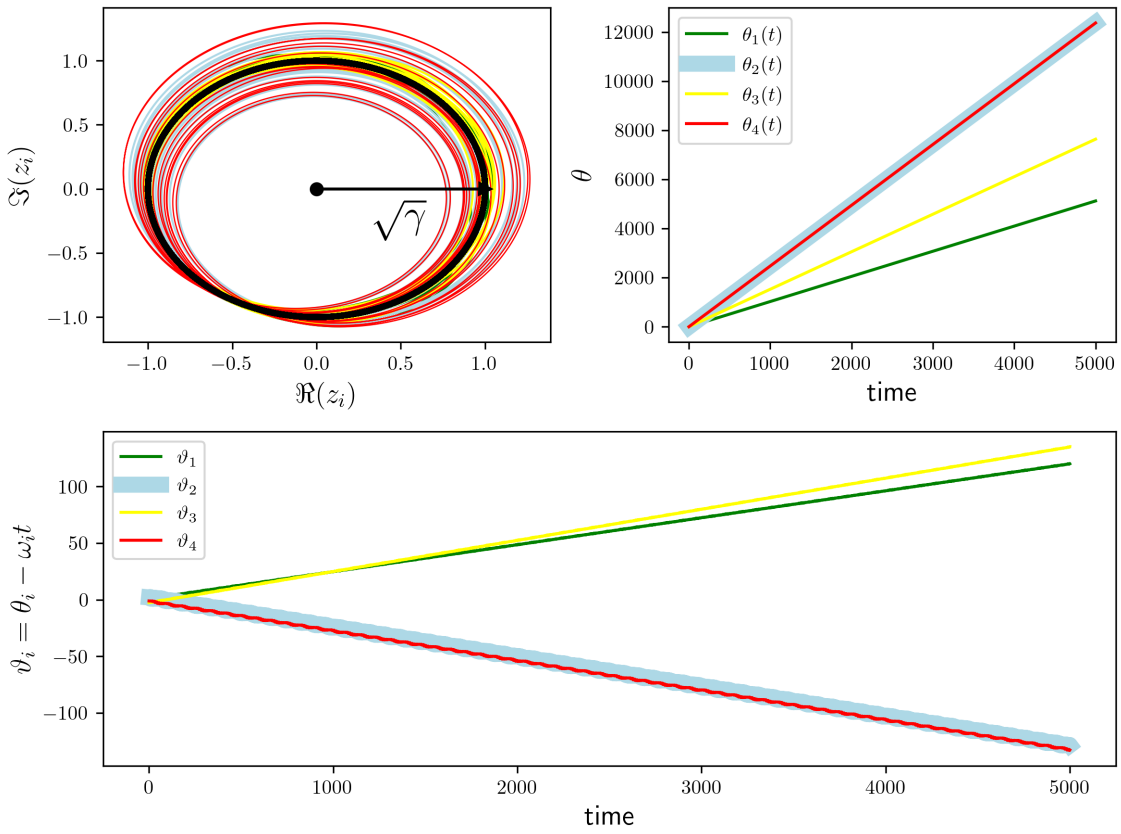

Figure 16 – **Simulations of the system** (4.53). a) Trajectories of the state variables z_k. All trajectories tend to a stable limit cycle with radius $r = \sqrt{\gamma}$. b) Time series of the unwrapped phases $\theta_k(t)$ of each oscillator k. c) The time series of the slow phases $\vartheta_k(t) = \theta_k(t) - \Omega_k t$ of each oscillator k. The parameter values are $\omega_k \in \{1.01, 2.5, 1.5, 2.49\}, \beta = -1, \alpha = 0.18$, and $\gamma = 1.0$. The system was simulated from time $t = 0$ to $t = 10000$ with a uniform time-step $\Delta t = 0.01$. We discard the first 5000 points as transient. A randomly chosen initial condition $z_k(0)$ was evolved using RK45.

Source: Elaborated by the author.

where each frequency Ω_k satisfies the resonance condition $\Omega_1 - \Omega_2 + \Omega_3 = 0$ and $\Omega_1 - \Omega_4 + \Omega_3 = 0$. Hence, we obtain a phase model from the data $\vartheta_k(t)$. The resulting phase time series $\{\vartheta_k(t_m) : t_m = m\Delta t, m = 1, \ldots, M; k = 1, 2, 3, 4\}$ of $M = 2.5 \times 10^6$ data points are used as the input for reconstructing the phase dynamics equations of each oscillator. This number of data points corresponds to approximately 4018 periods of the slowest oscillator 1 and to approximately 9948 periods of the fastest oscillators 2 and 4.

In reconstructing the phase equations, the next step is to compute numerically the time derivatives of all phases $\vartheta_k(t)$, and we aim to fit the unknown coefficients of the phase model of each oscillator. To this end, we assume that time derivatives $\dot{\vartheta}_i(t)$ can be written as linear combinations of a few subsets of a suitably chosen set of basis functions $\mathscr{L} = \{\boldsymbol{\phi}_1, \ldots, \boldsymbol{\phi}_K\}$,

with $\boldsymbol{\phi}_i : \mathbb{R}^N \to \mathbb{R}$, as

$$\dot{\vartheta}_i(t) = \sum_{k=1}^{K} c_{i,k}\boldsymbol{\phi}_k(\boldsymbol{\vartheta}(t)), \quad i = 1,2,3,4. \tag{4.91}$$

The choice of base functions for the inference needs to be determined so that the dynamics of the phases $\dot{\vartheta}_i(t)$ can be reconstructed effectively. Here, we choose the following K trigonometric basis functions $\boldsymbol{\phi}_k$:

$$\mathscr{L} = \{1, \sin(\vartheta_p), \cos(\vartheta_p), \sin(\vartheta_p - \vartheta_q), \cos(\vartheta_p - \vartheta_q), \sin(\vartheta_p + \vartheta_q - \vartheta_s), \cos(\vartheta_p + \vartheta_q - \vartheta_s)\}, \tag{4.92}$$

for each $p,q,s \in \{1,\ldots,N\}$ and $p \neq q \neq s$ for each basis function $\boldsymbol{\phi}_k \in \mathscr{L}$. One can see that the number of basis functions counts to $K = N^3 - 2N^2 + 3N + 1$, where $N = 4$. In counting the number of basis functions, we use the *variations without repetition* formula:

$$V_m(N) := \frac{N!}{(N-m)!},$$

which represents an ordered m-element group formed from a set of N elements. For example, $V_2(N) = N(N-1)$ corresponds to the total number of pairwise couplings without repetition.

Given the data set $\{\boldsymbol{\vartheta}(\boldsymbol{t})\}$, the derivative data $\{\dot{\boldsymbol{\vartheta}}(\boldsymbol{t})\}$, where $\boldsymbol{\vartheta}(t) = (\vartheta_1(t), \ldots, \vartheta_N(t))$ and $\boldsymbol{t} := \{t_1, \ldots, t_M\}$, and a set of library of functions $\mathscr{L}$, we attempt to solve the following linear problem

$$\dot{\Theta} = \boldsymbol{\Phi}(\Theta)\boldsymbol{C} \tag{4.93}$$

for the matrix of unknown coefficients $\boldsymbol{C} \in \mathbb{R}^{K\times 4}$, defined as

$$\boldsymbol{C} = \begin{bmatrix} c_{1,1} & c_{2,1} & c_{3,1} & c_{4,1} \\ \vdots & \vdots & \vdots & \vdots \\ c_{1,K} & c_{2,K} & c_{3,K} & c_{4,K} \end{bmatrix} = \begin{bmatrix} | & | & | & | \\ \boldsymbol{c}_1 & \boldsymbol{c}_2 & \boldsymbol{c}_3 & \boldsymbol{c}_4 \\ | & | & | & | \end{bmatrix}.$$

The matrices Θ and $\dot{\Theta}$ are M by 4 data and its time derivative data, defined as

$$\Theta := \begin{bmatrix} \vartheta_1(t_1) & \vartheta_2(t_1) & \vartheta_3(t_1) & \vartheta_4(t_1) \\ \vartheta_1(t_2) & \vartheta_2(t_2) & \vartheta_3(t_2) & \vartheta_4(t_2) \\ \vdots & \vdots & \vdots & \vdots \\ \vartheta_1(t_M) & \vartheta_2(t_M) & \vartheta_3(t_M) & \vartheta_4(t_M) \end{bmatrix} \quad \text{and} \quad \dot{\Theta} = \begin{bmatrix} \dot{\vartheta}_1(t_1) & \dot{\vartheta}_2(t_1) & \dot{\vartheta}_3(t_1) & \dot{\vartheta}_4(t_1) \\ \dot{\vartheta}_1(t_2) & \dot{\vartheta}_2(t_2) & \dot{\vartheta}_3(t_2) & \dot{\vartheta}_4(t_2) \\ \vdots & \vdots & \vdots & \vdots \\ \dot{\vartheta}_1(t_M) & \dot{\vartheta}_2(t_M) & \dot{\vartheta}_3(t_M) & \dot{\vartheta}_4(t_M) \end{bmatrix},$$

and $\boldsymbol{\Phi} := \boldsymbol{\Phi}(\Theta) \in \mathbb{R}^{M\times K}$ denotes the matrix of basis functions evaluated at each time point, where each column represents the K basis functions $\boldsymbol{\phi}_k$ whereas each row represents evaluations of the basis functions at each phase vector $\boldsymbol{\vartheta}^T(t_m)$ for each time step, and is known as the *library matrix* or *dictionary matrix*. Here M denotes the number of data points. We assume that we have sufficiently long enough time-series data, that is, $M \gg K$. Hence, we solve an overdetermined linear system (4.93).

In solving such inverse problems, e.g. using the ℓ_p-norm the least-squares solution of system (4.93) is obtained by solving the following ℓ_2-norm minimization problem:

$$\hat{\boldsymbol{c}}_i = \underset{\boldsymbol{c}_i \in \mathbb{R}^K}{\arg\min} \|\dot{\boldsymbol{\theta}}_i - \boldsymbol{\Phi}\boldsymbol{c}_i\|_2, \tag{4.94}$$

where $\boldsymbol{c}_i$ and $\boldsymbol{\theta}_i$ are columns of the matrices $\boldsymbol{C}$ and Θ, respectively, for each $i \in \{1,\ldots,N\}$. By the *singular value decomposition* (SVD), the problem (4.94) has an explicit solution

$$\boldsymbol{c}_i = \boldsymbol{\Phi}^{\dagger}\dot{\boldsymbol{\theta}}_i$$

where $\boldsymbol{\Phi}^{\dagger} = (\boldsymbol{\Phi}^T\boldsymbol{\Phi})^{-1}\boldsymbol{\Phi}^T$ is called the *Moore-penrose pseudo-inverse* of $\boldsymbol{\Phi}$. By assumption, the column vectors $\boldsymbol{c}_i$ of $\boldsymbol{C}$ are *sparse*, containing mostly zero entries, and the nonzero entries highlight the active terms in the dynamics of the ith oscillator.

As elaborated in section 4.2.2, we implement the SINDy algorithm (BRUNTON; PROCTOR; KUTZ, 2016). To this end, we attempt to obtain sparse solutions using regression techniques such as the sequentially thresholded least squares (STLSQ) with a thresholding parameter $\lambda > 0$. More precisely, we iteratively apply the least-squares method for the problem (4.93) with thresholding parameter $\lambda > 0$. In particular, a sparse vector $\boldsymbol{c}_i$, for each column $i = 1,\ldots,N$, which approximately solves Eq. (4.93) is generated by the following iterative scheme:

$$\boldsymbol{c}_i^{(0)} = \boldsymbol{\Phi}^{\dagger}\dot{\boldsymbol{\theta}}_i, \tag{4.95a}$$

$$S^{(n)} = \{1 \le k \le K \mid |c_{i,k}^{(n)}| \ge \lambda\},\ n \ge 0, \tag{4.95b}$$

$$\boldsymbol{c}_i^{(n+1)} = \underset{\boldsymbol{c}_i \in \mathbb{R}^K : \mathrm{supp}(\boldsymbol{c}_i) \subset S^{(n)}}{\arg\min} \|\dot{\boldsymbol{\theta}}_i - \boldsymbol{\Phi}\boldsymbol{c}_i\|_2,\ n \ge 0, \tag{4.95c}$$

where $\mathrm{supp}(\boldsymbol{c}_i)$ is the support set of $\boldsymbol{c}_i$, defined as the set of indices corresponding to its nonzero elements. Here $c_{i,k}^{(n)}$ is the kth component of the nth iteration $\boldsymbol{c}_i^{(n)}$. The procedure in Eq.(4.95) is iteratively repeated, for each oscillator $i \in \{1,\ldots,N\}$, until convergence or the maximum iteration is required. We denote the inferred sparse vector by $\hat{\boldsymbol{c}}_i$, for each i. In implementing the SINDy algorithm, we use *PySINDy*– an open-source software package that has been developed in Python (SILVA *et al.*, 2020).

Model selection: the choice of the thresholding parameter. Note that the estimated sparse vector $\hat{\boldsymbol{c}}_i$ depends on the choice of the thresholding parameter λ. At each iteration, all the coefficients with $|c_{i,k}| < \lambda$ are set to zero. Hence, the parameter λ is important because if λ is too small, the SINDy recovery model contains many nonzero coefficients and hence the sparsity fails. Conversely, if λ is large then basis functions required to emulate the dynamics of the system may be removed, resulting in a model that does not resemble the data. Hence we need to select an appropriate value of λ.

We first select *a priori* a set of 50 evenly spaced possible candidates of the thresholding parameter λ in the interval $[10^{-5}, 5\times10^{-3}]$. Each recovered coefficient vector $\hat{\boldsymbol{c}}_i := \hat{\boldsymbol{c}}_i(\lambda)$ produces an inferred phase model of varying accuracy and sparsity. From these models, we

calculate a Pareto front and select the most parsimonious model, as shown in figure 17. A Pareto front is calculated by plotting the number of terms on the x-axis vs an error indicating how well $\hat{\boldsymbol{c}}_i$ satisfies our equation ($\dot{\boldsymbol{\theta}}_i = \boldsymbol{\Phi}\boldsymbol{c}_i$), on the y-axis. The most parsimonious model is readily identifiable at the sharp drop-off in error. As we will show, this method succeeds at identifying the correct basis terms and coefficients.

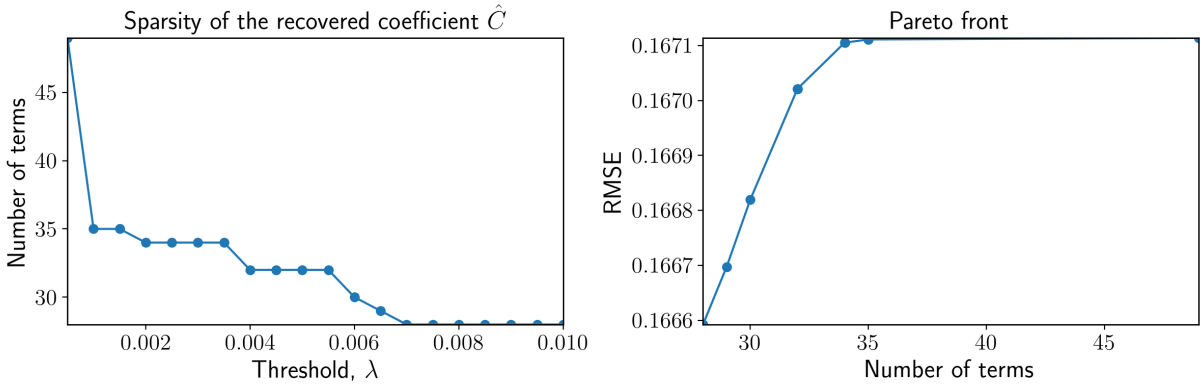

Figure 17 – Left panel: Increasing the sparsity parameter λ creates coefficient matrix $\hat{\boldsymbol{C}}$, with monotonically decreasing number of terms. Right panel: For each SINDy recovery $\hat{\boldsymbol{C}}$ we calculate RMSE and produce the Pareto front. The most parsimonious model is identified at the sharp drop-off in error, which is shown in the red spade. The parameter values are set to be $\omega_1 = 1.01, \omega_2 = 2.5, \omega_3 = 1.5, \omega_4 = 2.49, \beta = -1, \alpha = 0.18$, and $\gamma = 1.0$.

Source: Elaborated by the author.

In determining the accuracy of the recovered coefficients $\hat{\boldsymbol{c}}_i$, we choose an error metric known as *root-mean-squared error* (RMSE) on the test data. To accomplish this, we split the time-series data $\Theta \in \mathbb{R}^{M \times N}$ into a training set $\Theta_t \in \mathbb{R}^{M_t \times N}$ for inferring the parameters and a test set $\Theta_v \in \mathbb{R}^{M_v \times N}$ for evaluating the predictions. Here, M_t and M_v denote the number of data points in the training and test sets respectively. Then, for each oscillator i, the RMSE of predicted values $\hat{\dot{\boldsymbol{\theta}}}_i := \hat{\dot{\boldsymbol{\theta}}}_i(\lambda) = \boldsymbol{\Phi}\hat{\boldsymbol{c}}_i(\lambda)$ can be defined as

$$RMSE(\hat{\dot{\boldsymbol{\theta}}}_i) := \sqrt{\mathbb{E}((\hat{\dot{\boldsymbol{\theta}}}_i - \dot{\boldsymbol{\theta}}_i))^2}, \tag{4.96}$$

where $\mathbb{E}(\cdot)$ denotes the mean value. If the number of data points in the validation set is denoted by M_t, then we have

$$\mathbb{E}((\hat{\dot{\boldsymbol{\theta}}}_i - \dot{\boldsymbol{\theta}}_i))^2 = \frac{1}{M_v}\sum_{m=1}^{M_v}\left(\hat{\dot{\vartheta}}_i(t_m) - \dot{\vartheta}_i(t_m)\right)^2$$

where $\hat{\dot{\vartheta}}_i(t_m)$ and $\dot{\vartheta}_i(t_m)$ are the time derivatives and predicted values of the test data, respectively, at time t_m for each $m \in \{1, \ldots, M_v\}$.

The recovered phase equations with thresholding $\lambda = \lambda_{opt} = 0.00398$ are given by

$$\begin{aligned}
\dot{\vartheta}_1 &= 0.543 + 0.058\sin(\vartheta_2 - \vartheta_4) + 0.550\cos(\vartheta_2 - \vartheta_4) + 0.175\sin(\phi_2) - 0.170\cos(\phi_2) \\
&\quad + 0.155\sin(\phi_1) - 0.185\cos(\phi_1), \\
\dot{\vartheta}_2 &= -0.138 + 0.054\sin(\vartheta_2 - \vartheta_4) - 0.088\cos(\vartheta_2 - \vartheta_4) + 0.027\sin(\phi_2) + 0.140\cos(\phi_2) \\
&\quad - 0.021\sin(\phi_1) + 0.221\cos(\phi_1), \\
\dot{\vartheta}_3 &= 0.759 + 0.091\sin(\vartheta_2 - \vartheta_4) + 0.779\cos(\vartheta_2 - \vartheta_4) + 0.240\sin(\phi_2) - 0.231\cos(\phi_2) \\
&\quad + 0.216\sin(\phi_1) - 0.247\cos(\phi_1), \\
\dot{\vartheta}_4 &= 0.147 + 0.309\sin(\vartheta_2 - \vartheta_4) + 0.104\cos(\vartheta_2 - \vartheta_4) + 0.083\sin(\phi_2) + 0.021\cos(\phi_2) \\
&\quad + 0.258\sin(\phi_1) + 0.202\cos(\phi_1),
\end{aligned} \tag{4.97}$$

where ϕ_1 and ϕ_2 are given by the triplet interactions

$$\begin{aligned}
\phi_1 &:= \vartheta_1 + \vartheta_3 - \vartheta_2, \\
\phi_2 &:= \vartheta_1 + \vartheta_3 - \vartheta_4.
\end{aligned}$$

The recovered phase equations (4.97) show that although the data were generated from a network of pairwise couplings depicted on a ring topology (figure 15a), we recover triplet interactions and pairwise coupling as shown in figure 15b. Comparing equations (4.89) and (4.97) we see that the only mistake in the phase model reconstruction for $\gamma = 1$ is the existence of the pairwise coupling term $\cos(\vartheta_2 - \vartheta_4)$ in the dynamics of oscillator 1 and 3. Such reconstruction errors might result due to the SINDy algorithm, due to the choice of the basis functions $\boldsymbol{\phi}_k$, due to the length M of time series, or due to the choice of the model parameter values and so on. The predicted time series of $\vartheta_1(t)$ is displayed in figure 18.

In this subsection, we study the effect of varying the parameter γ on the length of the time series, and hence on the reconstruction using SINDy. To do this, we, hypothetically, consider the following values of γ:

$$\gamma = \{0.1, 0.15, 0.2, 0.25, 0.3, 0.4, 0.45, 0.65, 0.7, 0.8, 0.9, 1\}.$$

For each parameter γ, we construct the library matrix $\boldsymbol{\Phi} := \boldsymbol{\Phi}(\Theta; T(\gamma)) \in \mathbb{R}^{M(\gamma)\times K}$, where $M(\gamma) := T(\gamma)/\Delta t$ is the number of data points which depends on the choice of the parameter γ. To this end, we compute the time $T(\gamma)$, for each γ, for achieving the minimum singular value of the library matrix, denoted $\sigma_{min}(\boldsymbol{\Phi})$ satisfying the condition

$$\sigma_{min}(\boldsymbol{\Phi}) \geq \sigma^* \tag{4.98}$$

for some threshold value σ^*. Heuristically, we choose $\sigma^* = 0.5$, for each given parameter γ. The $T(\gamma)$ results are depicted in Table 3. Having the minimum values $T(\gamma)$ for each γ, we perform the mapping $T(\gamma) \mapsto 50T(\gamma)$ so that we get sufficient enough time-series for the reconstruction

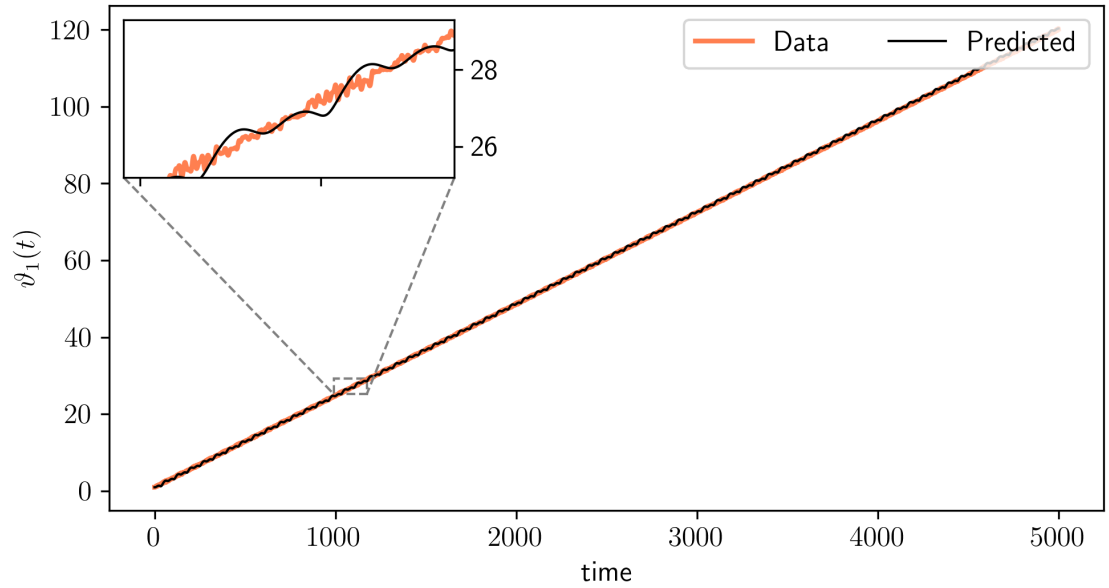

Figure 18 – Comparison of the predicted time series of $\vartheta_1(t)$ of a reconstructed phase model using the candidate functions library $\boldsymbol{\phi}_k \in \mathscr{L}$ defined in (4.92) with a hard thresholding parameter $\lambda = 0.0038$. The inset shows there is a reconstruction error.

γ	0.1	0.15	0.2	0.25	0.3	0.4	0.45	0.65	0.7	0.8	0.9	1.0
$T(\gamma)$	4400	1750	1300	1050	1000	950	950	600	550	500	450	250

Table 3 – Minimum time $T(\gamma)$ versus γ. The times $T(\gamma)$ satisfying condition (4.98) is shown in the second column. The starting test time was 100 with an increment of 50. A single random initial condition was considered.

Source: Elaborated by the author.

problem to be carried out for each choice of γ. Considering the new set of time $T(\gamma)$, we generate multiple data sets $\Theta^{\gamma} \in \mathbb{R}^{M(\gamma)\times N}$ for each parameter γ. Here, $M(\gamma) := \frac{T(\gamma)}{\Delta t}$ is the number of data points. Next, we build the corresponding library matrices $\boldsymbol{\Phi}^{\gamma}(\Theta^{\gamma})$ for each value of γ.

Next, we apply the SINDy algorithm with a thresholding $\lambda := \lambda(\gamma)$ separately for each data set Θ^{γ} to reconstruct the dynamics for each γ. To this end, we attempt to solve a sparse linear problem

$$\dot{\Theta}^{\gamma} = \boldsymbol{\Phi}^{\gamma}(\Theta^{\gamma})\boldsymbol{C}$$

for the coefficient matrix $\boldsymbol{C}$. We determine an optimal thresholding parameter λ corresponding to each parameter γ in estimating the coefficient matrix $\boldsymbol{C}(\gamma)$. In doing this we use the metric we introduced in this section. Based on this the "best" thresholding parameter values $\lambda_{opt}(\gamma)$ are displayed in table 4.

Table 4 shows that to effectively reconstruct the phase model from data with varying

γ	0.1	0.15	0.2	0.25	0.3	0.4	0.45	0.65	0.7	0.8	0.9	1.0
$\lambda_{opt}(\gamma)\times 10^{-4}$	4.95	1.72	1.28	10.4	4.17	9.1	21.3	27.8	10.3	32.7	28.6	39.8

Table 4 – Optimal thresholding parameter value $\lambda(\gamma)$ for varying γ. We considered 50 evenly spaced values of $\lambda(\gamma)$ between 10^{-5} and 0.003.

Source: Elaborated by the author.

parameter γ we need to choose different thresholding parameters λ. In the next subsection, we study the effects of varying γ in the phase model reconstruction using the SINDy algorithm.

4.4.5 Quantifying model reconstruction errors

In this subsection, we quantify the network and/or hypernetwork reconstructions, in particular, we identify the pairwise connections (*links* or *edges*) and/or triplet connections (*hyperlinks* or *hyperedges*), respectively. In this setting, typically there are two types of errors:

- *False positives links or hyperlinks* – are non-existing links or hyperlinks that are nevertheless present in the reconstructed network or hypernetwork, respectively
- *False negatives links or hyperlinks* – are existing links or hyperlinks that are not present in the reconstructed network or hypernetwork.

Let $\hat{\boldsymbol{c}}_i(\gamma) := [\hat{c}_{i,1},\ldots,\hat{c}_{i,K}] \in \mathbb{R}^K$ denote the reconstructed coefficient vector of the K-basis functions $\boldsymbol{\phi}_k(\boldsymbol{\vartheta})$ of oscillator $i \in \{1,\ldots,N\}$, obtained using SINDy algorithm with a given thresholding $\lambda := \lambda(\gamma)$, for each parameter γ. We see that $\hat{c}_{i,k} \neq 0$ if $\hat{c}_{i,k} > \lambda$, and $\hat{c}_{i,k} = 0$ if $\hat{c}_{i,k} < \lambda$. The vector $\hat{\boldsymbol{c}}_i$ is expected to be sparse. Let $\mathscr{P}$ and $\mathscr{T}$ denote the set of indices of the pairwise and triplet interactions, respectively, in the library $\mathscr{L}$. By reconstruction, we have

$$\mathscr{P} := \{9 \leq k \leq 20 : \boldsymbol{\phi}_k(\vartheta_p - \vartheta_q) \text{ is a pairwise basis element in } \mathscr{L}\},$$
$$\mathscr{T} := \{21 \leq k \leq 44 : \boldsymbol{\phi}_k(\vartheta_p + \vartheta_q - \vartheta_r) \text{ is a triplet basis element in } \mathscr{L}\}$$

For each oscillator i, let $\mathscr{P}_i$ and $\mathscr{T}_i$, respectively, denote the sets of indices of active pairwise interactions and triplet interactions of node i of the original network. Then we have

$$\mathscr{P}_i := \{k \in \mathscr{P} : \boldsymbol{\phi}_k(\vartheta_p - \vartheta_q) \text{ is an active pairwise coupling term in the dynamics of node } i\}, \text{ and}$$
$$\mathscr{T}_i := \{k \in \mathscr{T} : \boldsymbol{\phi}_k(\vartheta_p + \vartheta_q - \vartheta_r) \text{ is an active triplet coupling term in the dynamics of node } i\}.$$

From equation (4.89), we read the index sets of the true basis functions $\boldsymbol{\phi}_k$ in the dynamics of $\dot{\vartheta}_k$ for each oscillator i.

Let $\hat{\mathscr{P}}_i$ and $\hat{\mathscr{T}}_i$ denote the set of indices of the reconstructed links and hyperlinks associated with node $i \in \{1,\ldots,N\}$, respectively, using the SINDy algorithm with a given thresholding λ. Let the strength of the estimated links and hyperlinks of the reconstruction for node i be denoted by $w^p_{i,k} \in \{|\hat{c}_{i,k}| \ | k \in \hat{\mathscr{P}}_i\}$ and $w^t_{i,k} := \{|\hat{c}_{i,k}| \ | k \in \hat{\mathscr{T}}_i\}$. Then we define the

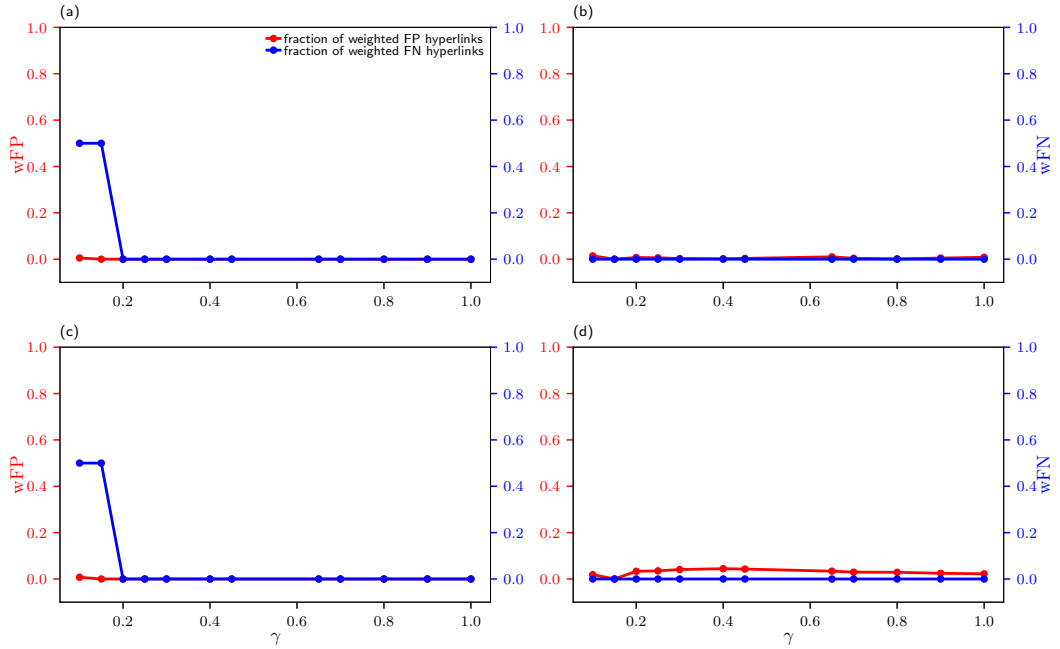

Figure 19 – The fractions of the false positive and false negative hyperlinks in the SINDy model reconstruction as a function of the parameter γ. For each parameter, γ, a maximum time of $T = 50T(\gamma)$, where $T(\gamma)$ is as provided in Table 3, was used to generate our time-series from the ring network. The choice of the thresholding parameter λ is provided in Table 4.

Source: Elaborated by the author.

weighted fractions of false positive links, wFP, and the weighted fractions of false negative links, wFN, in the reconstruction for each node i as:

$$wFP_i := \frac{\sum_{k\in\mathscr{P}} w_{i,k}\mathbb{1}_{\hat{\mathscr{P}}_i\cap\mathscr{P}_i^c}(k)}{\sum_{k\in\mathscr{P}}\left(w_{ik}\mathbb{1}_{\hat{\mathscr{P}}_i\cap(\mathscr{P}_i)^c}(k)+\mathbb{1}_{(\hat{\mathscr{P}}_i)^c\cap(\mathscr{P}_i)^c}(k)\right)}, \tag{4.99}$$

$$wFN_i := \frac{\sum_{k\in\mathscr{P}}\mathbb{1}_{(\hat{\mathscr{P}}_i)^c\cap\mathscr{P}_i}(k)}{\sum_{k\in\mathscr{P}}\mathbb{1}_{\mathscr{P}_i}(k)}, \tag{4.100}$$

where we have omitted the superscript p in the coefficient w_i^p for the sake of simplicity, and $\mathbb{1}_A$ is the indicator function of the set A, defined as

$$\mathbb{1}_A(k) = \begin{cases} 1 & \text{if } k \in A \\ 0 & \text{if } k \notin A \end{cases}$$

Similarly, the weighted fractions of false positive hyperlinks and the weighted fractions of false negative hyperlinks of each node i can be defined by replacing the sets $\mathscr{P}_i$ and $\hat{\mathscr{P}}_i$ by $\mathscr{T}_i$ and $\hat{\mathscr{T}}_i$, respectively.

The fractions of weighted false positives and false negatives in the reconstruction against varying the parameter γ are shown in figures 19 and 20.

The results in figure 19 show that there are missing true hyperlinks in the reconstructions of oscillators 1 and 3 when $\gamma = 0.1$ and $\gamma = 0.15$. This could be a result of the choice of the

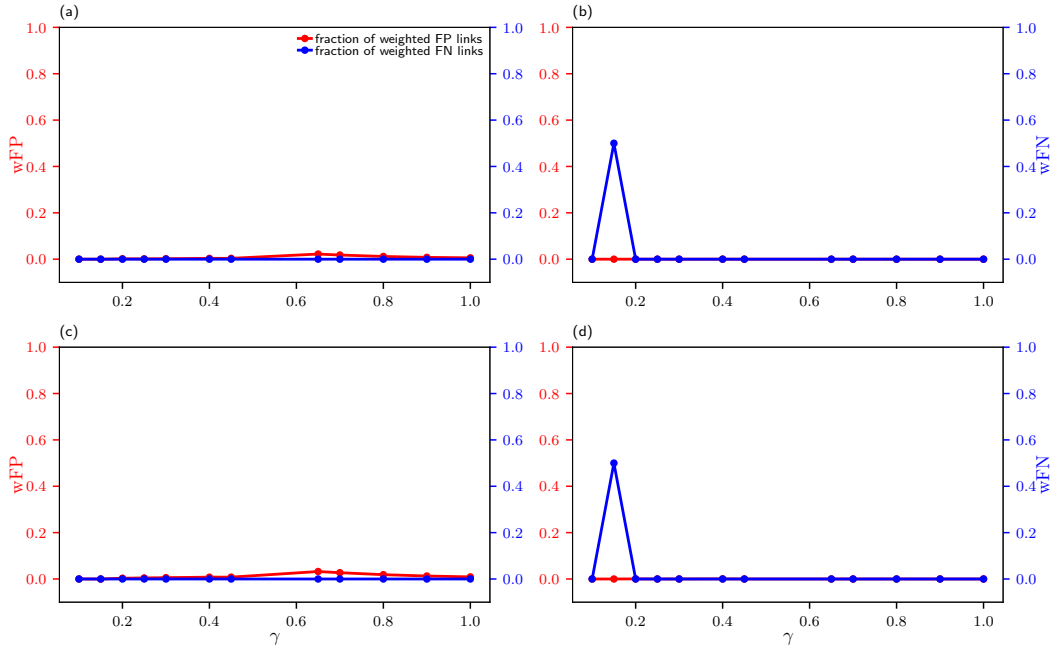

Figure 20 – The fractions of the false positive and false negative links in the SINDy model reconstruction as a function of the parameter γ. For each parameter, γ, a maximum time of $T = 50T(\gamma)$, where $T(\gamma)$ is as provided in Table 3, was used to generate our time-series from the ring network. The choice of the thresholding parameter λ is provided in Table 4.

Source: Elaborated by the author.

thresholding parameter. The results in figure 20 show that there is a missing true link in the reconstructions of oscillators 2 and 4, mainly for $\gamma = 0.15$.

CHAPTER

5

CONCLUSION

Many dynamical systems, both natural and man-made, are composed of interacting parts. Isolated dynamical systems such as the spiking of neurons, cardiac cells, and electrical circuits are periodic in nature. Mathematically, such periodic systems can be described by a limit cycle oscillator, which can be parameterized in terms of phases. In this thesis, we discussed the phase reduction approach in reducing high-dimensional, weakly interacting limit cycle oscillators theoretically.

Nowadays it is possible to collect and process enormous amounts of data from the units of many such interacting limit cycle oscillators. However, we do not have enough models of such systems to identify and parameterize the crucial features that must be incorporated into the model. To this end, in this thesis we aimed at reconstructing models of dynamical systems from available time-series data, using Bayesian inference and sparse recovery methods. Moreover, we studied the emergence of hypernetworks when reconstructing models of nonlinearly coupled oscillators from data. In particular, when the data comes from a network of weakly coupled Stuart-Landau oscillators, we showed that sparse recovery methods reveal hypernetworks. This result is verified theoretically using second-order phase reduction theory via the perturbation method.

Motivated by the time-variability of biological interactions, including neural delta-alpha interaction functions which were reconstructed based on Bayesian inference, a model of two coupled oscillators with time-evolving coupling functions has been shown to exhibit transitions to/from synchronization even when the net coupling strength remains constant. The analysis was carried out in terms of the phase difference between the oscillators. The corresponding numerical simulations show that, in the case of time-varying coupling functions, one can have sequential epochs of synchrony and asynchrony while the net coupling strength remains unchanged. Thus, by itself, the net coupling strength does not provide enough information to describe the dynamics of the interacting systems. To generalize the results, based on the model considered, we discussed three main ideas arising from the periodic function $f(t)$. The first of these was that, when

$\varphi(t) := f(t)t$ varies slowly with time, the dynamics of the two coupled oscillators induce synchrony over the slow timescale. The second was that when, by contrast, $\varphi(t)$ has rapid angular velocity, the oscillators do not synchronize. The third observation was the combined effect: the oscillators can exhibit sudden changes between synchrony and drifting phase differences occurring at transitions between slow variation and fast winding of $\varphi(t)$. So we have transitions in exhibited behavior due to the time-variability of the coupling functions despite constant net coupling strength. This confirms that, in the time-variable setting, the net coupling strength does not give sufficient information about the interaction of the oscillators to predict their behavior.

BIBLIOGRAPHY

ACEBRÓN, J. A.; BONILLA, L. L.; VICENTE, C. J. P.; RITORT, F.; SPIGLER, R. The kuramoto model: A simple paradigm for synchronization phenomena. **Rev. Mod. Phys.**, American Physical Society, v. 77, p. 137–185, Apr 2005. Available: <https://link.aps.org/doi/10.1103/RevModPhys.77.137>. Citation on page 45.

AHMAD, M.; RIYAZ, S.; RAND, R.; LIPSON, M. Design of dynamic neural observers. **IEE Proceedings of control theory applications**, v. 147, p. 257–263, 2015. Citation on page 73.

ASHRAF, I.; GODOY-DIANA, R.; HALLOY, J.; COLLIGNON, B.; THIRIA, B. Synchronization and collective swimming patterns in fish (hemigrammus bleheri). **Journal of The Royal Society Interface**, v. 13, n. 123, p. 20160734, 2016. Available: <https://royalsocietypublishing.org/doi/abs/10.1098/rsif.2016.0734>. Citation on page 81.

BARAHONA, M.; POON, C.-S. Detection of nonlinear dynamics in short, noisy time series. **Nature**, v. 381, p. 215–217, 1996. Available: <https://doi.org/10.1038/381215a0>. Citation on page 69.

BAYES, T. An essay towards a problem in the doctrine of chances. **Philos. Trans. R. Soc.**, v. 53, p. 370–418, 1763. Citation on page 63.

BILLINGS, S. A. **Nonlinear System Identification: NARMAX Methods in the Time, Frequency, and Spatio-Temporal Domains**. [S.l.]: Wiley, 2013. ISBN 9781119943594. Citations on pages 68 and 69.

BISHOP, C. M. **Pattern Recognition and Machine Learning**. [S.l.]: Springer New York, 2006. ISBN 9781493938438. Citation on page 63.

BJöRK, T. (Ed.). **Arbitrage Theory in Continuous Time**. [S.l.]: Oxford University Press, 2009. Citation on page 43.

BROMILEY, P. A. Products and convolutions of gaussian probability density functions. In: . [S.l.: s.n.], 2013. Citation on page 64.

BRUNTON, S. L.; PROCTOR, J. L.; KUTZ, J. N. Discovering governing equations from data by sparse identification of nonlinear dynamical systems. **Proceedings of the National Academy of Sciences**, v. 113, n. 15, p. 3932–3937, 2016. Available: <https://www.pnas.org/content/113/15/3932>. Citations on pages 71 and 93.

CESSAC, B. A view of neural networks as dynamical systems. **Intern. J. Bifurc. Chaos**, v. 20, p. 1585–1629, 01 2010. Citations on pages 22 and 45.

DAVIDSON, E. H. Emerging properties of animal gene regulatory networks. **Nature**, v. 468, p. 911–920, 2010. Citation on page 21.

DYKMAN, M. I. Large fluctuations and fluctuational transitions in systems driven by colored gaussian noise: A high-frequency noise. **Phys. Rev. A**, American Physical Society, v. 42, p. 2020–2029, Aug 1990. Available: <https://link.aps.org/doi/10.1103/PhysRevA.42.2020>. Citation on page 65.

ELDERING, J. **Normally Hyperbolic Invariant Manifolds: The noncompact case**. Sao Carlos: Springer, 2013. Citation on page 23.

____. Persistence of noncompact nhims. In: ____. **Normally Hyperbolic Invariant Manifolds: The Noncompact Case**. Paris: Atlantis Press, 2013. p. 75–140. ISBN 978-94-6239-003-4. Available: <https://doi.org/10.2991/978-94-6239-003-4_3>. Citations on pages 11, 23, and 83.

ERMENTROUT, B. Type i membranes, phase resetting curves, and synchrony. **Neural computation**, v. 8, n. 5, p. 979—1001, July 1996. ISSN 0899-7667. Available: <https://doi.org/10.1162/neco.1996.8.5.979>. Citation on page 40.

ERMENTROUT, G. B.; TERMAN, D. H. **Mathematical Foundations of Neuroscience**. NY: Springer New York, 2012. Citation on page 81.

FULLANA, J.-M.; ROSSI, M. Identification methods for nonlinear stochastic systems. **Phys. Rev. E**, American Physical Society, v. 65, p. 031107, Feb 2002. Available: <https://link.aps.org/doi/10.1103/PhysRevE.65.031107>. Citation on page 65.

GENGEL, E.; TEICHMANN, E.; ROSENBLUM, M.; PIKOVSKY, A. High-order phase reduction for coupled oscillators. **Journal of Physics: Complexity**, IOP Publishing, v. 2, n. 1, p. 015005, nov 2020. Available: <https://doi.org/10.1088/2632-072x/abbed2>. Citation on page 85.

GLASS, L.; MACKEY, M. C. Single pulse perturbation of biological oscillators. In: ____. **From Clocks to Chaos: The Rhythms of Life**. Princeton University Press, 1988. p. 98–118. ISBN 9780691084961. Available: <http://www.jstor.org/stable/j.ctv173dzwt.10>. Citation on page 21.

GOLUB, G. H.; LOAN, C. F. V. **Matrix computations**. Sao Carlos: The Johns Hopkins University Press, 1996. Citation on page 70.

Graham, R. Path integral formulation of general diffusion processes. **Zeitschrift fur Physik B Condensed Matter**, v. 26, n. 3, p. 281–290, Sep. 1977. Citation on page 65.

GUCKENHEIMER, J.; HOLMES, P. Introduction: Differential equations and dynamical systems. In: ____. **Nonlinear Oscillations, Dynamical Systems, and Bifurcations of Vector Fields**. New York, NY: Springer New York, 1983. p. 1–65. ISBN 978-1-4612-1140-2. Available: <https://doi.org/10.1007/978-1-4612-1140-2_1>. Citation on page 28.

GUCKENHEIMER, J. M. Isochrons and phaseless sets. **Journal of Mathematical Biology**, v. 1, p. 259–273, 1975. Citations on pages 29, 30, and 31.

HABER, R.; UNBEHAUEN, H. Structure identification of nonlinear dynamic systems—a survey on input/output approaches. **Automatica**, v. 26, n. 4, p. 651–677, 1990. ISSN 0005-1098. Available: <https://www.sciencedirect.com/science/article/pii/000510989090044I>. Citation on page 69.

Hagos, Z.; Stankovski, T.; Newman, J.; Pereira, T.; McClintock, P. V. E.; Stefanovska, A. Synchronization transitions caused by time-varying coupling functions. **Philosophical Transactions of the Royal Society of London Series A**, v. 377, n. 2160, p. 20190275, Dec. 2019. Citations on pages 25, 48, 49, 50, 51, 53, and 57.

HIRSCH, M. W.; PUGH, C. C.; SHUB, M. The local theory of normally hyperbolic, invariant, compact manifolds. In: ____. **Invariant Manifolds**. Berlin, Heidelberg: Springer Berlin Heidelberg, 1977. p. 39–53. ISBN 978-3-540-37382-7. Available: <https://doi.org/10.1007/BFb0092046>. Citations on pages 11, 23, 31, and 83.

IZHIKEVICH, E. M. Neural excitability, spiking and bursting. **International Journal of Bifurcation and Chaos**, v. 10, n. 06, p. 1171–1266, 2000. Available: <https://doi.org/10.1142/S0218127400000840>. Citation on page 21.

IZHIKEVICH, E. M.; ERMENTROUT, B. Phase model. **Scholarpedia**, v. 3, n. 10, p. 1487, 2008. Revision #129938. Citation on page 40.

Jensen, R. V. Synchronization of driven nonlinear oscillators. **American Journal of Physics**, v. 70, n. 6, p. 607–619, Jun. 2002. Citation on page 59.

JOSHI, S. K.; SEN, S.; KAR, I. N. Synchronization of master-slave oscillators: Analysis and experimental results. **IFAC-PapersOnLine**, v. 53, n. 1, p. 226–231, 2020. ISSN 2405-8963. 6th Conference on Advances in Control and Optimization of Dynamical Systems ACODS 2020. Available: <https://www.sciencedirect.com/science/article/pii/S2405896320300574>. Citation on page 73.

Kenwright, D. A.; Bahraminasab, A.; Stefanovska, A.; McClintock, P. V. E. The effect of low-frequency oscillations on cardio-respiratory synchronization. Observations during rest and exercise. **European Physical Journal B**, v. 65, n. 3, p. 425–433, Oct. 2008. Citation on page 52.

KRALEMANN, B.; CIMPONERIU, L.; ROSENBLUM, M.; PIKOVSKY, A.; MROWKA, R. Phase dynamics of coupled oscillators reconstructed from data. **Phys. Rev. E**, v. 77, n. 6, Part 2, p. 066205, 2008. Citation on page 47.

Kralemann, B.; Frühwirth, M.; Pikovsky, A.; Rosenblum, M.; Kenner, T.; Schaefer, J.; Moser, M. In vivo cardiac phase response curve elucidates human respiratory heart rate variability. **Nature Communications**, v. 4, p. 2418, Sep. 2013. Citation on page 49.

KURAMOTO, Y. (Ed.). **Chemical Oscillations, Waves, and Turbulence**. Berlin: Springer-Verlag, 1984. (Dover Books on Chemistry, 0486428818). Citations on pages 43, 44, and 85.

KURAMOTO, Y. Method of phase description i. In: ____. **Chemical Oscillations, Waves, and Turbulence**. Berlin, Heidelberg: Springer Berlin Heidelberg, 1984. p. 22–34. ISBN 978-3-642-69689-3. Available: <https://doi.org/10.1007/978-3-642-69689-3_3>. Citations on pages 37, 48, and 83.

LJUNG, L. **System Identification: Theory for the user**. PTR: Prentice Hall, 1999. Citations on pages 68 and 69.

LUCAS, M.; FANELLI, D.; STEFANOVSKA, A. Nonautonomous driving induces stability in network of identical oscillators. **Phys. Rev. E**, American Physical Society, v. 99, p. 012309, Jan 2019. Available: <https://link.aps.org/doi/10.1103/PhysRevE.99.012309>. Citation on page 59.

Lucas, M.; Newman, J.; Stefanovska, A. Stabilization of dynamics of oscillatory systems by nonautonomous perturbation. **Phys. Rev. E**, v. 97, n. 4, p. 042209, Apr. 2018. Citations on pages 22, 52, and 59.

LUCHINSKY, D. G.; SMELYANSKIY, V. N.; DUGGENTO, A.; MCCLINTOCK, P. V. E. Inferential framework for nonstationary dynamics. i. theory. **Phys. Rev. E**, American Physical Society, v. 77, p. 061105, Jun 2008. Available: <https://link.aps.org/doi/10.1103/PhysRevE.77.061105>. Citations on pages 65 and 68.

Luchinsky, D. G.; Smelyanskiy, V. N.; Millonas, M.; McClintock, P. V. E. Reconstruction of stochastic nonlinear dynamical models from trajectory measurements (Invited Paper). In: Kish, L. B.; Lindenberg, K.; Gingl, Z. (Ed.). **Noise in Complex Systems and Stochastic Dynamics III**. [S.l.: s.n.], 2005. (Society of Photo-Optical Instrumentation Engineers (SPIE) Conference Series, v. 5845), p. 173–181. Citations on pages 46 and 63.

MAIA, D. M. N.; MACAU, E. E. N.; PEREIRA, T. Persistence of network synchronization under nonidentical coupling functions. **SIAM Journal on Applied Dynamical Systems**, v. 15, n. 3, p. 1563–1580, 2016. Available: <https://doi.org/10.1137/15M1049786>. Citation on page 59.

MATHENY, M. H.; GRAU, M.; VILLANUEVA, L. G.; KARABALIN, R. B.; CROSS, M. C.; ROUKES, M. L. Phase synchronization of two anharmonic nanomechanical oscillators. **Phys. Rev. Lett.**, American Physical Society, v. 112, p. 014101, Jan 2014. Available: <https://link.aps.org/doi/10.1103/PhysRevLett.112.014101>. Citation on page 81.

MCKANE, A.; DROSSEL, B.; MCKANE, A.; BORNHOLDT, S.; SCHUSTER, H. Modelling food webs. In: ____. **Handbook of Graphs and Networks**. United Kingdom: John Wiley & Sons Ltd, 2003. p. 218–247. ISBN 3-527-40336-1. Citation on page 21.

MORELLI, M. S.; GRECO, A.; VALENZA, G.; GIANNONI, A.; EMDIN, M.; SCILINGO, E. P.; VANELLO, N. Analysis of generic coupling between EEG activity and PETCO2 in free breathing and breath-hold tasks using Maximal Information Coefficient (MIC). **Sci. Rep.**, 8, p. 4492, 2018. Citations on pages 22 and 45.

MORGAN, R. J.; SOLTESZ, I. Nonrandom connectivity of the epileptic dentate gyrus predicts a major role for neuronal hubs in seizures. **Proceedings of the National Academy of Sciences of the United States of America**, v. 105, p. 6179–6184, 2008. Available: <https://doi.org/10.1073/pnas.0801372105>. Citation on page 62.

NAKAO, H. Phase reduction approach to synchronisation of nonlinear oscillators. **Contemporary Physics**, Informa UK Limited, v. 57, n. 2, p. 188–214, Oct 2015. ISSN 1366-5812. Available: <http://dx.doi.org/10.1080/00107514.2015.1094987>. Citations on pages 22, 37, 39, 43, 81, and 83.

NEWMAN, M.; BARABÁSI, A.-L.; WATTS, D. J. Models of networks. In: ____. **The Structure and Dynamics of Networks:**. Princeton: Princeton University Press, 2006. chap. 4, p. 229–414. ISBN 9780691113579. Available: <http://www.jstor.org/stable/j.ctt7ssgv.7>. Citation on page 41.

NIJHOLT, E.; OCAMPO-ESPINDOLA, J. L.; EROGLU, D.; KISS, I. Z.; PEREIRA, T. Emergent hypernetworks in weakly coupled oscillators. **Nat Commun**, v. 13, p. 4849, 2022. Citation on page 90.

NIXON, M.; RONEN, E.; FRIESEM, A. A.; DAVIDSON, N. Observing geometric frustration with thousands of coupled lasers. **Phys. Rev. Lett.**, American Physical Society, v. 110, p. 184102, May 2013. Available: <https://link.aps.org/doi/10.1103/PhysRevLett.110.184102>. Citation on page 81.

ØKSENDAL, B. Stochastic differential equations. In: ____. **Stochastic Differential Equations: An Introduction with Applications**. Berlin, Heidelberg: Springer Berlin Heidelberg, 1992. p. 44–57. ISBN 978-3-662-02847-6. Available: <https://doi.org/10.1007/978-3-662-02847-6_5>. Citation on page 64.

OMEL'CHENKO, O. E.; WOLFRUM, M. Nonuniversal transitions to synchrony in the sakaguchi-kuramoto model. **Phys. Rev. Lett.**, American Physical Society, v. 109, p. 164101, Oct 2012. Available: <https://link.aps.org/doi/10.1103/PhysRevLett.109.164101>. Citations on pages 45, 62, and 81.

Pade, J. P.; Poignard, C.; Pereira, T. The Effects of Structural Perturbations on the Synchronizability of Diffusive Networks. **arXiv e-prints**, p. arXiv:1711.08909, Nov. 2017. Citation on page 59.

PEREIRA, T.; ELDERING, J.; RASMUSSEN, M.; VENEZIANI, A. Towards a theory for diffusive coupling functions allowing persistent synchronization. **Lond. Math. Soc. Nonlinearity**, v. 27, p. 501–525, 2014. Available: <doi:10.1088/0951-7715/27/3/501>. Citation on page 55.

PEREIRA, T.; EROGLU, D.; BAGCI, G. B.; TIRNAKLI, U.; JENSEN, H. J. Connectivity-driven coherence in complex networks. **Phys. Rev. Lett.**, American Physical Society, v. 110, p. 234103, Jun 2013. Available: <https://link.aps.org/doi/10.1103/PhysRevLett.110.234103>. Citation on page 59.

PIETRAS, B.; DAFFERTSHOFER, A. Network dynamics of coupled oscillators and phase reduction techniques. **Physics Reports**, v. 819, p. 1–105, 2019. ISSN 0370-1573. Network dynamics of coupled oscillators and phase reduction techniques. Available: <https://www.sciencedirect.com/science/article/pii/S0370157319302327>. Citation on page 22.

PIKOVSKY, A.; ROSENBLUM, M.; KURTHS, J. **Synchronization – A Universal Concept in Nonlinear Sciences**. Cambridge: Cambridge University Press, 2001. Citations on pages 22 and 50.

RIGATOS, G. Robust synchronization of coupled neural oscillators using derivative-free nonlinear kalman filter. **Cognitive neurodynamics**, v. 8, p. 465–478, 2014. Citation on page 73.

ROSENBLUM, M. G.; PIKOVSKY, A. S.; KURTHS, J. Phase synchronization of chaotic oscillators. **Phys. Rev. Lett.**, American Physical Society, v. 76, p. 1804–1807, Mar 1996. Available: <https://link.aps.org/doi/10.1103/PhysRevLett.76.1804>. Citations on pages 23 and 63.

RUDIN, W. Elementary hilbert space theory. In: ____. **Real and Complex Analysis**. 3. ed. New York, USA: McGraw-Hill, Inc., 1987. chap. 4, p. 76–94. Citation on page 49.

SAKAGUCHI, H.; KURAMOTO, Y. A soluble active rotater model showing phase transitions via mutual entertainment. **Progress of Theoretical Physics**, v. 76, p. 576–581, 1986. Citations on pages 45 and 62.

SANDERS, J. A.; VERHULST, F. The theory of averaging. In: ____. **Averaging Methods in Nonlinear Dynamical Systems**. New York, NY: Springer New York, 1985. p. 33–66. ISBN 978-1-4757-4575-7. Available: <https://doi.org/10.1007/978-1-4757-4575-7_3>. Citations on pages 38 and 57.

SANDERS, J. A.; VERHULST, F.; MURDOCK, J. **Averaging Methods in Nonlinear Dynamical Systems**. [S.l.]: Springer New York, 2007. (Applied Mathematical Sciences). ISBN 9780387489186. Citations on pages 84 and 89.

SCHÄFER, C.; ROSENBLUM, M. G.; KURTHS, J.; ABEL, H. H. Heartbeat synchronised with ventilation. **Nature**, v. 392, n. 6673, p. 239–240, 1998. Citations on pages 22 and 45.

SEBEK, M.; TÖNJES, R.; KISS, I. Z. Complex rotating waves and long transients in a ring network of electrochemical oscillators with sparse random cross-connections. **Phys. Rev. Lett.**, American Physical Society, v. 116, p. 068701, Feb 2016. Available: <https://link.aps.org/doi/10.1103/PhysRevLett.116.068701>. Citation on page 81.

SILVA, B. M. de; CHAMPION, K.; QUADE, M.; LOISEAU, J.-C.; KUTZ, J. N.; BRUNTON, S. L. Pysindy: A python package for the sparse identification of nonlinear dynamical systems from data. **Journal of Open Source Software**, The Open Journal, v. 5, n. 49, p. 2104, 2020. Available: <https://doi.org/10.21105/joss.02104>. Citations on pages 71 and 93.

Stankovski, T. Time-varying coupling functions: Dynamical inference and cause of synchronization transitions. **Phys. Rev. E**, v. 95, n. 2, p. 022206, Feb. 2017. Citations on pages 45, 50, and 51.

STANKOVSKI, T.; DUGGENTO, A.; MCCLINTOCK, P.; STEFANOVSKA, A. A tutorial on time-evolving dynamical bayesian inference. **Eur. Phys. J. Special Topics**, v. 223, p. 2685–2703, 2014. Citations on pages 46, 63, and 68.

STANKOVSKI, T.; DUGGENTO, A.; MCCLINTOCK, P. V. E.; STEFANOVSKA, A. Inference of time-evolving coupled dynamical systems in the presence of noise. **Phys. Rev. Lett.**, American Physical Society, v. 109, p. 024101, Jul 2012. Available: <https://link.aps.org/doi/10.1103/PhysRevLett.109.024101>. Citations on pages 46 and 52.

STANKOVSKI, T.; PEREIRA, T.; MCCLINTOCK, P. V. E.; STEFANOVSKA, A. Coupling functions: Universal insights into dynamical interaction mechanisms. **Rev. Mod. Phys.**, American Physical Society, v. 89, p. 045001, Nov 2017. Available: <https://link.aps.org/doi/10.1103/RevModPhys.89.045001>. Citations on pages 22, 33, 45, 46, and 62.

STANKOVSKI, T.; PETKOSKI, S.; RAEDER, J.; SMITH, A. F.; MCCLINTOCK, P. V. E.; STEFANOVSKA, A. Alterations in the coupling functions between cortical and cardio-respiratory oscillations due to anaesthesia with propofol and sevoflurane. **Philosophical Transactions of the Royal Society A: Mathematical, Physical and Engineering Sciences**, v. 374, n. 2067, p. 20150186, 2016. Available: <https://royalsocietypublishing.org/doi/abs/10.1098/rsta.2015.0186>. Citation on page 22.

STANKOVSKI, T.; TICCINELLI, V.; MCCLINTOCK, P. V. E.; STEFANOVSKA, A. Neural cross-frequency coupling functions. **Frontiers in systems neuroscience**, v. 11, p. 33, 2017. ISSN 1662-5137. Available: <https://europepmc.org/articles/PMC5471314>. Citations on pages 46 and 49.

STEFANOVSKA, A.; LUCHINSKY, D.; MCCLINTOCK, P. Modelling couplings among the oscillators of the cardiovascular system. **Physiological measurement**, v. 22, n. 3, p. 551—564, August 2001. ISSN 0967-3334. Available: <https://doi.org/10.1088/0967-3334/22/3/312>. Citation on page 52.

SUPRUNENKO, Y. F.; CLEMSON, P. T.; STEFANOVSKA, A. Chronotaxic systems: A new class of self-sustained nonautonomous oscillators. **Phys. Rev. Lett.**, American Physical Society, v. 111, p. 024101, Jul 2013. Available: <https://link.aps.org/doi/10.1103/PhysRevLett.111.024101>. Citation on page 59.

TAKEMURA, S.; BHARIOKE, A.; LU, Z.; NERN, A.; VITALADEVUNI, S.; RIVLIN, P.; KATZ, W.; OLBRIS, D.; PLAZA, S.; WINSTON, P.; ZHAO, T.; HORNE, J.; FETTER, R.; TAKEMURA, S.; BLAZEK, K.; CHANG, L.; OGUNDEYI, O.; SAUNDERS, M.; SHAPIRO, V.; SIGMUND, C.; RUBIN, G.; SCHEFFER, L.; MEINERTZHAGEN, I.; CHKLOVSKII, D. A visual motion detection circuit suggested by drosophila connectomics. **Nature**, v. 500, n. 7461, p. 175–181, 2013. Citation on page 21.

TIBSHIRANI, R. Regression shrinkage and selection via the lasso. **Journal of the Royal Statistical Society. Series B (Methodological)**, p. 267–288, 1996. Citation on page 70.

TICCINELLI, V.; STANKOVSKI, T.; IATSENKO, D.; BERNJAK, A.; BRADBURY, A. E.; GALLAGHER, A. R.; CLARKSON, P. B. M.; MCCLINTOCK, P. V. E.; STEFANOVSKA, A. Coherence and coupling functions reveal microvascular impairment in treated hypertension. **Frontiers in Physiology**, v. 8, p. 749, 2017. ISSN 1664-042X. Available: <https://www.frontiersin.org/article/10.3389/fphys.2017.00749>. Citation on page 46.

WIESENFELD, K.; COLET, P.; STROGATZ, S. H. Synchronization transitions in a disordered Josephson series array. **Phys. Rev. Lett.**, v. 76, n. 3, p. 404–407, 1996. Citation on page 22.

WINFREE, A. Biological rhythms and the behavior of populations of coupled oscillators. **Journal of theoretical biology**, v. 16, n. 1, p. 15—42, July 1967. ISSN 0022-5193. Available: <https://doi.org/10.1016/0022-5193(67)90051-3>. Citations on pages 28, 37, and 48.

____. Patterns of phase compromise in biological cycles. **Journal of Mathematical Biology**, v. 1, p. 73–93, 1974. Citation on page 22.

WINFREE, A. T. **The Geometry of Biological Time**. New York: Springer-Verlag, 1980. Citation on page 48.

____. Attracting cycles and isochrons. In: ____. **The Geometry of Biological Time**. New York, NY: Springer New York, 2001. p. 161–197. ISBN 978-1-4757-3484-3. Available: <https://doi.org/10.1007/978-1-4757-3484-3_6>. Citation on page 21.

WITTHAUT, D.; TIMME, M. Braess's paradox in oscillator networks, desynchronization and power outage. **New Journal of Physics**, IOP Publishing, v. 14, n. 8, p. 083036, aug 2012. Available: <https://dx.doi.org/10.1088/1367-2630/14/8/083036>. Citation on page 21.

APPENDIX

A

PROOFS OF THEOREMS

Proof of Theorem 2.2.3. By construction, for each $x_0 \in \gamma$, x_0 is a fixed point of g. Note that x_0 has both a transversal direction (i.e. stable) and a direction tangent to the limit cycle at x_0 (see Figure 21). We can introduce a suitable local coordinate systems $z = (u, v) \in \mathbb{R} \times \mathbb{R}$, where $u \in \mathbb{R}$ and $v \in \mathbb{R}$, to a point z in the neighborhood $B_\varepsilon(x_0)$ for some small $\varepsilon > 0$. Assume the point x_0 corresponds to the origin. Using the coordinate system, the time-1 map can be redefined as

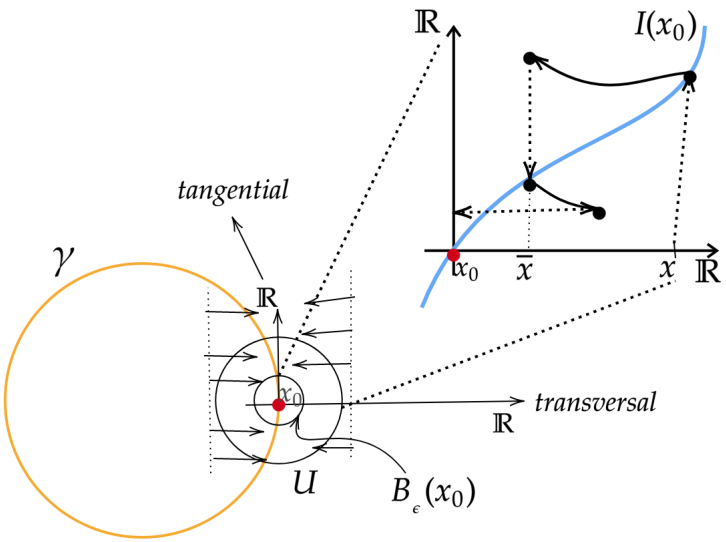

Figure 21 – The coordinate transformation near a limit cycle γ. The point x_0 is the base point of the transversal vector.

Source: Elaborated by the author.

$g : \mathbb{R} \times \mathbb{R} \longrightarrow \mathbb{R}^2$ such that

$$\begin{aligned} \bar{u} &= Au + R(u, v) \\ \bar{v} &= v + S(u, v) \end{aligned} \tag{A.1}$$

where $u \in \mathbb{R}, v \in \mathbb{R}, A \in (-1,1)$, $R : \mathbb{R}\times\mathbb{R} \to \mathbb{R}, S : \mathbb{R}\times\mathbb{R} \to \mathbb{R}$ are at least C^1 with

$$R(0,0) = 0 = S(0,0) \quad \text{and} \quad DR(0,0) = 0 = DS(0,0).$$

Moreover, let us introduce a map $H : \mathbb{R}\times\mathbb{R} \to \mathbb{R}$ such that

$$H(u,v) := v + S(u,v)$$

where S is as defined above. So that $H(0,0) = 0$ and $DH(0,0) = 0$. By construction, $R(\cdot,\cdot)\colon B_\varepsilon(0,0) \to \mathbb{R}^2$ is continuously differentiable. By the mean value theorem,

$$|R(u,v)| \leq \sup_{(u,v)\in B_\varepsilon(0,0)} |DR(u,v)||(u,v)|.$$

Note that $|DR(0,0)| = 0$. Then by continuity, given a $\delta > 0$, there is $\varepsilon = \varepsilon(\delta) > 0$ such that if $(u,v) \in B_\varepsilon(0,0)$ then $|DR(u,v)| < \delta$. This implies that

$$|R(u,v)| \leq \delta|(u,v)|.$$

So that we can make $\delta \ll 1$ and $Lip(R) < \delta$. Similarly, one can show that $Lip(H) < \mu \ll 1$.

Using the local coordinate systems, we consider the set

$$\mathscr{I}_{loc}(x_0) = \{(u,v) \in B_\varepsilon(x_0) \ : \ |g^m(u,v) - x_0| < Ke^{-\lambda m}\} \tag{A.2}$$

in the neighborhood of γ (see Figure 21). Here K and λ are positive constants.

We want to show that there is a function $\alpha\colon \mathbb{R} \to \mathbb{R}$ which depends on the base point x_0 such that

$$\mathscr{I}_{loc}(x_0) = \{(u,v)\colon v = \alpha(u)\} = graph(\alpha) \tag{A.3}$$

which is invariant under the action of g. We have shown that $Lip(A^{-1})Lip(H) < 1$ and $Lip(R) < \delta$. At this stage, we note that all the hypothesis of the *graph transform theorem* are satisfied. Hence we draw the conclusions of the graph transform. Thus, there is a unique function $\alpha_{x_0}\colon B_\varepsilon(x_0) \to \mathbb{R}$ with $\alpha_{x_0}(0) = 0$ and $Lip(\alpha_{x_0}) \leq \delta \ll 1$ such that

$$graph(\alpha_{x_0}) = g(graph(\alpha_{x_0})).$$

Hence, for each $x_0 \in \gamma$ the set $\mathscr{I}_{loc}(x_0)$ is represented in some local coordinates as the graph of a function $v = \alpha_{x_0}(u)$. That is, $\mathscr{I}_{loc}(x_0) =: graph(\alpha_{x_0})$ which depends on the base point x_0. Thus, through each point of the orbit γ there is a unique isochron $\mathscr{I}_{loc}(x_0)$ which is locally a graph of a function. The dependence on the base point $x_0 \in \gamma$ is continuous, but it may or may not be smooth.

Next, we want to show that isochrons are mapped to isochrons under the flow φ. To do this, let us assume that a base point $x_0 \in \mathscr{I}_{loc}(x_0)$ is mapped to another base point $y_0 \in \mathscr{I}_{loc}(y_0)$

under the flow φ, i.e., there is time t such that $\varphi(t,x_0) = y_0$. It remains to show that every $x \in \mathscr{I}_{loc}(x_0)$ is mapped to $y_0 \in \mathscr{I}_{loc}(y_0)$ under the flow φ. Let $x \in \mathscr{I}_{loc}(x_0)$ be arbitrary. By construction, $g^n(x) \to x_0$ exponentially fast. By the group property of the flow φ

$$g^m(\varphi(t,x)) = \varphi(m+t,x) = \varphi(t,\varphi(m,x)) = \varphi(t,g^m(x)).$$

By the continuity of the flow φ in x, we have

$$\varphi(t,g^m(x)) = \varphi(t,x_0) = y_0.$$

Thus, we can conclude that $\varphi(t,\mathscr{I}_{loc}(x_0)) = \mathscr{I}_{loc}(\varphi(t,x_0)) =: \mathscr{I}_{loc}(y_0)$, that is, the isochrons are mapped to isochrons under the flow φ.

Consider two distinct base points x_0 and y_0. We can conclude that their corresponding isochrons $\mathscr{I}_{loc}(x_0)$ and $\mathscr{I}_{loc}(y_0)$ are distinct. For if there is a point x in common, the asymptotic phase $\Theta(x) = \Theta(x_0) = \Theta(y_0)$ which is a contradiction to the assumption on x_0 and y_0. This implies that $\mathscr{I}_{loc}(x_0) \cap \mathscr{I}_{loc}(y_0) = \emptyset$ for $x_0, y_0 \in \gamma, x_0 \neq y_0$, where $\emptyset$ is the empty set. This implies that locally the isochrons form a foliation of the small neighborhood V of γ. This completes the proof of the theorem. □

Proof of Theorem 2.3.1. Assume that $\varepsilon \ll 1$. By construction, $\varphi_\varepsilon(t,x,\vartheta) = (\varphi_\varepsilon(\vartheta,x,t,\varepsilon),\vartheta(t))$ is the flow of the perturbed system (2.23). Let us define the corresponding time-one map as the mapping

$$\begin{aligned} g_\varepsilon := \varphi_\varepsilon(1,\cdot,\cdot) \;:\; \mathbb{R}^n \times \mathbb{S}^1 &\longrightarrow \mathbb{R}^n \times \mathbb{S}^1 \\ (x,\vartheta) &\longmapsto \left(g_\varepsilon(x,\vartheta),\bar{\vartheta}\right). \end{aligned} \tag{A.4}$$

For $\varepsilon = 0$, the time-one map $g_0(x,\vartheta) = g(x,\vartheta)$, where $g : \mathbb{R}^n \to \mathbb{R}^n$ is the time-one map for the unperturbed system. By construction g is a contraction, i.e. $\exists k \in (0,1)$ Lipschitz constant and a unique fixed point z. Indeed, $g(\gamma) = \gamma$. Let us introduce the composition

$$g_\varepsilon^n(\cdot,\boldsymbol{\vartheta}) = g_\varepsilon(\cdot,\vartheta_n) \circ g_\varepsilon(\cdot,\vartheta_{n-1}) \circ \ldots g_\varepsilon(\cdot,\vartheta_1)$$

of transformations, and assume that the transformations satisfy

$$\sup_{x\in\mathbb{R}^n} \|g(x) - g_\varepsilon(x,\theta)\| \leq \varepsilon. \tag{A.5}$$

Consider a fixed ϑ and let $G = g_\varepsilon$, then note that

$$\begin{aligned} \|G(x) - G(y)\| &\leq \|G(x) - g(x)\| + \|g(y) - G(y)\| + \|g(x) - g(y)\| \\ &\leq 2\varepsilon + k\|x - y\| \end{aligned}$$

and,

$$\begin{aligned} \|G(x) - g(y)\| &\leq \|G(x) - G(y)\| + \|g(y) - G(y)\| \\ &\leq 3\varepsilon + k\|x - y\|. \end{aligned}$$

Now, consider a ball $x \in W(z,\delta)$. We claim that if $\delta = \frac{3\varepsilon}{1-k}$ then $g_\varepsilon^n(x,\vartheta) \in W(z,\delta)$. Indeed, consider the action of a generic element G

$$\begin{aligned} \|G(x)-z\| &= \|G(x)-g(z)\| \\ &\leq 3\varepsilon + k\|x-z\| \leq \delta \end{aligned}$$

but since $x \in W(z,\delta)$ we have the following bound $\delta \geq 3\varepsilon/(1-k)$, and by induction the claim follows. This shows that for each $g_\varepsilon(x,\theta)$ is contraction on W.

□

Proof of Theorem 4.2.2. By definition, the Jacobian of transformation is given by

$$J(\boldsymbol{\theta}_m) = \frac{\partial(\zeta_{m,1},\ldots,\zeta_{m,N})}{\partial(\theta_{m+1,1},\ldots,\theta_{m+1,N})} = \begin{pmatrix} \frac{\partial\zeta_{m,1}}{\partial\theta_{m+1,1}} & \cdots & \frac{\partial\zeta_{m,1}}{\partial\theta_{m+1,N}} \\ \vdots & \ddots & \vdots \\ \frac{\partial\zeta_{m,N}}{\partial\theta_{m+1,1}} & \cdots & \frac{\partial\zeta_{m,N}}{\partial\theta_{m+1,N}} \end{pmatrix}. \tag{A.6}$$

For sake of simplicity, we proof for the case $N=2$, and generalize the result for an arbitrary N. In this case, Equation (4.7) leads us to the following two equations:

$$\begin{aligned} \zeta_{m,1} &= \theta_{m+1,1} - \theta_{m,1} - \Delta t F_1(\boldsymbol{\theta}_m^*;\boldsymbol{c}) \\ \zeta_{m,2} &= \theta_{m+1,2} - \theta_{m,2} - \Delta t F_2(\boldsymbol{\theta}_m^*;\boldsymbol{c}). \end{aligned} \tag{A.7}$$

It follows that

$$\boldsymbol{J}(\boldsymbol{\theta}_m) = \begin{pmatrix} \frac{\partial\zeta_{m,1}}{\partial\theta_{m+1,1}} & \frac{\partial\zeta_{m,1}}{\partial\theta_{m+1,2}} \\ \frac{\partial\zeta_{m,2}}{\partial\theta_{m+1,1}} & \frac{\partial\zeta_{m,2}}{\partial\theta_{m+1,2}} \end{pmatrix} = \begin{pmatrix} 1-\frac{\Delta t}{2}\frac{\partial F_1(\boldsymbol{\theta}_m^*;\boldsymbol{c})}{\partial\theta_{m+1,1}} & -\frac{\Delta t}{2}\frac{\partial F_1(\boldsymbol{\theta}_m^*;\boldsymbol{c})}{\partial\theta_{m+1,2}} \\ -\frac{\Delta t}{2}\frac{\partial F_2(\boldsymbol{\theta}_m^*;\boldsymbol{c})}{\partial\theta_{m+1,1}} & 1-\frac{\Delta t}{2}\frac{\partial F_2(\boldsymbol{\theta}_m^*;\boldsymbol{c})}{\partial\theta_{m+1,2}} \end{pmatrix} \tag{A.8}$$

If Δt is sufficiently small, then the determinant of $\boldsymbol{J}(\{\boldsymbol{\theta}_m\})$ can be approximated by the product of the elements of the diagonal, that is,

$$\det\boldsymbol{J}(\boldsymbol{\theta}_m) \approx \left(1-\frac{\Delta t}{2}\frac{\partial F_1(\boldsymbol{\theta}_m^*;\boldsymbol{c})}{\partial\theta_{m+1,1}}\right)\left(1-\frac{\Delta t}{2}\frac{\partial F_2(\boldsymbol{\theta}_m^*;\boldsymbol{c})}{\partial\theta_{m+1,2}}\right) \tag{A.9}$$

$$= \prod_{i=1}^{2}\left(1-\frac{\Delta t}{2}\frac{\partial F_i(\boldsymbol{\theta}_m^*;\boldsymbol{c})}{\partial\theta_{m,i}}\right) \tag{A.10}$$

$$= \exp -\frac{\Delta t}{2}\sum_{i=1}^{2}\left(\frac{\partial F_i(\boldsymbol{\theta}_m^*;\boldsymbol{c})}{\partial\theta_{m,i}}\right) \tag{A.11}$$

where we have used the fact from Taylor expansion that

$$1-\frac{\Delta t}{2}\frac{\partial F_i(\boldsymbol{\theta}_m^*;\boldsymbol{c})}{\partial\theta_{m,i}} \approx \exp\left(-\frac{\Delta t}{2}\frac{\partial F_i(\boldsymbol{\theta}_m^*;\boldsymbol{c})}{\partial\theta_{m,i}}\right)$$

to the first-order approximation in Δt. This result can be generalized for an arbitrary N. And hence, for a sufficiently small Δt, we have that

$$\begin{aligned}\det \boldsymbol{J}(\{\boldsymbol{\theta}_m\}) &\approx \prod_{i=1}^{N}\left(1-\frac{\Delta t}{2}\frac{\partial F_i(\boldsymbol{\theta}_m^*;\boldsymbol{c})}{\partial \theta_{m,i}}\right)\\ &\approx \exp\left(-\frac{\Delta t}{2}\sum_{i=1}^{N}\frac{\partial F_i(\boldsymbol{\theta}_m^*;\boldsymbol{c})}{\partial \theta_{m,i}}\right)\\ &= \exp -\frac{\Delta t}{2}\left(\boldsymbol{\nabla}\cdot\boldsymbol{F}(\boldsymbol{\theta}_m^*;\boldsymbol{c})\right)\end{aligned}$$

□

APPENDIX

B

DEFINITIONS OF COUPLING FUNCTIONS OF THE SECOND-ORDER PHASE APPROXIMATION

In this section, we define the explicit expressions of the coupling functions in the second-order phase reduction of the four weakly coupled Stuart-Landau oscillators. In this case, the functions Γ_k^2 in equations (4.83)–(4.86) are given by the following expressions.

$$
\begin{aligned}
\Gamma_1^2 = {} & B^{(1)}_{0,0,0,0} + A^{(1)}_{1,0,0,0}\sin\theta_1 + B^{(1)}_{1,0,0,0}\cos\theta_1 + A^{(1)}_{0,1,0,0}\sin\theta_2 + \sqrt{\gamma}b_1\cos\theta_2 + A^{(1)}_{0,0,1,0}\sin\theta_3 \\
& + B^{(1)}_{0,0,1,0}\cos\theta_3 + A_{0,0,0,1}\sin\theta_4 + \sqrt{\gamma}b_1\cos\theta_4 + A^{(1)}_{1,-1,0,0}\sin(\theta_1-\theta_2) - b_1\cos(\theta_1-\theta_2) \\
& + A^{(1)}_{1,0,-1,0}\sin(\theta_1-\theta_3) + B^{(1)}_{1,0,-1,0}\cos(\theta_1-\theta_3) + A^{(1)}_{1,0,0,-1}\sin(\theta_1-\theta_4) - b_1\cos(\theta_1-\theta_4) \\
& - b_3\cos(\theta_3-\theta_2) + A^{(1)}_{0,1,0,-1}\sin(\theta_2-\theta_4) + B^{(1)}_{0,1,0,-1}\cos(\theta_2-\theta_4) + a_3\sin(\theta_3-\theta_4) \\
& - a_1\sin(\theta_1+\theta_2) + b_1\cos(\theta_1+\theta_2) - a_3\sin(\theta_2-\theta_3) + b_3\cos(\theta_2+\theta_3) - a_3\sin(\theta_3+\theta_4) \\
& + b_3\cos(\theta_3+\theta_4) - a_1\sin(\theta_1+\theta_4) + b_1\cos(\theta_1+\theta_4) + A^{(1)}_{-1,2,0,0}\sin(2\theta_2-\theta_1) \\
& + A^{(1)}_{-1,0,0,2}\sin(2\theta_4-\theta_1) + B^{(1)}_{-1,0,0,2}\cos(2\theta_4-\theta_1) - c_{2,3}\sin(2\theta_2-\theta_3) + d_{2,3}\cos(2\theta_2-\theta_3) \\
& + \sqrt{\gamma}a_1\sin(2\theta_1-\theta_4) - \sqrt{\gamma}b_1\cos(2\theta_1-\theta_4) + \sqrt{\gamma}a_1\sin(2\theta_1-\theta_2) - \sqrt{\gamma}b_1\cos(2\theta_1-\theta_2) \\
& - 2\sqrt{\gamma}[d_{1,2}\cos(2\theta_1-2\theta_2) + d_{1,4}\cos(2\theta_1-2\theta_4)] - c_{4,3}\sin(2\theta_4-\theta_3) + d_{4,3}\cos(2\theta_4-\theta_3) \\
& + A^{(1)}_{2,-1,0,-1}\sin(2\theta_1-\theta_2-\theta_4) + B^{(1)}_{2,-1,0,-1}\cos(2\theta_1-\theta_2-\theta_4) + A^{(1)}_{1,-1,0,-1}\sin(\theta_2-\theta_1+\theta_4) \\
& + \sqrt{\gamma}a_3\left[\sin(\theta_1+\theta_3-\theta_4) + \sin(\theta_1+\theta_3-\theta_2)\right] - \sqrt{\gamma}b_3\left[\cos(\theta_1+\theta_3-\theta_4) + \cos(\theta_1+\theta_3-\theta_2)\right] \\
& + B^{(1)}_{1,-1,0,-1}\cos(\theta_2-\theta_1+\theta_4) + \sqrt{\gamma}b_3\cos(\theta_3-\theta_1+\theta_2) - \sqrt{\gamma}b_2\cos(\theta_2+\theta_1-\theta_4) \\
& + \sqrt{\gamma}a_2\sin(\theta_2+\theta_1-\theta_4) + \sqrt{\gamma}a_3\sin(\theta_1-\theta_3-\theta_4) + \sqrt{\gamma}b_3\cos(\theta_1-\theta_3-\theta_4) + a_3\sin(\theta_3-\theta_2) \\
& + \sqrt{\gamma}d_{4,3}\cos(2\theta_4-\theta_3-\theta_1) - \sqrt{\gamma}c_{2,3}\sin(2\theta_2-\theta_3-\theta_1) + \sqrt{\gamma}d_{2,3}\cos(2\theta_2-\theta_3-\theta_1) \\
& - b_3\cos(\theta_3-\theta_4) + B^{(1)}_{-1,2,0,0}\cos(2\theta_2-\theta_1) - \sqrt{\gamma}c_{4,3}\sin(2\theta_4-\theta_3-\theta_1) + \sqrt{\gamma}a_3\sin(\theta_1-\theta_3-\theta_2)
\end{aligned}
\tag{B.1}
$$

$$
\begin{aligned}
\Gamma_2^2 = {} & B^{(2)}_{0,0,0,0} + A^{(2)}_{1,0,0,0}\sin\theta_1 + \sqrt{\gamma}b_2\cos\theta_1 + A^{(2)}_{0,1,0,0}\sin\theta_2 + B^{(2)}_{0,1,0,0}\cos\theta_2 + A^{(2)}_{0,0,1,0}\sin\theta_3 \\
& + \sqrt{\gamma}b_2\cos\theta_3 + A^{(2)}_{0,0,0,1}\sin\theta_4 + B^{(2)}_{0,0,0,1}\cos\theta_4 + A^{(2)}_{1,-1,0,0}\sin(\theta_1-\theta_2) - b_2\cos(\theta_1-\theta_2) \\
& + B^{(2)}_{1,0,-1,0}\cos(\theta_1-\theta_3) - a_4\sin(\theta_1-\theta_4) - b_4\cos(\theta_1-\theta_4) + A^{(2)}_{0,1,-1,0}\sin(\theta_2-\theta_3) \\
& + A^{(2)}_{0,1,0,-1}\sin(\theta_2-\theta_4) + B^{(2)}_{0,1,0,-1}\cos(\theta_2-\theta_4) - a_4\sin(\theta_3-\theta_4) - b_4\cos(\theta_3-\theta_4) \\
& + A^{(2)}_{2,-1,0,0}\sin(2\theta_1-\theta_2) + B^{(2)}_{2,-1,0,0}\cos(2\theta_1-\theta_2) + A^{(2)}_{0,-1,2,0}\sin(2\theta_3-\theta_2) + d_{3,2}\cos(2\theta_2-2\theta_3)) \\
& - c_{3,4}\sin(2\theta_3-\theta_4) + d_{3,4}\cos(2\theta_3-\theta_4) - c_{1,4}\sin(2\theta_1-\theta_4) + d_{1,4}\cos(2\theta_1-\theta_4) \\
& - b_2\cos(\theta_2-\theta_3) + \sqrt{\gamma}a_2\sin(2\theta_2-\theta_1) - \sqrt{\gamma}b_2\cos(2\theta_2-\theta_1) + 2(d_{1,2}\cos(2\theta_1-2\theta_2) \\
& - a_2\sin(\theta_1+\theta_2) + b_2\cos(\theta_1+\theta_2) - a_4\sin(\theta_1+\theta_4) + b_4\cos(\theta_1+\theta_4) - a_2\sin(\theta_2+\theta_3) \\
& + A^{(2)}_{1,-1,1,0}\sin(\theta_1-\theta_2+\theta_3) + B^{(2)}_{1,-1,1,0}\cos(\theta_1-\theta_2+\theta_3) - a_4\sin(\theta_3+\theta_4) + b_4\cos(\theta_3+\theta_4) \\
& + A^{(2)}_{-1,2,-1,0}\sin(2\theta_2-\theta_1-\theta_3) + B^{(2)}_{-1,2,-1,0}\cos(2\theta_2-\theta_1-\theta_3) - \sqrt{\gamma}a_4\sin(\theta_1-\theta_2-\theta_4) \\
& + \sqrt{\gamma}b_4\left[\cos(\theta_1-\theta_2+\theta_4) - \cos(\theta_1-\theta_2-\theta_4) - \cos(\theta_2-\theta_3-\theta_4) + \cos(\theta_2-\theta_3-\theta_4)\right] \\
& + \sqrt{\gamma}a_4\left[\sin(\theta_2-\theta_3+\theta_4) - \sin(\theta_1-\theta_2+\theta_4) + \sin(\theta_2-\theta_3-\theta_4)\right] - c_{3,4}\sin(2\theta_3-\theta_2-\theta_4) \\
& + \sqrt{\gamma}d_{3,4}\cos(2\theta_3-\theta_2-\theta_4) + \sqrt{\gamma}a_2\sin(2\theta_2-\theta_3) + A^{(2)}_{1,0,-1,0}\sin(\theta_1-\theta_3) \\
& + B^{(2)}_{0,-1,2,0}\cos(2\theta_3-\theta_2) + \sqrt{\gamma}b_2\cos(2\theta_2-\theta_3) + b_2\cos(\theta_2+\theta_3),
\end{aligned}
\tag{B.2}
$$

$$
\begin{aligned}
\Gamma_3^2 = {} & B^{(3)}_{0,0,0,0} + A^{(3)}_{1,0,0,0}\sin(\theta_1) + B^{(3)}_{1,0,0,0}\cos(\theta_1) + A^{(3)}_{0,1,0,0}\sin\theta_2 + \sqrt{\gamma}b_3\cos\theta_2 + A^{(3)}_{0,0,1,0}\sin\theta_3 \\
& + B^{(3)}_{0,0,1,0}\cos\theta_3 + A^{(3)}_{0,0,0,1}\sin\theta_4 + \sqrt{\gamma}b_3\cos\theta_4 + A^{(3)}_{0,1,0,-1}\sin(\theta_2-\theta_4) + B^{(3)}_{0,1,0,-1}\cos(\theta_2-\theta_4) \\
& + B^{(3)}_{0,2,-1,0}\cos(2\theta_2-\theta_3) - A^{(3)}_{0,0,-1,2}\sin(2\theta_4-\theta_3) + B^{(3)}_{0,0,-1,2}\cos(2\theta_4-\theta_3) - b_1\cos(\theta_1-\theta_2) \\
& + a_1\sin(\theta_1-\theta_2) + A^{(3)}_{1,0,-1,0}\sin(\theta_1-\theta_3) + B^{(3)}_{1,0,-1,0}\cos(\theta_1-\theta_3) + a_1\sin(\theta_1-\theta_4) \\
& + A^{(4)}_{0,0,1,-1}\sin(\theta_3-\theta_4) - b_3\cos(\theta_3-\theta_4) + A^{(3)}_{0,1,-1,0}\sin(\theta_2-\theta_3) - b_3\cos(\theta_2-\theta_3) \\
& + b_1\cos(\theta_1+\theta_2) - a_3\sin(\theta_2+\theta_3) + b_3\cos(\theta_2+\theta_3) - c_{2,1}\sin(2\theta_2-\theta_1) + d_{2,1}\cos(2\theta_2-\theta_1) \\
& - a_3\sin(\theta_3+\theta_4) + b_3\cos(\theta_3+\theta_4) - a_1\sin(\theta_1+\theta_4) + b_1\cos(\theta_1+\theta_4) - c_{4,1}\sin(2\theta_4-\theta_1) \\
& + d_{4,1}\cos(2\theta_4-\theta_1) + \sqrt{\gamma}a_3\sin(2\theta_3-\theta_2) - \sqrt{\gamma}b_3\cos(2\theta_3-\theta_2) + \sqrt{\gamma}a_3\sin(2\theta_3-\theta_4) \\
& + 2\sqrt{\gamma}d_{2,3}\cos(2\theta_2-2\theta_3) - \sqrt{\gamma}b_3\cos(2\theta_3-\theta_4) - 2\sqrt{\gamma}d_{3,4}\cos(2\theta_3-2\theta_4) \\
& + \sqrt{\gamma}a_1\left[\sin(\theta_1+\theta_3-\theta_2) + \sin(\theta_1+\theta_3-\theta_4)\right] - \sqrt{\gamma}b_1\left[\cos(\theta_1+\theta_3-\theta_2) + \cos(\theta_1+\theta_3-\theta_4)\right] \\
& + B^{(3)}_{0,1,-1,1}\cos(\theta_2-\theta_3+\theta_4) + A^{(3)}_{0,1,-1,1}\sin(\theta_2-\theta_3+\theta_4) + A^{(3)}_{0,-1,2,-1}\sin(2\theta_3-\theta_2-\theta_4) \\
& + \sqrt{\gamma}b_1\left[\cos(\theta_1-\theta_3+\theta_2) + \cos(\theta_1-\theta_3+\theta_4)\right] - \sqrt{\gamma}a_1\left[\sin(\theta_1-\theta_3+\theta_2) + \sin(\theta_1-\theta_3+\theta_4)\right] \\
& + \sqrt{\gamma}a_2\sin(\theta_2+\theta_3-\theta_4) - \sqrt{\gamma}b_2\cos(\theta_2+\theta_3-\theta_4) + \sqrt{\gamma}a_4\sin(\theta_4+\theta_3-\theta_2) \\
& + \sqrt{\gamma}d_{2,1}\cos(2\theta_2-\theta_1-\theta_3) + B^{(3)}_{0,-1,2,-1}\cos(2\theta_3-\theta_2-\theta_4) - \sqrt{\gamma}c_{2,1}\sin(2\theta_2-\theta_1-\theta_3) \\
& + \sqrt{\gamma}d_{4,1}\cos(2\theta_4-\theta_1-\theta_3) - \sqrt{\gamma}b_4\cos(\theta_4+\theta_3-\theta_2) - \sqrt{\gamma}c_{4,1}\sin(2\theta_4-\theta_1-\theta_3) \\
& - A^{(3)}_{0,2,-1,0}\sin(2\theta_2-\theta_3) - b_1\cos(\theta_1-\theta_4) - a_1\sin(\theta_1+\theta_2)
\end{aligned}
\tag{B.3}
$$

$$
\begin{aligned}
\Gamma_4^2 = {} & B^{(4)}_{0,0,0,0} + A^{(4)}_{1,0,0,0}\sin\theta_1 + \sqrt{\gamma}b_4\cos\theta_1 + A^{(4)}_{0,1,0,0}\sin\theta_2 + B^{(4)}_{0,1,0,0}\cos\theta_2 - \sqrt{\gamma}a_4\sin\theta_3) \\
& + A^{(4)}_{0,0,0,1}\sin\theta_4 + B^{(4)}_{0,0,0,1}\cos\theta_4 - b_2\cos(\theta_1-\theta_2) + A^{(4)}_{1,0,-1,0}\sin(\theta_1-\theta_3) \\
& + A^{(4)}_{1,0,0,-1}\sin(\theta_1-\theta_4) - b_4\cos(\theta_1-\theta_4) + a_2\sin(\theta_2-\theta_3) - b_2\cos(\theta_2-\theta_3) \\
& + A^{(4)}_{0,1,0,-1}\sin(\theta_2-\theta_4) + B^{(4)}_{0,1,0,-1}\cos(\theta_2-\theta_4) + A^{(4)}_{0,0,1,-1}\sin(\theta_3-\theta_4) - b_4\cos(\theta_3+\theta_4) \\
& + b_2\cos(\theta_1+\theta_2) - a_4[\sin(\theta_1+\theta_4)+\sin(\theta_3+\theta_4)] + b_4[\cos(\theta_1+\theta_4)+\cos(\theta_3+\theta_4)] \\
& + b_2\cos(\theta_2+\theta_3) - c_{3,2}\sin(2\theta_3-\theta_2) + d_{3,2}\cos(2\theta_3-\theta_2) + \sqrt{\gamma}a_4\sin(2\theta_4-\theta_3) \\
& + A^{(4)}_{0,0,2,-1}\sin(2\theta_3-\theta_4) + B^{(4)}_{0,0,2,-1}\cos(2\theta_3-\theta_4) + 2\sqrt{\gamma}d_{3,4}\cos(2\theta_3-2\theta_4) \\
& + \sqrt{\gamma}a_4\sin(2\theta_4-\theta_1) - \sqrt{\gamma}b_4\cos(2\theta_4-\theta_1) + A^{(4)}_{1,0,1,-1}\sin(\theta_1+\theta_3-\theta_4) \\
& + A^{(4)}_{-1,0,-1,2}\sin(2\theta_4-\theta_1-\theta_3) + B^{(4)}_{-1,0,-1,2}\cos(2\theta_4-\theta_1-\theta_3) - \sqrt{\gamma}c_{1,2}\sin(2\theta_1-\theta_2-\theta_4) \\
& + \sqrt{\gamma}a_2(\sin(\theta_2+\theta_4-\theta_3)-\sin(\theta_2-\theta_4+\theta_3)) - \sqrt{\gamma}a_2(\sin(\theta_1-\theta_2-\theta_4)-\sin(\theta_1+\theta_2-\theta_4)) \\
& + \sqrt{\gamma}b_2(\cos(\theta_2-\theta_4+\theta_3)-\cos(\theta_2+\theta_4-\theta_3)) - \sqrt{\gamma}b_2(\cos(\theta_1-\theta_2-\theta_4)+\cos(\theta_1+\theta_2-\theta_4)) \\
& + \sqrt{\gamma}d_{3,2}\cos(2\theta_3-\theta_2-\theta_4) - \sqrt{\gamma}c_{3,2}\sin(2\theta_3-\theta_2-\theta_4) + \sqrt{\gamma}a_1\sin(\theta_1-\theta_3+\theta_4) \\
& + \sqrt{\gamma}d_{1,2}\cos(2\theta_1-\theta_2-\theta_4) - \sqrt{\gamma}a_3\sin(\theta_1-\theta_3-\theta_4) - \sqrt{\gamma}b_3\cos(\theta_1-\theta_3-\theta_4) \\
& + \sqrt{\gamma}b_4\cos\theta_3 - a_2\sin(\theta_1-\theta_2) + B^{(4)}_{1,0,-1,0}\cos(\theta_1-\theta_3) - a_4\sin(\theta_3-\theta_4) - a_2\sin(\theta_1+\theta_2) \\
& - a_2\sin(\theta_2+\theta_3) - \sqrt{\gamma}b_4\cos(2\theta_4-\theta_3) + 2\sqrt{\gamma}d_{1,4}\cos(2\theta_1-2\theta_4) + B^{(4)}_{1,0,1,-1}\cos(\theta_1+\theta_3-\theta_4) \\
& - \sqrt{\gamma}b_1\cos(\theta_1-\theta_3+\theta_4)
\end{aligned}
\tag{B.4}
$$

The coefficients $A^{(m)}_{\boldsymbol{l}}, B^{(m)}_{\boldsymbol{l}}$ in equations (B.1)–(B.4) are listed in tables 5–7 and 8. Here the four-component vector $\boldsymbol{l} = (l_1, l_2, l_3, l_4)$ is used to signify the term with the combination of the phases $l_1\theta_1 + l_2\theta_2 + l_3\theta_3 + l_4\theta_4$. Moreover, we used notations

$$
a_m = \frac{a'_m}{2},\ b_m = \frac{b'_m}{2},\ c_{m,k} = \frac{c'_{m,k}}{2},\ \text{and}\ d_{m,k} = \frac{d'_{m,k}}{2},
$$

where $a'_m, b'_m, c'_{m,k}$, and $d'_{m,k}$ are defined as

$$
\begin{aligned}
a'_m &= \frac{2\gamma^2}{4\gamma^2+\omega_m^2}, \quad b'_m = \frac{\omega_m\gamma}{4\gamma^2+\omega_m^2}, \\
c'_{m,k} &= \frac{2\gamma^2}{4\gamma^2+(\omega_m-\omega_k)^2}, \quad d'_{m,k} = \frac{(\omega_m-\omega_k)\gamma^{3/2}}{4\gamma^2+(\omega_m-\omega_k)^2}.
\end{aligned}
$$

Table 5 – Definitions of the coupling coefficients $A_{\boldsymbol{l}}^{(1)}, B_{\boldsymbol{l}}^{(1)}$ in equation (B.1) of the first oscillator.

$A^{(1)}_{1,0,0,0}$	$-c_{4,1}-c_{2,1}+\sqrt{\gamma}a_4+\sqrt{\gamma}a_2$
$B^{(1)}_{1,0,0,0}$	$-d_{4,1}-d_{2,1}-\sqrt{\gamma}b_4-\sqrt{\gamma}b_2$
$A^{(1)}_{0,0,1,0}$	$-c_{4,3}-c_{2,3}$
$B^{(1)}_{0,0,1,0}$	$-d_{4,3}-d_{2,3}$
$A^{(1)}_{0,0,0,1}$	$-c_0-\sqrt{\gamma}a_1$
$A^{(1)}_{1,-1,0,0}$	$a_1+2\sqrt{\gamma}c_0$
$A^{(1)}_{1,0,-1,0}$	$c_{4,3}+c_{2,3}$
$B^{(1)}_{1,0,-1,0}$	$-d_{4,3}-d_{2,3}$
$A^{(1)}_{1,0,0,-1}$	$a_1+2\sqrt{\gamma}c_0$
$A^{(1)}_{0,1,0,-1}$	$\sqrt{\gamma}(c_{1,2}-c_{1,4})$
$B^{(1)}_{0,1,0,-1}$	$\sqrt{\gamma}(d_{1,2}+d_{1,4})$
$A^{(1)}_{-1,0,0,2}$	$-c_{4,1}-\sqrt{\gamma}a_4$
$B^{(1)}_{-1,0,0,2}$	$d_{4,1}+\sqrt{\gamma}b_4$
$A^{(1)}_{-1,2,0,0}$	$-c_{2,1}-\sqrt{\gamma}a_2$
$B^{(1)}_{-1,2,0,0}$	$d_{2,1}+\sqrt{\gamma}b_2$
$A^{(1)}_{2,-1,0,-1}$	$\sqrt{\gamma}(c_{1,2}+c_{1,4})$
$B^{(1)}_{2,-1,0,-1}$	$-\sqrt{\gamma}(d_{1,2}+d_{1,4}$
$A^{(1)}_{1,-1,0,-1}$	$\sqrt{\gamma}(a_2+a_4)$
$B^{(1)}_{1,-1,0,-1}$	$\sqrt{\gamma}(b_2+b_4)$
$B^{(1)}_{0,0,0,0}$	$2\sqrt{\gamma}(d_{1,4}+d_{1,2})$

Source: Elaborated by the author.

Table 6 – Definitions of the coupling coefficients $A_{\boldsymbol{l}}^{(2)}, B_{\boldsymbol{l}}^{(2)}$ in equation (B.2) of the second oscillator.

$A^{(2)}_{1,0,0,0}$	$-c_0 - \sqrt{\gamma}a_2$
$A^{(2)}_{0,1,0,0}$	$-c_{1,2} - c_{3,2} + \sqrt{\gamma}a_1 + \sqrt{\gamma}a_3$
$B^{(2)}_{0,1,0,0}$	$-d_{1,2} - d_{3,2} - \sqrt{\gamma}b_1 - \sqrt{\gamma}b_3$
$A^{(2)}_{0,0,1,0}$	$-c_0 - \sqrt{\gamma}a_2$
$A^{(2)}_{0,0,0,1}$	$-(c_{1,4} + c_{3,4})$
$B^{(2)}_{0,0,0,1}$	$-(d_{1,4} + d_{3,4})$
$A^{(2)}_{1,0,-1,0}$	$c_{2,1} - c_{2,3}$
$B^{(2)}_{1,0,-1,0}$	$d_{2,3} + d_{2,1}$
$A^{(2)}_{0,1,-1,0}$	$a_2 + 2\sqrt{\gamma}c_0$
$A^{(2)}_{0,1,0,-1}$	$\sqrt{\gamma}(c_{1,4} + c_{3,4})$
$B^{(2)}_{0,1,0,-1}$	$-\sqrt{\gamma}(d_{1,4} + d_{3,4})$
$A^{(2)}_{2,-1,0,0}$	$-c_{1,2} - \sqrt{\gamma}a_1$
$B^{(2)}_{2,-1,0,0}$	$d_{1,2} + \sqrt{\gamma}b_1$
$A^{(2)}_{0,-1,2,0}$	$-c_{3,2} - \sqrt{\gamma}a_3$
$B^{(2)}_{0,-1,2,0}$	$d_{3,2} + \sqrt{\gamma}b_3$
$B^{(2)}_{0,0,0,0}$	$-2\sqrt{\gamma}(d_{1,2} + d_{3,2})$
$A^{(2)}_{-1,2,-1,0}$	$\sqrt{\gamma}(c_{2,3} + c_{2,1})$
$B^{(2)}_{-1,2,-1,0}$	$-\sqrt{\gamma}(d_{2,3} + d_{2,1})$
$A^{(2)}_{1,-1,1,0}$	$-\sqrt{\gamma}(a_3 + a_1)$
$B^{(2)}_{1,-1,1,0}$	$\sqrt{\gamma}(b_3 + b_1)$

Source: Elaborated by the author.

Table 7 – Definitions of the coupling coefficients $A_l^{(3)}, B_l^{(3)}$ in equation (B.3) of the third oscillator.

$A^{(3)}_{1,0,0,0}$	$-c_{2,1} - c_{4,1}$
$B^{(3)}_{1,0,0,0}$	$-d_{2,1} - d_{4,1}$
$A^{(3)}_{0,1,0,0}$	$-c_0 - \sqrt{\gamma}a_3$
$A^{(3)}_{0,0,1,0}$	$-c_{2,3} - c_{4,3} + \sqrt{\gamma}a_2 + \sqrt{\gamma}a_4$
$B^{(3)}_{0,0,1,0}$	$-d_{2,3} - d_{4,3} - \sqrt{\gamma}b_2 - \sqrt{\gamma}b_4$
$A^{(3)}_{0,0,0,1}$	$-c_0 - \sqrt{\gamma}a_3$
$A^{(3)}_{1,0,-1,0}$	$-\sqrt{\gamma}(c_{2,1} + c_{4,1})$
$B^{(3)}_{1,0,-1,0}$	$-\sqrt{\gamma}(d_{2,1} + d_{4,1})$
$A^{(3)}_{0,1,-1,0}$	$-a_3 - 2\sqrt{\gamma}c_0$
$A^{(3)}_{0,0,1,-1}$	$a_3 + 2\sqrt{\gamma}c_0$
$A^{(3)}_{0,1,0,-1}$	$\sqrt{\gamma}(c_{3,2} - c_{3,4})$
$B^{(3)}_{0,1,0,-1}$	$\sqrt{\gamma}(d_{3,2} + d_{3,4})$
$A^{(3)}_{0,2,-1,0}$	$-c_{2,3} - \sqrt{\gamma}a_2$
$B^{(3)}_{0,2,-1,0}$	$d_{2,3} + \sqrt{\gamma}b_2$
$A^{(3)}_{0,0,-1,2}$	$-c_{4,3}\sqrt{\gamma}a_4$
$B^{(3)}_{0,0,-1,2}$	$d_{4,3} + \sqrt{\gamma}b_4$
$B^{(3)}_{0,0,0,0}$	$\sqrt{\gamma}(2d_{3,2} + 2d_{3,4})$
$A^{(3)}_{0,1,-1,1}$	$-\sqrt{\gamma}(a_4 + a_2)$
$B^{(3)}_{0,1,-1,1}$	$\sqrt{\gamma}(b_4 + b_2)$
$A^{(3)}_{0,-1,2,-1}$	$\sqrt{\gamma}(c_{3,4} + c_{3,2})$
$B^{(3)}_{0,-1,2,-1}$	$-\sqrt{\gamma}(d_{3,4} + d_{3,2})$

Source: Elaborated by the author.

Table 8 – Definitions of the coupling coefficients $A_{\boldsymbol{l}}^{(4)}, B_{\boldsymbol{l}}^{(4)}$ in equation (B.4) of the fourth oscillator.

$A^{(4)}_{1,0,0,0}$	$-c_0 - \sqrt{\gamma}a_4$
$A^{(4)}_{0,1,0,0}$	$-c_{3,2} - c_{1,2}$
$B^{(4)}_{0,1,0,0}$	$-d_{3,2} - d_{1,2}$
$A^{(4)}_{0,0,0,1}$	$-c_{3,4} - c_{1,4} + \sqrt{\gamma}a_3 + \sqrt{\gamma}a_1$
$B^{(4)}_{0,0,0,1}$	$-d_{3,4} - \sqrt{\gamma}d_{1,4} + b_3 + \sqrt{\gamma}b_1$
$A^{(4)}_{1,0,-1,0}$	$c_{4,1} - c_{4,3}$
$B^{(4)}_{1,0,-1,0}$	$d_{4,1} + d_{4,3}$
$A^{(4)}_{1,0,0,-1}$	$-a_4 - 2\sqrt{\gamma}c_0$
$A^{(4)}_{0,1,0,-1}$	$-\sqrt{\gamma}(c_{3,2} + c_{1,2})$
$B^{(4)}_{0,1,0,-1}$	$-\sqrt{\gamma}(d_{3,2} + d_{1,2})$
$A^{(4)}_{0,0,2,-1}$	$-c_{3,4} - \sqrt{\gamma}a_3$
$B^{(4)}_{0,0,2,-1}$	$d_{3,4} + \sqrt{\gamma}b_3$
$A^{(4)}_{2,0,0,-1}$	$-c_{1,4} - \sqrt{\gamma}a_1$
$B^{(4)}_{2,0,0,-1}$	$d_{1,4} + \sqrt{\gamma}b_3$
$A^{(4)}_{1,0,1,-1}$	$-\sqrt{\gamma}(a_1 + a_3)$
$B^{(4)}_{1,0,1,-1}$	$\sqrt{\gamma}(b_1 + b_3)$
$A^{(4)}_{-1,0,-1,2}$	$\sqrt{\gamma}(c_{4,1} + c_{4,3})$
$B^{(4)}_{-1,0,-1,2}$	$\sqrt{\gamma}(d_{4,1} + d_{4,3})$
$B^{(4)}_{0,0,0,0}$	$-2\sqrt{\gamma}(d_{3,4} + d_{1,4})$

Source: Elaborated by the author.


ICMC
USP
SÃO CARLOS